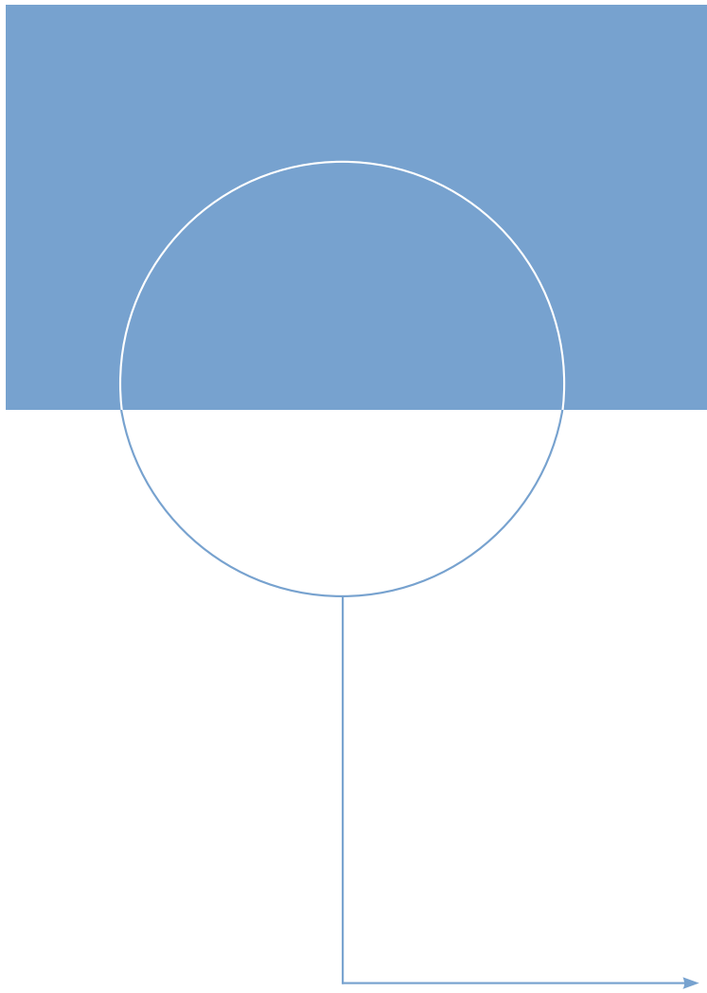

Master's thesis

2019

Håkon Pedersen

NTNU
Norwegian University of
Science and Technology
Faculty of Natural Sciences
Department of Physics

Håkon Pedersen

Spin Wave Modulation in Antiferromagnetic Magnonic Crystals with Interfacial Dzyaloshinskii-Moriya Interaction

May 2019

NTNU
Norwegian University of
Science and Technology

NTNU
Norwegian University of
Science and Technology

NTNU

Norwegian University of
Science and Technology

Spin Wave Modulation in Antiferromagnetic Magnonic Crystals with Interfacial Dzyaloshinskii-Moriya Interaction

MSc in Physics
Submission date: May 2019
Supervisor: Arne Brataas
Co-supervisor: Roberto Troncoso

Norwegian University of Science and Technology
Department of Physics

ABSTRACT

The advent of spintronics has opened up a new field of physics, interesting from both a technological and theoretical viewpoint. Motivated by the possibility of novel forms of information transfer, processing and storage, along with recent experimental realizations of these spin-based systems, we study the excitation spectrum of spin waves in a antiferromagnetic bipartite lattice with spatially modulated interfacial Dzyaloshinskii-Moriya interaction. These kinds of modulated systems are called magnonic crystals.

Collinear easy-axis antiferromagnets can support two degenerate excitation modes associated with the two sublattices of the antiferromagnetic bipartite lattice, a novel degree of freedom not present in conventional charge-based electronic systems. The combined time- and inversion-symmetry breaking in the form of a external magnetic field and the antisymmetric Dzyaloshinskii-Moriya-interaction completely lifts the degeneracy of the modes, which presents a possibility of controlling the propagation of the individual modes. This degree of control has several applications in the emerging field of wave based computing, including spin wave-filters for the creation of spin-polarized currents, one-way magnonic waveguides, phase shifters and much more.

To obtain the low-frequency spin wave spectrum, we study a continuum model formulated in terms of two convenient antiferromagnetic order parameter fields. The coupled differential equations describing their semi-classical dynamics will be decoupled and reduced to a single equation, which will be used to obtain an effective spin wave equation for the two antiferromagnetic modes. This equation will be used to model 1- and 2D magnonic crystals with periodic modulation of the Dzyaloshinskii-Moriya interaction strength. The 2D case in particular has not been previously studied with the theoretical framework presented in this thesis.

The spin wave dispersion of the magnonic crystals will be obtained and discussed, with special attention directed towards the features of the dispersion which make the systems interesting for novel applications.

SAMMENDRAG

Framveksten av fagområdet spinntronikk har åpnet et nytt, interessant felt i fysikken fra både teoretisk og teknologisk ståsted. Motivert av muligheten for nye måter å sende, prosessere og lagre informasjon, samt nylige eksperimentelle realiseringer av denne typen systemer, velger vi å studere eksitasjonsspekteret til spinn-bølger i et vekselvirkende antiferromagnetisk gitter med en romlig modulert Dzyaloshinskii-Moriya-vekselvirkning mellom nærmeste gitterpunkter. Denne typen modulerte systemer kalles for magnoniske krystaller.

To degenererte spinn-bølge-moder, assosiert med dekomposisjonen av det antiferromagnetiske gitteret i to separate under-gitter, kan propagere i antiferromagneter med kollineære, akse-rettede spinn. Disse to modene representerer en ny frihetsgrad som ikke finnes i konvensjonelle ladnings-baserte elektroniske systemer. Brytningen av den kombinerte tids- og inversjonssymmetrien med et eksternt magnetisk felt og den antisymmetriske Dzyaloshinskii-Moriya-interaksjonen opphever degenerasjonen i modene, og presenterer en mulighet for å kontrollere propageringen deres individuelt. Denne graden av kontroll har flere applikasjoner i det voksende feltet omkring bølge-baserte beregninger, som inkluderer blant annet spinn-bølge-filtre, danningen av spinn-polariserte strømmer, en-veis magnoniske bølgeledere og faseskiftere.

For å finne det lavfrekvente spinn-bølge-spekteret studerer vi en kontinuerlig modell, formulert ved hjelp av to passende antiferromagnetiske ordensparameter-felt. De koblede differensialligningene som beskriver den semi-klassiske dynamikken til feltene vil bli dekoblet og redusert til en enkelt ligning. Denne vil bli brukt til å utarbeide en effektiv spinn-bølge-ligning for de to antiferromagnetiske modene, som vi deretter bruker til å modellere en- og todimensjonale krystaller gjennom periodisk variasjon av styrken til Dzyaloshinskii-Moriya-vekselvirkingen. Det todimensjonale tilfellet har ikke blitt studert tidligere i det teoretiske rammeverket som presenteres her.

Spinn-bølge-dispersjonen til de magnoniske krystallene vil bli utarbeidet og diskutert, med fokus på egenskapene som gjør systemet interessant for mulige applikasjoner.

PREFACE

This thesis was written during the 2nd year of the two-year Master in Physics programme at the Norwegian University of Science and Technology in Trondheim. I would like to thank my supervisor Dr. Roberto Troncoso for the thesis idea, and for guidance and discussion throughout my time working on the subject. Special thanks go to my family for supporting me throughout these five years in Trondheim, and to my friends and fellow physics students for all the good times we've had, both the productive and the not-so-productive.

Håkon Pedersen
Trondheim, Norway
May 2019

CONTENTS

1 Introduction **1**
- 1.1 Antiferromagnetic spintronics and context . . . 1
- 1.2 Spin waves . . . 4
- 1.3 Magnonics and magnonic crystals . . . 7
- 1.4 The Dzyaloshinskii-Moriya interaction . . . 8
- 1.5 Proposal and structure of thesis . . . 11

2 AFM spin systems and semi-classical spin wave theory **13**
- 2.1 The torque equation . . . 13
- 2.2 The AFM lattice and ground states . . . 16
- 2.3 The continuum description of a AFM lattice . . . 18
  - 2.3.1 Alternative formulation: Haldane's mapping . . . 19
- 2.4 Antiferromagnetic exchange . . . 20
  - 2.4.1 Magnetic anisotropy . . . 21
  - 2.4.2 Zeeman coupling . . . 22
  - 2.4.3 The Dzyaloshinskii-Moriya interaction . . . 23
- 2.5 Complete form of free energy . . . 25
  - 2.5.1 Discarding anisotropic and parity-breaking terms . . . 26
- 2.6 Semi-classical equations of motion for the Neél AFM . . . 27
- 2.7 Klein-Gordon-equation of in-plane SW-fluctuations . . . 32

3 1D magnonic crystal **37**
  - 3.0.1 Effects of DMI on spin wave spectrum . . . 38
  - 3.0.2 1D modulation and the DMI Kronig-Penney model . . . 40
- 3.1 1D magnonic crystal results . . . 44

4 2D magnonic crystal and the plane wave expansion **53**
- 4.1 General formulation of PWM . . . 53
- 4.2 PWE for AFM spin waves . . . 55
  - 4.2.1 Inclusion of magnetic field . . . 60
- 4.3 2D cosine-modulated periodic potential . . . 61
- 4.4 2D results . . . 63

5 Summary, discussion and outlook **77**

A Derivation of AFM free energy, lattice approach **79**

B Obtaining the semi-classical equations of motion in the exchange approximation **86**

C Equations of motion for Néel order fluctuations **93**

D Fourier transform of the effective Dzyaloshinskii-Moriya term and matrix elements **95**

NOMENCLATURE

Abbreviations

AFM	Antiferromagnet
FM	Ferromagnet
SW	Spin wave
RH/LH	Right-handed / Left-handed
(I)DMI	(Interfacial) Dzyaloshinskii-Moriya Interaction
SOC	Spin-orbit coupling
MC	Magnonic crystal
EM	Electromagnetic (field)
MBZ	(Magnetic) Brillouin zone

Notation

D	Inhomogeneous DMI strength
d_h	Homogeneous DMI strength
γ	Gyromagnetic ratio
T_N	Néel-temperature
$\mathcal{L}, \mathcal{F}, \mathcal{K}$	Lagrangian-, free energy- and kinetic density
$\mathcal{S}$	Classical action

Conventions

Vectors in the text will be noted in **bold** , and a overhead arrow $\rightarrow$ in figures
The constant background DMI d_h will be referred to as *homogeneous* DMI
The Einstein summation convention is invoked for repeated indices

CHAPTER 1

INTRODUCTION

In this chapter, we will motivate the work done in this thesis with historical context, a general introduction to the main constituents of this thesis, namely magnonic crystals, spin waves and antiferromagnets, and a overview of current research on the topic. We will then present the structure of the thesis itself.

1.1 Antiferromagnetic spintronics and context

The demand for better computational efficiency, lower power consumption, increased reliability and streamlined production of components necessitates insight into what physics allows us to realistically achieve in technology. This naturally leads us to the fundamentals of how we physically transfer and store information today. Until recently, the fundamental particles of choice, or perhaps more accurately necessity, in technological applications has been the *electron* and the *photon*. The former is arguably the most well known and "accessible" fermion for technological applications, while the bosonic photon is the fundamental quantum of the electromagnetic field, meaning it is the mediator, or gauge boson, carrying the electromagnetic force.

Historically, only the the electron mass and charge has been applied technologically, even before the discovery of the fundamental particle itself by Thomson in late 19^{th} century through his experiments with cathode rays [78]. The photon has had a similar fundamental importance in practically all of modern technology. A suitable description of the interactions between these particles depend on the energy scales and distances involved: the theory of electromagnetism [39], classical electrodynamics [37], and later quantum electrodynamics [36] (QED) are all theories which describe the interplay between currents, charges and fields, but at different field intensities and length scales.

Modern technological applications do not necessarily need the fundamental insight into the interactions of the electron and the photon obtained in e.g. QED. However, one can argue that the theoretical framework of quantum mechanics (QM) is almost essential in driving modern technology. In the context of this thesis, QM is a necessity to obtain a understanding of magnetic materials, another fundamental part of modern technology. Being inherently quantum-mechanical and requiring QM-properties to explain their microscopic ordering and resulting macroscopic effects, magnetic systems are a natural arena to study the dynamics and physical effects of *spin*, its consequences and possible applications.

In the mid-1920s, Heisenberg proposed an *exchange interaction* between neighbouring magnetic moments, or spins, as an explanation for the observed

spontaneous magnetization in certain materials below the *Curie temperature* T_C, a critical temperature which separates a ordered magnetic state where spins point predominantly in the same direction, from a state dominated by thermal fluctuations, resulting in randomly disordered spins [45]. The state characterized by collinear spins for $T < T_C$ is called *ferromagnetic*, with the material as a whole naturally called a *ferromagnet* (FM). The two states are separated by a *phase transition*, a reordering which the system undergoes to minimize its free energy subject to external conditions such as temperature, field and pressure. These transitions are, loosely speaking, classified as 1^{st} or 2^{nd} order based on if they involve latent heat (1^{st}) or not (2^{nd}). To quantify the amount of order in the system, one introduces a *order parameter* which typically ranges from zero in a disordered phase (e.g. a $T > T_C$-phase) to a finite value in a ordered phase, often with a divergent susceptibility at a critical point denoted by some critical parameter C. In the case of ferromagnetism, the order parameter is the *net magnetization* $\mathbf{M}$ of the system. The language of phase transitions are of course completely general and constitutes a vast field of study on its own [17, 23], and does not apply to magnetism alone.

In the 1930s, Néel discovered that certain magnetic materials such as Fe did not exhibit ferromagnetic order below a certain critical temperature, as one might expect. The net magnetization of the system vanished below some critical *Néel temperature* T_N [27], which Néel proposed was due to an exchange interaction between neighbouring magnetic moments which favoured antiparallel alignment, and not parallel as in typical FMs, thus introducing the *antiferromagnet* (AFM) to the types of known magnetic order. Above T_N, the moments are disalligned due to thermal fluctuations, and the material undergoes a phase transition into a disordered state. For AFMs, this state is typically *paramagnetic* [45], exhibiting weak ferromagnetism which can couple to magnetic fields.

As the theory of magnetic materials evolved, one took interest in smaller scale properties of the magnetic arrangements of coupled spin systems, such as the formation of magnetic structures. This physical domain needed a new, practical framework. In the 40s, Brown provided the starting point for the field of *micromagnetics* [18], which considers the physical regime between the small scale atomic structures and magnetic structures such as *domain walls* and *magnetic textures*, about which more later. In the length scales relevant in magnetic material textures and structures, $\sim 10^{-(6\sim12)}$ m, one can ignore the complicated internal structure and quantized nature of the atom itself in favour of resolving interesting magnetic structures and configurations in the system.

The physical regime of micromagnetics lends itself very well to a description in terms of *continuum mechanics* [26]. This approach to modelling physical systems assumes that quantities like mass and fields take on a continuum of values. In other words, notions of point-particles are discarded. In this limit, where all quantities are defined at every point in space, one ignores the fact that physics at the smallest energy- and length-scales is discrete. However, from the sub-micrometer range of micromagnetics and up, the continuum description of matter proves to be very accurate, and has significant overlap with well-known

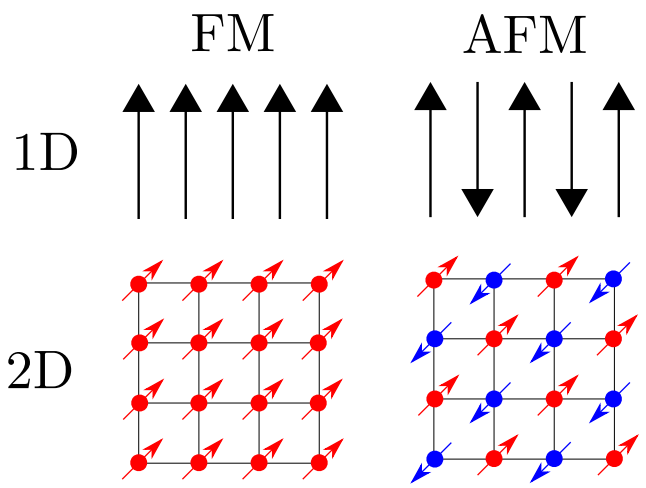

Figure 1.1: Sketch illustrating the idealized microscopic ordering of the magnetic moments in a FM and AFM for $T < T_C$ and $T < T_N$ respectively. Red arrows indicate a "up"-spin and blue indicate "down"-spin. In reality, the spins can be canted at some angle with respect to each other, as opposed to being perfectly collinear.

theories of classical fields and solid- and fluid-mechanics [16].
One of the successors to micromagnetics is the field of *spintronics* [112], which seek to exploit the spin degree of freedom of electrons in addition to its charge and mass. The emergence of spintronics has had a profound impact on the field of solid state physics in the last 20 years, with many regarding the discovery of *giant magnetoresistance* [25, 29] in the late 80s as the starting point of the field. An example of a important technological application made possible by the advent of spintronics and giant magnetoresistance is *spin-valves*. The device is made possible by an understanding of spin-transfer torque (STT) in thin films [34], as a spin-valve involves stacks of thin magnetic layers which can support electric current, and allows for switching between a high- and low-resistance state depending on the relative orientations of the magnetization in the layers. One of the most promising technological applications of spin-valves is *magnetic random access memory* (MRAM) [120], which stores data in magnetic domains, in contrast to transistor-based flash memory or dynamic random-access memory (DRAM).

Today, FMs constitute virtually all technological applications of magnets in modern devices. One of the reasons is that AFMs are generally harder to manipulate. Change and detection of the magnetic state is challenging due to the lack of macroscopic magnetization in AFMs. However, AFMs in spintronics has in recent years attracted considerable interest due to a renewed understanding of their interactions with currents, in addition to several other favourable properties making them attractive for applications.

In contrast to FMs, AFMs do not produce stray fields due to the lack of net magnetization at macroscopic scales. This renders the interactions in the mag-

netic moments (for the most part) local, eliminating the phenomena of domain splitting in larger systems, as is seen in FMs due to the *demagnetization effect* [45] which reduces the magnetic dipole energy by splitting the system into areas of different magnetization-directions, so called *domains*. AFMs are associated with considerably faster dynamics than FMs, exhibiting characteristic frequencies in the THz-range [65] compared to the GHz-ranges in ferromagnets. AFMs are very resistant to external EM-fields, which serves as both a challenge when manipulating their dynamics, and favourable when one does not want outside agents to perturb the AFM system.

A serious challenge in AFM spintronics is being able to detect and manipulate the AFM-order. It is proposed that the detection can be done through *anisotropic magnetoresistive tunneling* [82], and *current-induced torques* in AFMs has been hinted at in experiments [53], opening up for altering the order parameter with external currents. In addition, *spin-pumping* in AFMs has been theoretically proposed [93], which indicates that the generation of spin-polarized currents can be viable for detecting the AFM-state and manipulating the system despite its lack of net magnetization.

Another challenge in adapting AFMs in modern technology is controlling the spin degree of freedom at practical temperatures. This has been demonstrated in NiO at room temperature ($\sim$ 300 K), where optical methods was used to measure AFM spin excitations of the order $\sim$ 1 THz, induced by a EM-field [72]. In general, AFM order occurs under less extreme conditions than FM order, making them easier to study. Another important property of collinear AFMs is that they can support two degenerate excitation-modes which can be separated by the symmetry of the material and external fields, allowing for a novel degree of freedom in encoding information. We will treat this property more closely in sec. 1.2.

1.2 Spin waves

Spin waves (SWs) are collective excitations of the coupled spin systems in magnetic solid materials [68, 133]. Their properties are sensitive to many different parameters, and can be altered by the type of magnet, EM-fields of different intensities and orientations, and the geometry and size of the system or sample in which they propagate. One can associate a quasiparticle corresponding to this excitation, called a *magnon*. Being bosons, these quasiparticles obey *Bose-Einstein statistics*, and can carry *spin current*, making their properties as information carriers fundamentally different from the conventional electron transport used in today's computing technologies. We will use the terms "spin waves" and "magnons" interchangably.

SWs offers the possibility of encoding more information than what is possible for data processing with conventional electron charge carriers due to its spin degree of freedom. This paradigm of *wave based computing* represents a entirely new era of information processing if one can find reliable ways of encoding, propagating and extracting information with SWs.

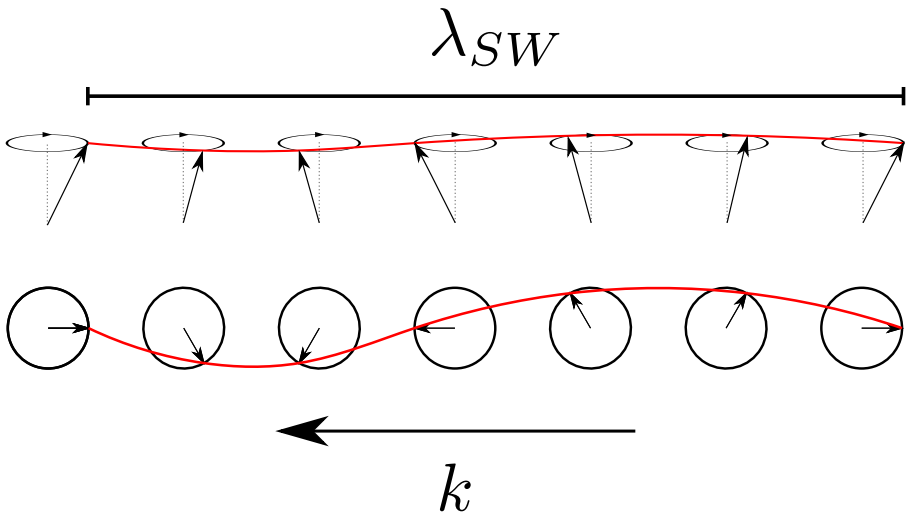

Figure 1.2: A chain of vectors precessing clockwise, which can be imagined as local magnetic moments. The 2nd row is the same as the 1st, but seen from above. The "spin wave" is the deviation in the precessional motion w.r.t. the equilibrium direction, shown with perforated lines in the top row, and transfers spin wave momentum to the left. The wavelength of the spin wave λ_{SW} is defined by the length of one period of rotation of the spin. The figure is adapted from [45].

In the 30s, Bloch proposed magnon excitations as an explanation for the observed reduced spontaneous magnetization in FMs when approaching T_C from below [1]. In a semi-classical picture, spin waves can be visualized as a small disturbance in the local magnetization in a material: a precessing magnetic moment about some equilibrium orientation, where the amplitude is the deviation from this ground state orientation, and the propagation is in the direction which the angle of precession varies, see fig. 1.2. Another leap in SW-theory came in the 40s, with Holstein and Primakoffs quantization-approach in terms of bosonic creation- and annihilation-operators [3]. Uniformly precessing SW-modes were first observed in the 40s using ferromagnetic resonance [4].

Spin waves are able to propagate through both conductors and insulators because they are collective excitations of the precessing magnetic moments themselves, and not point-particles and charge carriers like electrons. Thus, there is no *Joule-heating* associated with their propagation, meaning a higher computational energy efficiency can theoretically be achieved. Excitation of the SWs can be performed with e.g. a oscillating magnetic field [113], optical excitation [38], or thermal excitation through the *spin Seebeck effect* [107]. The measurement and detection of SWs is possible with magnetic probing/optical spectroscopy [73, 94], the detection of currents by the *inverse spin Hall effect* by virtue of spin-pumping [91, 93], or by inelastic neutron scattering [121], although the latter is not the most practical.

The physics and comprising literature on SWs are rich and varied due to a multitude of interesting and experimentally realizable phenomena, as they exhibit the same type of properties as sound or light waves, such as reflection and refraction, interference and the *Doppler effect* [59], among others. The waves exhibit *non-linearity*, allowing for suppression or amplification of magnon currents by means of other magnon-currents [68]. The waves also exhibit *nonreciprocivity* in certain systems [89]. Such non-reciprocal-magnons were first measured experimentally [121] by inelastic neutron scattering (BT7/SPINS) in the non-centrosymmetric AFM α-$Cu_2V_2O_7$. SWs exhibit different propagation modes in different geometries subject to external fields, e.g. thin film/slab arrangements (*Damon-Eshbach-geometry*) [12] or at the boundaries of samples [92]. SWs also have properties which make them very different from sound and light waves, e.g. a high degree of dispersion, appearance of frequency gaps in zero-response and anisotropic dispersion even in isotropic media.

Magnons have attracted considerable interest due to their interplay with magnetic *solitons* and *textures*. A prominent example of such structures is the *skyrmion* [66, 122], a excitation of collective magnetic moments where the resulting configuration is said to be *topologically protected*. The skyrmion spin structure acquires a conserved quantum number of topological origin, a *topological charge*, whose conservation makes the excitation metastable and manipulable e.g. by external currents [128]. The structures represent a minimum of the free energy of the system, and with the conserved "exotic" topological quantum number and the possibility of manipulating its state, the skyrmion is attractive for future technological applications. The quantum number, or *winding number*, characterizing the structure can take on positive and negative integer values, making it a possible qubit-candidate [102]. Another example of interesting topological excitations are *band-gap solitons* in periodic magnetic structures [55]. Other interesting SW phenomena and realizations include the creation of caustic beams [88] and Bose-Einstein-condensation of room-temperature magnons achieved through spin-pumping in a magnon gas [48].

The recent theoretical interest in AFMs also extends to SWs. Anderson studied AFM-SWs in a semi-classical approach as early as in the 50s [7]. AFM-SWs was first experimentally observed by neutron diffraction around the same time [6]. As mentioned in the last section, one of the features of collinear, easy-axis AFMs in spintronics is that they exhibit two degenerate SW-modes with opposite polarization, see fig. 1.3. This reflects the description of AFMs as two coupled FM-sublattices, which we will return to in chap. 2. The polarization of the modes is analogous to EM-polarization, and implies that it can be used to encode information.

As an alternative to the basis in fig. 1.3, one can also describe the polarization in terms of oscillations of the some AFM order parameter Θ, e.g. $\Theta \propto \mathbf{m}_1 - \mathbf{m}_2$. Suitable order parameters will be discussed further in chap. 2. The up/down-spins in each AFM unit cell can individually travel clockwise or counterclockwise, but the order parameter can still exhibit linear oscillations in a single direction, e.g. along the x- or y-axes. Analogous to EM-waves, this polarization can be ro-

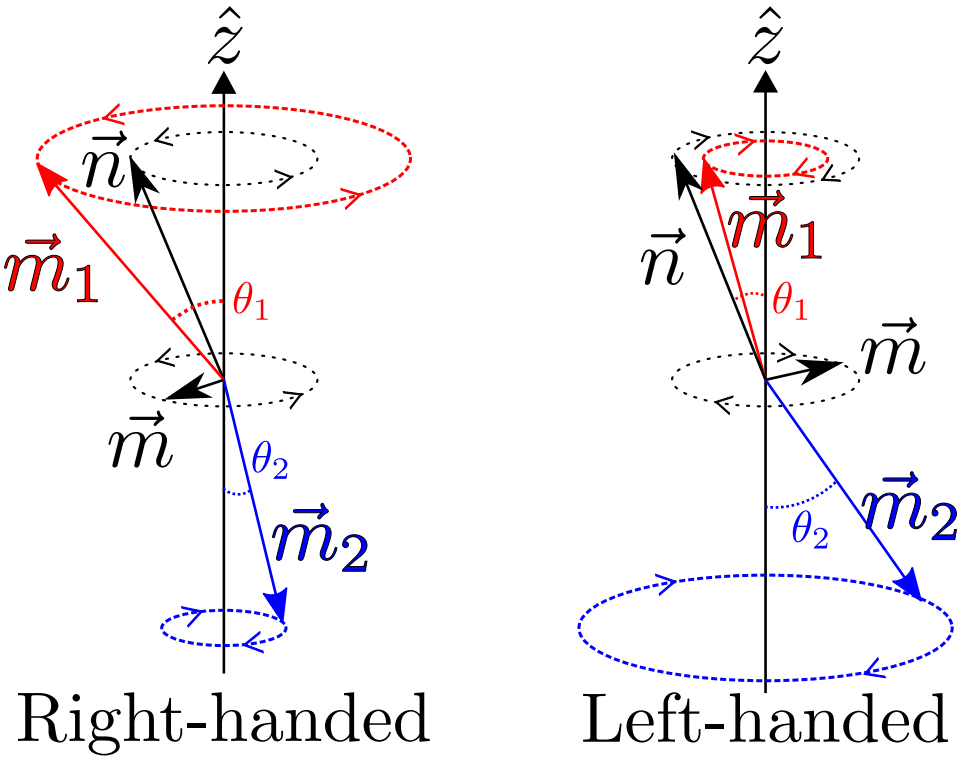

Figure 1.3: RH/LH circularly polarized precessional modes of the order parameters **n** and **m**. $\mathbf{m}_1$ and $\mathbf{m}_2$ can be any magnetic moment, most commonly a classical spin **S** confined to a lattice. The figure is adapted from [93].

tated if we alter the two modes by opposite phase shifts, allowing for a magnonic analogue of *Faraday-rotation* [14]. This mechanism is proposed for a possible realization of a *SW field effect transistor* [113], where the polarization direction is used to encode a bit of information. However, to achieve this, one needs to lift the degeneracy of the SW-modes. We will return to this issue in sec. 1.4.

1.3 Magnonics and magnonic crystals

Magnonics considers itself with how the wave-like magnons behave in magnetic materials, which includes excitation, detection and dynamics [73]. The field is motivated by the possibility of harnessing the wave-like characteristics of SWs introduced in section 1.2. Devices based on magnonics has many possible advantages over traditional electronics, e.g. easier manipulation by EM-fields and faster dynamics, resulting in higher read/write-speeds. SWs also have characteristic frequencies several orders of magnitude higher than in EM-waves, making them more suited for miniaturization [133].

An integral part of magnonics is the study of artificial magnetic systems, where some parameter of the system is periodic in space or time. These systems are often dubbed *magnonic crystals* (MCs) due to this periodicity-property, and serves as a magnetic analogue to *photonic* [49] and *phononic* [67] crystals. Research on these *magnetic superlattices* started with Elachi in the mid 70s [15], and has since then become the primary magnonic system of study which exhibits a *band gap*. These gaps occur due to Bragg-scattering at the potential barriers represented by a change in the modulated parameter, analogous to the Bragg-scattering on families of crystal planes in ordinary crystals [24, 45]. The most common type of magnonic crystal is a slab or thin film-system, where the periodicity is grown by layering alternating magnetic materials in one direction, and the width and thickness of the material is very small compared to its length. This *waveguide* is a 1D MC, since the SWs can essentially only propagate in a single direction.

The creation of MCs can be realized by several different procedures. As mentioned, a common procedure is to layer varying stripes or regions of alternating width or magnetic material [69]. A proposal which has been realized experimentally is modulation of a magnetic field [61] by the layering of current-carrying wires on top of a magnetic thin film, where the current is reversed in consecutive wires. *Chiral magnonic crystals*, where one modulates a property which induces antisymmetric interactions which breaks the symmetry of SWs propagating in different directions, has been proposed by consecutive layering of heavy-metal wires on a FM thin film [132], which may be possible by etching [136]. Other methods of creation includes laser-induced heating [110] or a material sputtering approach [81, 96]. Among many proposals and realizations of MCs, one can imagine a more exotic form of modulation made possible by the technological advancement in the creation of nanomaterials: the possibility of making the geometry of the system itself periodic, or indeed any shape [101]. SWs in such deformed nanostructures has not yet been studied, and is currently a open problem.

On the topic of low energy SW-excitations in AFM materials, the procedure and creation of reliable magnonic crystals necessitates the use of AFM insulators. There are many materials of this type, with some examples of such materials being NiO [44], FeF_2 and MnF_2.

1.4 The Dzyaloshinskii-Moriya interaction

The *Dzyaloshinskii-Moriya-interaction* (DMI) is a antisymmetric contribution to the exchange energy made possible by the lack of inversion symmetry in spin systems [10, 11]. The interaction is an example of a *superexchange mechanism*. This mechanism, first proposed by Kramers [2] was generalized by Anderson [5], who in his work used the example of the fcc-structured manganese oxide (MnO). In MnO, the strongly coupled Mn^{++}-ions are separated by non-magnetic O^{--}-ions. However, the (then) reported Néel-temperature of MnO, $T_N = 122$K, implied that the exchange between the Mn^{++}-ions was still present, and with a magnitude of about a tenth of ordinary exchange magnitudes. This relatively strong interaction

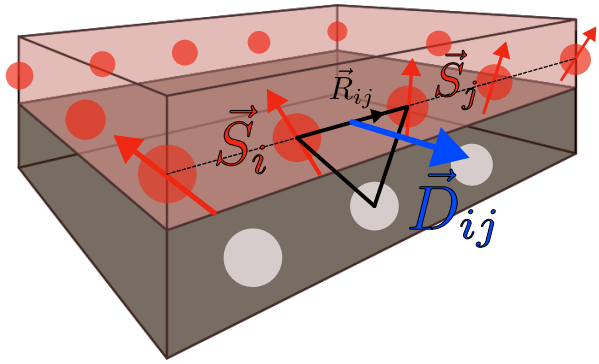

Figure 1.4: Visualization of the superexchange mechanism in the interfacial Dzyaloshinskii-Moriya interaction. The top layer is a thin FM/AFM-layer, and the bottom layer is a material with strong SOC, typically a heavy metal like Pt or Bi. The interaction favours relative canting of the spins.

prompted Anderson to suggest superexchange through a ligand ion as the cause. Dzyaloshinskii posed superexchange when he proposed magnetic dipole interactions and relativistic interactions between electron spins and the crystal lattice as an explanation for the weak ferromagnetic behaviour in α-Fe_2O_3-crystals [10]. Moriya later showed [11] that the microscopic origin of the effect was *spin-orbit coupling* (SOC), which he derived in 2^{nd}-order perturbation theory in the superexchange formalism developed by Anderson. The theory was later extended to noncentrosymmetric magnetic materials [20], and to magnetic multilayers, i.e. DMI-interaction due to inversion symmetry breaking at interfaces [31].

DMI favours canting of neighbouring magnetic moments, see fig. 1.4 , and makes a deviation from the uniform collinearity of FMs/AFMs energetically favourable. The interaction is thus a source of weak ferromagnetism in antiferromagnetic materials. DMI occurs in one of two forms: *bulk* or *interfacial* (IDMI). Bulk DMI appears as the name suggests in the bulk of a magnetic material lacking inversion symmetry. Interfacial DMI, which we will consider in this thesis, occurs at the interface of noncentrosymmetric systems; magnons are scattered due to the lack of inversion symmetry in the material [87]. Coupled spin systems that lack inversion symmetry can host IDMI in the presence of strong SOC, often supplied by a layer of a heavy metal like Pt or Ir. Large interfacial DMI of the order of the exchange interaction, and resulting spin textures, were first observed in such thin-film IDMI systems: spin spirals in Mn on W [50] and skyrmions in Fe on Pd [80].

DMI in AFMs has interesting consequences for the two degenerate SW-modes present in the system [113]. The degeneracy of the modes is protected by time-reversal symmetry $\mathcal{T}$ and sublattice exchange (inversion symmetry or parity symmetry) $\mathcal{I}$ of the FM-lattices that make up the AFM. Thus, to separate and control

the modes, we need to break either or both of these symmetries. A in plane magnetic field can be applied to break the former symmetry, while the DMI can be utilized to break the latter, since DMI reverses sign under exchange of the two magnetic sublattices, leading to phase shifts of different signs for the two modes. This gives us control mechanisms that allow us to separate and manipulate the modes, and even rotate the polarization direction of the order parameter oscillations as noted in the last section [113]. As a remark, SWs subject to DMI is very similar to electrons subject to the *Rashba interaction* in bulk crystals and low-dimensional systems [99]: spin bands are subject to a momentum dependent splitting by the combination of crystal/potential inversion symmetry breaking and SOC resulting from the interaction between the spin and a magnetic field, which is present in the frame of reference of the electron due to its motion in the electric potential of the crystal. Similarly, in AFMs subject to DMI, the degenerate SW-modes, analogous to the spin-degree of freedom of the electron, are split due to the chiral DMI interaction, which plays the role as a effective magnetic field acting on the precessional motion of the magnetic moments.

The analogue between encoding information in electron spins and AFM spin wave modes can be made explicit by mapping the SW state to the *Bloch sphere* [113]. In summary, AFM-SWs constitute a system of two states which can store information as a superposition of precessional modes of magnetic moments. In many regards, it can be seen as a classical analogue of the quantum bit. One might speculate that polarization of the AFM precessional modes might even be easier to manipulate than a electron-based quantum bit, but until this type of setup has been verified experimentally one cannot draw conclusions regarding its practicality.

The theoretical interest in DMI is due to a multitude of possible technological applications. The interaction is perhaps most notably able to stabilize non-collinear magnetic structures and spin textures in magnetic materials, such as skyrmions in FMs [66] and AFMs [119], and magnetic vortices [30], where the former has attracted considerable interest in recent years due to its potential usage in data storage, e.g. in the form of *"racetrack"-memory* [98]. DMI can give rise to and control FM [111] and AFM [130] domain walls, a proponent in controlling and moving magentic textures. The role of DMI in the separation of degenerate AFM-SW-modes have already been commented on. The *magnon Hall effect*, a magnonic analogue to the *Hall effect* [39], involves propagating magnons being deflected by a vector potential, which can take the form of e.g. IDMI. This is a possible method of controlling the direction of magnonic currents, and has been observed experimentally [75].

DMI-based magnonic crystals have been proposed as a fundamental building block in one-way SW-filters and circulators by utilizing the strong nonreciprocivity, see fig. 1.5, of SWs [97]. An example of a FM-type of bi-component MC waveguide can be realized by the alternate layering of materials, e.g. Co and permalloy (Py) [97]. Spatially modulated DMI can be achieved by means of patterning heavy metal-wires on top of thin magnetic films [132]. In addition to giving rise to magnonic bandgaps due to spatial modulation of a system parameter,

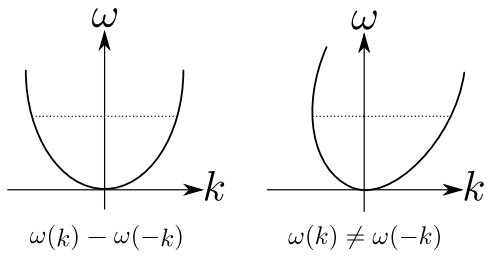

Figure 1.5: A sketch illustrating dispersion nonreciprocity. Particles of the same energy travelling in opposite directions have different energies. One of the defining features of SWs are their strong nonreciprocity. Nonreciprocity can be induced e.g. by antisymmetric interactions such as DMI or a external electric field.

the nonreciprocity effect of the DMI breaks the symmetry between SWs travelling in different directions. As a result, the bandgaps do not occur at the the edges of the Brillouin zone (BZ), but is shifted in k-space. Other peculiar effects include the relative shifting of frequency bands of different Bragg-planes, and direction-dependent band gaps for the low-frequency excitations.

1.5 Proposal and structure of thesis

In this thesis, we present spatially modulated IDMI in collinear easy-axis AFMs as a possible means of creating a spin wave polarizer, a bandpass filter for the two degenerate SW-modes present in the system for $T << T_N$. This might be a possible component in future technological magnon-based applications; the mechanism can be used to create spin polarized-currents by propagating AFM-SWs through a DMI-modulated waveguide, with the frequency bandwidth being adjustable by the excitation direction, the lattice parameter of the effective DMI-potential and the strength of the modulation. We will also show features of the filter which allow us to make a one-way waveguide, which confines SW-propagation to a single direction. To achieve this, the $\mathcal{TI}$-protected degeneracy of the modes will be lifted by the combination of a in-plane magnetic field and IDMI. Due to the periodic modulation of the DMI strength, bandgaps occur in the spectrum, with additional effects characteristic to periodic IDMI mentioned in this chapter. The magnetic field will lift the degeneracy of the gapped precessional modes, allowing for selective propagation of SW-modes in the system. We will show this by means of a effective model for the low-frequency precessional modes, valid for long SW-wavelength and at sufficiently low temperatures.

Chapter 2 introduces the theoretical framework in the thesis, with focus on the intermediate important results and explanations. A general introduction to the AFM lattice and the continuum model will be given, with a subsequent presentation of the interactions in the micromagnetic model of the system: symmetric exchange, easy-axis anisotropy, the Zeeman-effect and the interfacial Dzyaloshinskii-Moriya-interaction. Their form in the continuum limit will also

be stated. We will outline the procedure of obtaining the classical dynamics of the system, and state the most important steps. At the end of the chapter, we will present the effective continuum model for the AFM-SWs.

In chapter 3, we start by showcasing the general features of SWs. We will then model a 1D MC as a Krönig-Penney-type potential, and a analytical solution for the SW-dispersion will be obtained. In chapter 4, a 2D MC will be modelled as a continuous cosine-potential. We will introduce and discuss the method of calculation, before presenting the SW dispersion-relation through magnonic band-structure diagrams and highlighting their features. Lastly, the results of chapter 3 and 4 will be summarized in chapter 5. We will discuss the findings, how to iterate and improve upon them, and make an attempt at connecting them to the larger context of magnonics.

CHAPTER 2

AFM SPIN SYSTEMS AND SEMI-CLASSICAL SPIN WAVE THEORY

In this chapter, we will present the basic components of describing SWs in a AFM insulator in the continuum limit by means of an effective SW-equation. Our starting point will be to introduce the AFM system, including the micromagnetic description of interacting spins confined to a lattice. The thermodynamic free energy of the antiferromagnet $\mathcal{F}_{AFM}$, as derived in appendix A, will be introduced, and the semi-classical equations of motion will be presented. After introducing the appropriate order parameters, we obtain the dynamics of the SWs by the *principle of least action* [41].

In appendix A, the free energy density $\mathcal{F}_{AFM}$ is obtained from the micromagnetic Hamiltonian. Taking the continuum limit of the discrete lattice allows for the identification of the physical parameters of the theory. In the derivation, two anisotropic contributions to $\mathcal{F}_{AFM}$ will appear. These will be commented on, but discarded for the rest of the thesis due to them dropping out of the semi-classical equations of motion.

We are interested in the low-frequency, $T << T_N$-regime, implying slowly precessing and ordered spins. This is the regime of validity of the many-body spin-wave theory. In the end, we present the effective SW-equation, where the "exact" Hamiltonian $\mathcal{H}$ is replaced by an effective one, $\mathcal{H}^{eff}$. The *renormalization* procedure results in a Hamiltonian which act on a lower energy subspace [32, 35].

As mentioned in the last chapter, a continuum description of the magnetization dynamics is well suited in the sub-micrometer regime in which excitations in the form of spin waves are relevant. In describing the dynamics of the AFM in terms of a set of appropriate order parameters, one takes the collective excitations of the system to be the precessional modes of a semi-classical description, very similar to e.g. *Larmor precession* of electrons in homogeneous magnetic fields [68]. This "spinning top"-model, where the order parameters are described as classical vectors in 3D-space subject to a torque induced by a effective field (analogous to the magnetic field in Larmor precession), can be fairly accurate in systems with large number of particles and long-wavelength excitations [33].

2.1 The torque equation

The time evolution of some general field $\mathbf{M}$, which could be any classical field, which we without loss of generality take to be magnetization, in the absence

of dissipation or external currents can be written down as a torque-equation [21]

$$\begin{aligned}\frac{d\mathbf{M}(\mathbf{r},t)}{dt} &= \mathbf{M}(\mathbf{r},t)\times\mathbf{H}_{eff}[\mathbf{M}(\mathbf{r},t)] \\ &= -\gamma\mathbf{M}(\mathbf{r},t)\times\frac{\delta E_{mm}[\mathbf{M}]}{\delta\mathbf{M}}\end{aligned} \tag{2.1}$$

where γ is some proportionality constant which relates the precessional frequency to the field strength, often called the *gyromagnetic ratio*. This equation preserves $|\mathbf{M}|$, is invariant under a global rotation of all magnetic moments in the system, with higher order time derivatives assumed to be negligible. These are necessary conditions in our approximation, which will be shown throughout the chapter. $\mathbf{H}_{eff}[\mathbf{M}]$ is an *effective field*, which in general can contain a multitude of effects like crystal anisotropy, external magnetic field, SOC, demagnetization effects etc. $\mathbf{H}_{eff}[\mathbf{M}]$ is determined by the minimalization of the *antiferromagnetic free energy* of the system [21]. We seek a energy minimum w.r.t. constant volume, magnetic field and temperature, which explains the choice of free energy as thermodynamic potential. At low T and long wavelengths, the dissipation of energy as $\mathbf{M}$ precesses is taken to be negligible, and is set to zero. In this thesis, the cases of dissipation and damping will not be considered. In general, $\mathbf{H}_{eff}[\mathbf{M}]$ is defined as the functional derivative of some *micromagnetic energy functional* E_{mm}. As mentioned, we take this functional to be the AFM free energy density: $\mathbf{H}_{eff} \equiv \delta E_{mm}[\mathbf{M}]/\delta\mathbf{M} = \delta\mathcal{F}_{AFM}[\mathbf{M}]/\delta\mathbf{M}$
Equation 2.1 can be derived in the context of quantum mechanics as the time evolution of the expectation value of the spin operator $\hat{S}_i$.

$$\frac{d}{dt}\langle\hat{S}_i\rangle = \frac{1}{i\hbar}\langle[\hat{S}_i,\hat{H}]\rangle + \left\langle\frac{\partial\hat{S}_i}{\partial t}\right\rangle \tag{2.2}$$

where $\hat{H}$ is a Hamiltonian operator. The macroscopic magnetization is defined as the expectation value of the spins. We set $i = z$ to find the expectation value of the time-independent (dissipationless) spin operator in the z-direction, and insert the *Zeeman interaction* $\hat{H} = -S_iH_i$, with H in units of energy, to investigate the dynamics of the spin in a magnetic field.

$$\frac{d}{dt}\langle\hat{S}_z\rangle = -\frac{1}{i\hbar}\langle[S_z, S_iH_i]\rangle \tag{2.3}$$

$$= \frac{1}{\hbar}\langle(S_xH_y - S_yH_x)\rangle \tag{2.4}$$

$$= \frac{1}{\hbar}(\langle\mathbf{S}\rangle\times\mathbf{H})_z \tag{2.5}$$

where we in the 2$^{\text{nd}}$ line used the angular momentum commutation relation $[S_i, S_j] = i\hbar\epsilon_{ijk}S_k$, with ϵ_{ijk} being the *Levi-Civita*-tensor. We define the magnetization $\mathbf{M}$ as the expectation value of the spins $\langle\mathbf{S}\rangle$. The magnetic field $\mathbf{H}$ corresponds to $\mathbf{H}_{eff}$ in eq. 2.1.

In sec. 2.3, we will introduce the continuum description of the AFM lattice. Two continuous fields $\mathbf{l}$ and $\mathbf{m}$ will be introduced in the process. $\mathcal{F}_{AFM}$ is a functional of these two fields: $\mathcal{F}_{AFM} = [\mathbf{l}(\mathbf{r},t), \mathbf{m}(\mathbf{r},t)]$.

We note that the total energy is the integral over the energy density

$$F_{AFM}[\mathbf{l}(\mathbf{r},t), \mathbf{n}(\mathbf{r},t)] \;=\; \int d\mathbf{r}\; \mathcal{F}[\mathbf{l}(\mathbf{r},t), \mathbf{m}(\mathbf{r},t)] \tag{2.6}$$

We will often refer to the free energy density as just "free energy". The energy dissipation of the fields is given by the derivative of F with respect to time, with a additional minus sign implying dissipation. A infinitesimal variation of the free energy with respect to the fields $\mathbf{l}$ and $\mathbf{m}$ is expressed as

$$\delta F[\mathbf{l}(\mathbf{r},t), \mathbf{m}(\mathbf{r},t)] \;=\; -\int d\mathbf{r}\; \{\mathbf{f}_\mathbf{l} \cdot \delta\mathbf{l} + \mathbf{f}_\mathbf{m} \cdot \delta\mathbf{m}\} \tag{2.7}$$

The quantities $\mathbf{f}$ are the effective fields introduced in the torque equation 2.1. They represent the combined effects of the physical interactions on the precession of the magnetic moments $\mathbf{l}$ and $\mathbf{m}$. Without dissipation, the fields are constant w.r.t. time, and is zero in equilibrium. The condition of no dissipation takes the form

$$-\frac{\partial F}{\partial t} \;=\; \int d\mathbf{r}\; \left\{\mathbf{f}_\mathbf{l} \cdot \frac{\partial \mathbf{l}}{\partial t} + \mathbf{f}_\mathbf{m} \cdot \frac{\partial \mathbf{m}}{\partial t}\right\} \;=\; 0 \tag{2.8}$$

The effects of dissipation in FMs and AFMs are normally included by adding a phenomenological *Gilbert damping*-term [56] to eq. 2.1. Formally, the energy of the AFM is conserved in eq. 2.1 for some minimal configuration of the field (i.e. magnetization $\mathbf{m}$ or staggered magnetization $\mathbf{l}$), but this means that for a given initial configuration, the low-energy equilibrium state can not be reached dynamically by the system on its own. However, the Gilbert damping allows for this by including a term which reduces the precessional amplitude with time w.r.t. the equilibrium direction of the field. Adding the damping term to eq. 2.1, we have

$$\frac{d\mathbf{M}(\mathbf{r},t)}{dt} \;= = -\gamma \mathbf{M}(\mathbf{r},t) \times \frac{\delta E_{mm}[\mathbf{M}]}{\delta \mathbf{M}} - \alpha_G \mathbf{M}(\mathbf{r},t) \times \frac{\partial \mathbf{M}(\mathbf{r},t)}{\partial t} \tag{2.9}$$

where the damping is expressed through the term $\propto \alpha_G$. The term makes the magnetization amplitude decay exponentially, resulting in a spiralling motion towards the equilibrium configuration of the field $\mathbf{M}$. The constant $\alpha_G > 0$ determines the damping, and is typically in the range $\alpha_G \sim .01 - .1$. Equation 2.9 is called the *Landau-Lifshitz-Gilbert-equation* (LLG). It describes the low-frequency precessional motion of the magnetic moments subject to external interactions expressed through the effective field $\mathbf{H}_{eff} = -\delta E_{mm}[\mathbf{M}]/\delta\mathbf{M}$. As mentioned, the Gilbert-damping will not be treated, and is subsequently neglected. We note that this is consistent with assuming no dissipation in the system, which implies excitations with infinite lifetime if we neglect relativistic interactions. At the quantum

level, adding dissipation means adding interactions between magnons and other quasi-particles such as phonons, resulting in a finite lifetime for the quasiparticles [21].

2.2 The AFM lattice and ground states

Consider a 2D lattice of localized spins $\mathbf{S}_{ij}$, represented by vectors in 3D space of equal mangitude. The lattice can be divided into two sublattices α, β, where neighbouring spins are of the opposite type, as in fig. 1.1 or 2.1. A general spin $\mathbf{S}_{ij}$ of either type α, β is labeled by indices i, j, denoting its position on the lattice. We note that for a 3D structure, the formalism is similar, with $i, j \to i, j, k$. The total lattice will be referred to as the *bipartite lattice* [35]. A set of lattice vectors $\{\mathbf{a}_q\}$ generates the entire lattice by translation of the *antiferromagnetic unit cell*, shown in red in fig. 2.1.

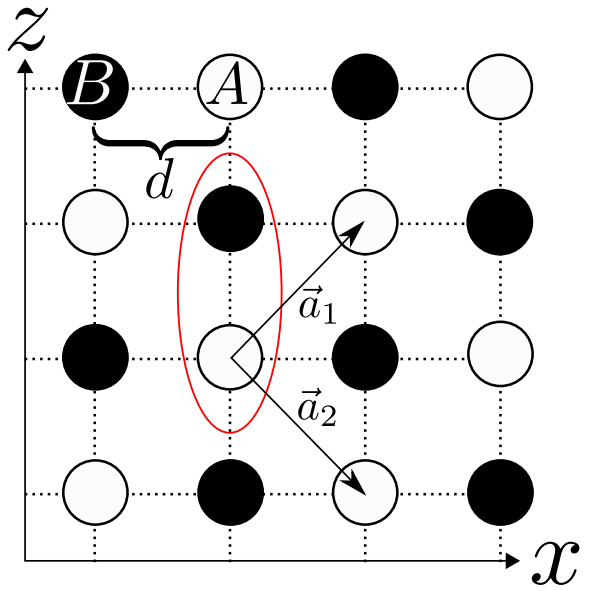

Figure 2.1: Sketch of the microscopic bipartite lattice, where sites $A \in \alpha$ and $B \in \beta$ belong to different sublattices. The AFM unit cell is marked in red, with our choice of lattice vectors. The spacing between the sites is d, and the unit cell width $\Delta = \sqrt{2}d$.

The magnetization of the two sublattices are denoted $\{\mathbf{M}_\alpha, \mathbf{M}_\beta\}$. An important point is that below T_N, the magnitude of the magnetization is assumed to be conserved, as we noted was a necessary condition in sec. 2.1. We can then write $\mathbf{M}_{\alpha,\beta} = M^S_{\alpha,\beta}\mathbf{m}(\mathbf{r}, t)_{\alpha,\beta}$, where $\{M^S_\alpha, M^S_\beta\}$ denotes the *saturation magnetization* of the sublattices, the magnetization when the spins are maximally ordered. $\mathbf{m}$ can thus be viewed as the direction of the magnetization. In sec. 2.3, we will define the order parameter fields $\{\mathbf{l}, \mathbf{m}\}$ in terms of the spins $\{\mathbf{S}^\alpha_{ij}, \mathbf{S}^\beta_{ij}\}$.

The uniform *Néel state* [35] is the state where spins on neighbouring lattice sites are aligned oppositely w.r.t. its neighbours, see fig. 1.1 or 2.1.

$$|\Psi^{\text{Néel}}\rangle = \prod_{i\in\alpha} |S_i\rangle \prod_{j\in\beta} |-S_j\rangle \tag{2.10}$$

If the equilibrium direction of magnetization is taken to be e.g. $\hat{\mathbf{z}}$, then all spins are aligned along $\pm\hat{\mathbf{z}}$. This configuration corresponds to Ising spins on a 2D lattice, and can also be called the *Ising configuration* [35].

However, the Néel state is *not* the ground state, nor even a eigenstate, of the Heisenberg Hamiltonian, which we will come back to in sec. 2.4. Restrictions on the ground state can be set, and it turns out that the true ground state $|\Psi^0\rangle$ of the QM AFM is the state that has the minimal possible total spin S_{tot} [13], which for equal size sublattices $\{\alpha, \beta\}$ is at $S_{tot} = 0$. It can thus thus be shown that $|\Psi^0\rangle$ is a singlet state of total spin 0. The true ground state is then

$$|\Psi^0\rangle = \frac{|\Psi^{\text{Néel}}\rangle - |-\Psi^{\text{Néel}}\rangle}{\sqrt{2}} = \frac{\prod_{i\in\alpha}|S_i\rangle\prod_{j\in\beta}|-S_j\rangle - \prod_{i\in\alpha}|-S_i\rangle\prod_{j\in\beta}|S_j\rangle}{\sqrt{2}} \tag{2.11}$$

which can be shown to have $S_{tot} = 0$. However, the Néel state *is* the *classical* ground state of the AFM system. We will take the continuum limit of the micromagnetic Heisenberg Hamiltonian, which will result in a classical theory. Thus, we can take the ground state equilibrium configuration to be the Néel-state.

Motivated by the advantages of research into IDMI over bulk DMI, being much easier to study and manufacture and able to host strong antisymmetric interaction, we will consider a thin-film geometry for the insulating AFM in this thesis. As a comment on low-dimensional-systems, an apparent problem with the assumption of ordered spins for $T << T_N$, and not $T = 0$, for a 2D lattice comes from Mermin and Wagner's theorem [35]. It states that there cannot be spontaneously broken symmetry at $T > 0$ in one and two dimensions. Thus, the spin wave approach we seek to apply would not be valid, since we must have ordered spins and O(3)-symmetry breaking for SW-theory to be applicable. Thermal fluctuations ruin the ordered ground state for infinitessimally small temperatures in 1- and 2D. The problem is resolved in the (semi-)classical limit of the Heisenberg antiferromagnet: if the classical Hamiltonian is short ranged, then so are the correlations. Thus, in the classical limit we can expect at least short range order of the classical spins [35]. However, we will bypass this problem by assuming that our system is three-dimensional, but that the SW-propagation is restricted to a single plane. For this approximation to be feasible, we must assume that in this limit, the in-plane SW-momenta $\mathbf{k}_\parallel$ parallel to the thin film plane satisfies the condition $\mathbf{k}_\parallel c \ll 1$ [58], where c is the thickness of the film.

The validity and correlations of the continuum limit of the Heisenberg Hamiltonian is a whole nother topic in itself, which we will not explore further in this thesis.

2.3 The continuum description of a AFM lattice

We now introduce the necessary machinery for constructing a continuum model of the AFM-system, starting by defining the classical fields **n** and **m**. Consider the two identical 2D lattices α and β from the previous section, with magnetization of the same magnitudes M_α, M_β pointing in opposite directions on neighbouring lattice sites as described by the Néel-ground state. The magnetization of the two sublattices is taken to be due to the aforementioned localized spins $\{\mathbf{S}_{ij}^{\alpha}, \mathbf{S}_{ij}^{\beta}\}$ on the bipartite lattice, where i, j denotes position on the lattice. We now define two order parameter fields

$$\mathbf{m}_{ij} = \frac{(\mathbf{S}_{ij}^{\alpha} + \mathbf{S}_{ij}^{\beta})}{2S} \tag{2.12}$$

$$\mathbf{l}_{ij} = \frac{(\mathbf{S}_{ij}^{\alpha} - \mathbf{S}_{ij}^{\beta})}{2S} \tag{2.13}$$

$\{\mathbf{m}, \mathbf{l}\}$ are called the *magnetization* and *staggered magnetization* respectively. The interpretation of $\mathbf{m}_{ij}$ is that it is the direction of the total magnetization of the spins in one unit cell of the bipartite lattice, or in other words, the relative canting of the magnetic sublattices in the AFM, see fig. 1.3. Since the magnetization from the two sublattices $\{\alpha, \beta\}$ compensate each other perfectly in a equilibrium AFM, we expect **m** to be very small, which we will make use of in later approximations. $\mathbf{l}_{ij}$ is the difference in the magnetization direction of the two spins in the unit cell. Since these contributions are equal in equilibrium, but with different signs, we expect $\mathbf{l}_{ij}$ to be much larger than $\mathbf{m}_{ij}$. Note that we have $\mathbf{m}_{ij}^2 + \mathbf{l}_{ij}^2 = 1$. These order parameters are more convenient to work with than individual spins.

Typically, the exchange interaction between spins J, treated in sec. 2.4, represents the dominating energy scale in the magnetic system, $E_J \gg E_K, E_{DMI}, E_H$. This condition is in a sense already included in the last section, in which the phenomenological torque equation 2.1 for a field **M** was written down with the assumption of slowly varying dynamics. We call this simplification the *exchange approximation* [21]. In addition, we will invoke the *adiabatic condition* that the fields are varying slowly in time. With these conditions in place, we have that

$$|\mathbf{l}|^2 \gg |\mathbf{m}|^2 \tag{2.14}$$

Thus, we can safely drop terms of higher order than $|\mathbf{m}|^2$.

In the regime described by the above conditions, it is convenient to define the *normalized staggered magnetization*

$$\mathbf{n}(\mathbf{r}, t) = \frac{\mathbf{l}(\mathbf{r}, t)}{|\mathbf{l}(\mathbf{r}, t)|} \tag{2.15}$$

We call this field the *Néel* field, even if it strictly speaking is a small abuse of terminology, see sec. 2.3.1. In the exchange approximation, we impose constraints on the **n**- and **m**-fields, setting $|\mathbf{n}| = 1$ and $\mathbf{n} \cdot \mathbf{m}$. These constraints enforce the

conditions that $\mathbf{m}$ is so much smaller than $\mathbf{n}$ that we take $\mathbf{n}$ to be a unit vector, or *unimodular*, and that $\mathbf{n}$ and $\mathbf{m}$ are perpendicular. Formally, these requirements need to be enforced at the level of the classical Lagrangian for the model to be valid. We will do this by the method of *Lagrange multipliers* [41] in app. B.

With the above constraints, we have effectively "suppressed" longitudinal degrees of freedom in the system, since $\mathbf{m}$ points in the "longitudinal" direction (in the SW-propagation plane) and is assumed very small compared to $\mathbf{n}$, and $\mathbf{n}$ is pointing (approximately) perpendicular to the propagation direction of SWs. We assume that $\mathbf{n}$ and $\mathbf{m}$ are able to describe the low-frequency dynamics of the system for $T << T_N$.

In the exchange approximation, $|\mathbf{n}|^2 \gg |\mathbf{m}|^2$, all expressions in the fields $\mathbf{n}$ and $\mathbf{m}$ must be invariant under a global rotation of the magnetic moments in the lattice. This is a reflection of the equivalence of the two magnetic moments constituting each unit cell of the bipartite AFM lattice. In other words, we should be able to exchange the two magnetic sublattices $\{\alpha, \beta\}$ and obtain the same physics. This requires invariance under the transformations $\mathbf{n}(\mathbf{r}, t) \to -\mathbf{n}(\mathbf{r}, t)$ and $\mathbf{m}(\mathbf{r}, t) \to \mathbf{m}(\mathbf{r}, t)$ under sublattice exchange [21].

Before introducing the contributions to the free energy in the upcoming sections, we note that the above symmetry requirements for the order parameters can be used to obtain $\mathcal{F}_{AFM}$ in a more direct manner. One can construct a energy density up to some power in the fields which satisfies the condition of invariance under global rotation of the magnetic moments of the lattice, and invariance under sublattice exchange. Mote details can be found in Landau & Lifshitz treatment of the subject in [21]. We note that in the reference, the field $\mathbf{n}$ is the transverse oscillations $\mathbf{n} \equiv \mathbf{n}_\perp$ from some equilibrium configuration $\mathbf{n}_0$. As noted in [118], this difference will yield a anisotropic dispersion relation, with additional magnetization buildup on the edges of the AFM.

2.3.1 Alternative formulation: Haldane's mapping

There is another way of defining the continuum fields used to describe the AFM. However, this approach carries with it some subtleties. We mention briefly this other formalism, called *Haldane's mapping* [35]. In this framework, each spin $\{\mathbf{S}_{ij}^{\alpha}, \mathbf{S}_{ij}^{\beta}\}$ is mapped onto two fields reflecting the "slow" and "fast" fluctuations of the spin-dynamics. Each spin of either type at site i is parametrized as

$$\Omega_i \;=\; \eta_i \mathbf{n}_i'(\mathbf{r}) \sqrt{1 - \left|\frac{\mathbf{L}_i(\mathbf{r})}{S}\right|^2} + \frac{\mathbf{L}_i(\mathbf{r})}{S}$$

where $\mathbf{n}_i'$ is the unimodular *Néel field* fulfilling $|\mathbf{n}_i'| = 1$, and $\mathbf{L}_i$ is the *canting field*, which satisfies the orthogonality condition $\mathbf{L}_i \cdot \mathbf{n}_i' = 0$. Each site previously had two degrees of freedom for describing a spin, the angles (θ, ϕ), which we now have replaced by four degrees of freedom, since the fields $\mathbf{n}'$ and $\mathbf{L}$ has three each, minus the two constraints. The last two degrees of freedom are eliminated by

reducing the number of Fourier components in the classical path integral measure [35].

The goal of the mapping is to separate the fluctuations at short wavelengths and keep the modes corresponding to long wavelengths. Even if the formalism seems equivalent to the continuum fields defined in sec. 2.3, there is a crucial difference [118]: **L** is not the total magnetization, but a dynamic magnetization arising from the time-variation of the field **n**'. AFMs can have a *intrinsic magnetization density* which varies as the gradient of the order parameter, which can happen in e.g. magnetic textures. This intrinsic magnetization arises in a parity-breaking term in the energy functional which does not appear with Haldane's mapping, but *does* appear in the definitions of the fields applied in this thesis. We will not treat this intrinsic magnetization further since magnetic textures are not the focus of this thesis, but it is noted that the above (seemingly minor) detail in formalism can have substantial consequences for the system.

2.4 Antiferromagnetic exchange

Consider a simple system of spins **S** close to the ground state, as we have done in previous sections. The spins can point in any direction in 3D space, and is endowed with some non-zero spin angular momentum $S \neq 0$. The spins are confined to a bipartite lattice as discussed earlier, where neighbouring spins are of opposite type. A spin of type $\mathbf{S}^\alpha$ only has neighbours of spin $\mathbf{S}^\beta$ and vice versa.

The *Heisenberg model* [21, 70] describes the spins confined to lattice sites as 3D vectors, and can be seen as a limit of the *Hubbard model* at half-filling when tunneling between sites is suppressed [35, 70]. The exchange interaction between two spins on a lattice take the form

$$\hat{\mathcal{H}}_{exch.} = \frac{1}{2}\sum_{ij} J_{ij}\mathbf{S}_i\mathbf{S}_j \tag{2.16}$$

where the summation extends over all lattice sites, where a single index i or j denotes the lattice site. The exchange parameter J_{ij} determines the strength and type of interaction, and is given by the overlap of the wave-functions of the electrons [68]. In the ferromagnetic case, $J_{ij} < 0$, while $J_{ij} > 0$ for antiferromagnets. The exchange coupling is a function of the distance between the sites, $J_{ij} = J(\mathbf{r}_i - \mathbf{r}_j)$. The factor 1/2 accounts for double counting of lattice sites in the sum. The exchange interaction is symmetric w.r.t. the lattice indices: $J_{ij} = J_{ji}$.

Due to its definition in terms of overlapping wavefunctions, the exchange interaction falls of as $\sim e^{-x}$ [68]. If we take the individual spins of the lattice to be far apart, effectively describing an *insulating system*, we can model the exchange interaction as a coupling between nearest neighbour-pairs, $\sum_{ij} = \sum_{<ij>}$, where $\langle\cdots\rangle$ denotes nearest neighbour summation. A further simplification comes from assuming the system to be *isotropic*, reducing the tensor J_{ij} to a constant J characterizing the pairwise interaction. For more complicated lattices, this tensorial

character must be included. For example, in α-$Cu_2V_2O_7$, the isotropic exchange interaction can be modeled by three AFM coupling parameters $J_1, J_2, J_3 < 0$ for different directions in the unit cell.

We can now explain why the Néel state is not the ground state (nor an eigenstate) of the QM Heisenberg Hamiltonian [134]. Writing the spin operators in eq. 2.16 in terms of ladder operators $S_j^{\pm} = S_j^x \pm iS_j^y$ [35, 115], and denoting the neighbouring sites as $i = j + \mathbf{r}_D$, where $\mathbf{r}_D$ is a 1/2/3D vector pointing to the nearest neighbour lattice site (we will take $\mathbf{r}_D$ to run over only half the sites to avoid double counting), we have

$$\hat{\mathcal{H}}_{exch.} = \frac{1}{2}\sum_{<ij>} J_{ij}\mathbf{S}_i\mathbf{S}_j \;=\; J\sum_{i,\mathbf{r}_D}\left(\frac{1}{2}(S_i^+S_{i+\mathbf{r}_D}^- + S_i^-S_{i+\mathbf{r}_D}^+) + S_i^zS_{i+\mathbf{r}_D}^z\right) \tag{2.17}$$

Acting with the above operator on the Néel state defined in eq. 2.10, the spin-flip terms, e.g. S^+S^-, connect $|\Psi^{\text{Néel}}\rangle$ to other ground states, returning a new state. Thus, $|\Psi^{\text{Néel}}\rangle$ cannot be a eigenstate nor a ground state of the QM AFM. Again, we bypass this problem in our classical model. We now choose to specialize to *square lattices* to keep the calculations and expressions simple. In the continuum limit, the free energy contribution of the exchange interaction on a square lattice in the exchange approximation takes the form (see app. A)

$$\mathcal{F}_{exch}^{AFM} \;=\; \frac{a}{2}\mathbf{m}^2 + \frac{A}{2}\left[\sum_i(\partial_i\mathbf{n})^2 + \frac{1}{2}\sum_{i\neq j}\partial_i\mathbf{n}\partial_j\mathbf{n}\right] + B\sum_i\mathbf{m}\partial_i\mathbf{n} \tag{2.18}$$

with N_n being the number of nearest neighbours, $\Delta = \sqrt{2}d$ is the width of the AFM unit cell, the *exchange energy* $a = 4N_nJS^2$, and *exchange stiffness* $A = N_n\Delta^2JS^2/2$ and $B = N_n\Delta JS^2$.

The parity-breaking terms $\propto \{\partial_i\mathbf{n}\partial_j\mathbf{n}, \mathbf{m}\partial_i\mathbf{n}\}$ will be discussed in sec. 2.5.1. Neglecting these terms, as we will do, implies zero intrinsic magnetization in the AFM at equilibrium. This is the case even if the ground state is in the form of a magnetic texture [118].

2.4.1 Magnetic anisotropy

Generally, anisotropy introduces some directional preference of the order parameter. The parameters characterizing these preferred directions are thus tensorial. More specifically, for magnetic materials, we consider *crystalline magnetic anisotropy*: the alignment of the magnetization along some energetically favourable direction in the crystal, determined by the crystal symmetry. In a macroscopic theory, the effect is captured as a *magnetic anisotropy energy density* K. The magnetocrystalline anisotropy determines the equilibrium direction of the spontaneous magnetization [21]. At the microscopic level, the magnetic anisotropy arise due to relativistic interactions between the magnetization and the

magnetic field, i.e. SOC. The electrons experience a magnetic field in their frame of reference due to the electric field of the lattice. This electric field (experienced as a magnetic field for the electrons) constitutes the magnetic anisotropy, which the electrons align their spins along to reduce their energy. As a consequence, the magnetization gains a preferred equilibrium direction.

Due to the weakness of these interactions relative to the exchange coupling, it is often treated through perturbation theory. In general, the strength of the SOC increases with atomic number due to stronger nuclear fields [24], and as a result, so too does the anisotropy. One therefore can expect relatively large anisotropies for sufficiently large atomic numbers, i.e. TM/Fe/MgO(001) [126], which is favourable in many technological applications

The anisotropy-part of the spin Hamiltonian along a specified direction in the crystal $\hat{\mathbf{r}}$, which we assume can be expressed as the temperature-independent (which in general is not the case) energy density K, takes the form

$$\hat{\mathcal{H}}_{anis.} = -K \sum_i (\mathbf{S}_i \cdot \hat{\mathbf{r}})^2 \tag{2.19}$$

where the sum goes over all lattice-sites of the bipartite lattice. If $K > 0$, alignment along $\hat{\mathbf{r}}$ is energetically favourable, and the axis is a so-called *easy axis*. If $K < 0$, the axis is a *hard axis*, and the equilibrium magnetization will lie in a plane $\perp \hat{\mathbf{r}}$.

With the z-axis as a easy axis, the free energy contribution from magnetocrystalline anisotropy takes the form

$$\mathcal{F}_{anis.}^{AFM} = -K_z \Big[(\mathbf{m} \cdot \hat{\mathbf{z}})^2 + (\mathbf{n} \cdot \hat{\mathbf{z}})^2 \Big] \tag{2.20}$$

with $K_z = 2KS^2$.

2.4.2 Zeeman coupling

The *Zeeman interaction* describes the interaction between magnetic moments and magnetic fields. The magnetic moment can arise from both orbital- and spin-angular momentum, where we will neglect the former. One can consider the effect of a external magnetic field by addition of the operator

$$\hat{\mathcal{H}}_{ext} = -\rho\gamma \sum_i \mathbf{S_i} \cdot \mathbf{H}$$

to the Hamiltonian, where the sum goes over all lattice sites. We will eventually take the magnetic field to be constant, and point along $\hat{z}$. The Zeeman coupling will then take the form

$$\hat{\mathcal{H}}_{ext} = -\rho H \gamma \sum_i S_{i,z}$$

where $S_{i,z}$ is the spin projection of the i^{th} spin along the $\hat{z}$-axis. γ is the *gyromagnetic ratio*, and the factor ρ is a angular momentum magnitude with units $[\rho] = J \cdot s$.

We will take it to be the magnitude of the angular momentum in each AFM unit cell, $\rho = 2\hbar S$.

The Zeeman-interaction aligns the magnetic moments along the magnetic field, as is evident from the dot product between the magnetic field and the spin. In the continuum limit, the free energy density contribution amounts to a substitution of the spin sum with the magnetization. In general, neglecting for a moment that we take $\mathbf{H} \propto \hat{z}$ later in the thesis, we thus have

$$\mathcal{F}_{ext}^{AFM} = -\rho\gamma(\mathbf{m} \cdot \mathbf{H})$$

2.4.3 The Dzyaloshinskii-Moriya interaction

The *Dzyaloshinskii-Moriya-interaction* induces canting of the collinear spins in the equilibrium FM/AFM. It is a chiral interaction, increasing the spin energy depending on whether the spins rotate clockwise or anticlockwise relative to the direction of the DMI, dictated by the symmetry of the material. It is a source of weak ferromagnetism in AFMs, as it causes a deviation in the sponataneous magnetization due to the spin canting, emerging from the antisymmetric exchange interaction between neighbouring spins. The nearest neighbour DMI-interaction takes the form

$$\hat{\mathcal{H}}_{DMI} = \sum_{<ij>} \mathbf{D}_{ij} \cdot (\mathbf{S}_i \times \mathbf{S}_j) \tag{2.21}$$

where the indices $\{i, j\}$ dente the lattice sites. The interaction is characterized by the vector $\mathbf{D}_{ij}$, whose strength and direction is determined by the symmetries of the magnetic material. The chiral nature of the interaction is seen from the cross-product, which yields a minus-sign under interchange of spins. The DMI, typically at least a order of magnitude smaller than the exchange interaction, with some exceptions [75], can in the presence of out-of-plane anisotropy give rise to magnetic domains separated by *Néel-type domain walls*, where the spins rotate in-plane with the domain wall determined by the $\mathbf{D}$-vector. For completeness, we mention the *Bloch-type* domain wall, where the magnetization rotates out-of-plane with the domain wall.

Néel-type domain walls is the most common in thin film arrangements. The DMI can also give rise to non-collinear ground states like magnetic skyrmions and vortices [30, 119], as noted in chap. 1. Skyrmions in particular have been stabilized by IDMI in magnetic multilayers at room temperature [116].

In app. A, we derive the form of the free energy contribution of the IDMI $\mathcal{F}_{DMI}^{AFM}$ in terms of *Lifshitz-invariants* [30, 43, 86], combinations of linear derivatives of the order parameter which is determined by the crystal symmetry of the material. In this section, we will apply the more direct approach, see sup. mat. of [113].

We consider IDMI in a thin film with broken inversion/mirror symmetry along the y-axis, ignoring any DMI-contribution from the bulk. In such thin-film systems, the DMI-vector is taken to be completely in-plane with the xz-plane.

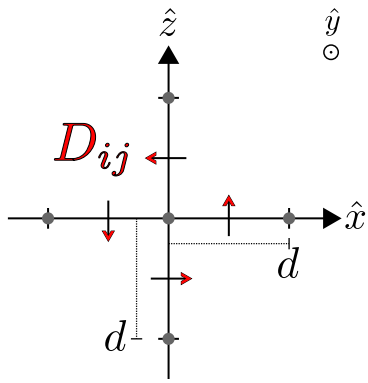

Figure 2.2: The direction of the in-plane IDMI-vector between neighbouring sites of the square lattice. The mirror symmetry is broken along $\hat{y}$, and the DMI D_{ij} is completely confined to the xz-plane.

With the expressions for the magnetization $\mathbf{m}$ and the staggered magnetization $\mathbf{l}$ given by eqs. 2.12 and 2.13, we take $\mathbf{l} \to \mathbf{n}$ as explained in sec. 2.3, and assume that the spins at site i belong to the α-sublattice, while the spins at j belong to the β-sublattice. We express the spins on site i and j in terms of the fields as

$$\mathbf{S}_i = S(\mathbf{m}_i + \mathbf{n}_i)$$
$$\mathbf{S}_j = S(\mathbf{m}_j - \mathbf{n}_j)$$

We then perform an expansion in the gradients of the fields at the lattice sites j, writing them in terms of the directional derivatives of the fields at lattice sites i.

$$\mathbf{n}_j \approx \mathbf{n}_i + \Delta(\hat{\mathbf{r}}_{ij} \cdot \nabla)\mathbf{n}_i + \Theta((\nabla^2 n))$$
$$\mathbf{m}_j \approx \mathbf{m}_i + \Delta(\hat{\mathbf{r}}_{ij} \cdot \nabla)\mathbf{m}_i + \Theta((\nabla^2 m))$$

where we neglect terms of higher than linear order in the derivatives. The vectors $\hat{\mathbf{r}}_{ij}$ denote the direction of the nearest neighbour-site, and $\Delta = \sqrt{2}d$ is the centered square lattice unit cell width.

We can now rewrite the Hamiltonian for in-plane interfacial DMI as

$$\sum_{<ij>} \mathbf{D}_{ij} \cdot (\mathbf{S}_i \times \mathbf{S}_j) = -D \sum_i \mathbf{S}_i \cdot \left\{ \sum_{<j>} (\hat{\mathbf{y}} \times \hat{\mathbf{r}}_{ij}) \times \mathbf{S}_j \right\} \tag{2.22}$$

where the brackets $\langle \cdots \rangle$ represents summation over nearest-neighbour lattice sites. Inserting the expansions of the fields into eq. 2.22 and keeping terms up to linear order in the gradients, we obtain the continuum limit of the chiral part of the Hamiltonian density as

$$\mathcal{F}_{DMI}^{AFM} = \mathcal{D}\Big[\mathbf{n} \cdot (\tilde{\nabla} \times \mathbf{n}) + \tilde{\nabla} \cdot (\mathbf{n} \times \mathbf{m}) - \mathbf{m} \cdot (\tilde{\nabla} \times \mathbf{m})\Big] \tag{2.23}$$

where $\mathcal{D} \equiv \Delta S^2 D$. As in [113], we have defined the in-plane ∇-operator: $\tilde{\nabla} \equiv \hat{y} \times \nabla$. The 2nd term of $\mathcal{F}_{DMI}^{AFM}$ amounts to a total derivative, which can be shown to have no effect on the dynamics of the fields, and is subsequently dropped. We remind that we are working with the energy density i.e. we are leaving out a integral over space from the notation.

The expression for the continuum limit contribution of the DMI to the AFM free energy density thus has the form

$$\mathcal{F}_{DMI}^{AFM} = \mathcal{D}\Big[\mathbf{n} \cdot (\tilde{\nabla} \times \mathbf{n}) - \mathbf{m} \cdot (\tilde{\nabla} \times \mathbf{m})\Big] \tag{2.24}$$

where we have chosen to keep the contribution from the magnetization $\mathbf{m}$ for now. As mentioned in the discussion about Lifshitz- invariants in app. A, a magnetic material with T-symmetry has the same structure as the terms in 2.24, with the $\sim$ on the ∇-operators dropped. In this case, the operator $\tilde{\nabla}$ is responsible for restricting the DMI to lie in the xz-plane.

Letting $\hat{y}$ be the direction perpendicular to the basal plane of the thin film (xz-plane), the term $\mathbf{n} \cdot (\tilde{\nabla} \times \mathbf{n})$ can be written as

$$\begin{aligned}\Big[\mathbf{n} \cdot (\tilde{\nabla} \times \mathbf{n})\Big] =& \mathbf{n} \cdot ((\hat{y} \times \nabla) \times \mathbf{n}) \\ =& \Big[(\hat{y} \cdot \boldsymbol{n})(\nabla \cdot \boldsymbol{n}) - (\boldsymbol{n} \cdot \nabla)(\hat{y} \cdot \boldsymbol{n})\Big]\end{aligned} \tag{2.25}$$

In this thesis, we will consider spatially modulated IDMI. This IDMI will be taken as a function of $\mathbf{r}$: $D \equiv D(\mathbf{r})$. However, we include in the definition of the DMI a constant interfacial background-DMI in addition to the spatially modulated inhomogeneous DMI. This situation can be imagined as e.g. periodic layering of a material (modulated DMI) on top of a single-component layer with non-zero interfacial DMI (homogeneous DMI). We will often denote the constant IDMI as *homogeneous*, and the modulated IDMI *inhomogeneous*. We thus include a constant term in the definition of $D(\mathbf{r})$

$$D(\mathbf{r}) = d_h + D(\mathbf{r}) \equiv D(\mathbf{r})$$

The homogeneous DMI is denoted by d_h, and will taken to be zero until we say otherwise. We continue to use the notation $D(\mathbf{r})$ (and its redefinitions) for the sum of the homogeneous and modulated contributions to avoid cluttering the notation. When $D(\mathbf{r})$ is redefined for ease of notation, d_h is redefined in the same manner.

In this thesis, we will consider two types of spatial modulation $D(\mathbf{r})$: a Krönig-Penney model for the 1D magnonic crystal in chapter 3, and a continuous cosine potential for the 2D magnonic crystal in chapter 4.

2.5 Complete form of free energy

We are now ready to present the complete form of $\mathcal{F}_{AFM}$. We started out with a micromagnetic model in terms of isolated lattice spins $\{\mathbf{S}_i, \mathbf{S}_j\}$ including sym-

metric exchange, magnetocrystalline anisotropy, magnetic field and IDMI. The complete Hamiltonian for this chiral AFM-model where all the terms discussed in the previous sections has been included reads

$$H = J\sum_{<ij>}\mathbf{S}_i\cdot\mathbf{S}_j + \sum_{<ij>}\mathbf{D}_{ij}\cdot(\mathbf{S}_i\times\mathbf{S}_j) - \sum_i \mathbf{H}\cdot\mathbf{S}_i - K\sum_i(\mathbf{S}_i\cdot\hat{z})^2 \tag{2.26}$$

where $< ij >$ denotes summation over all pairs of n.n. spins on the two sublattices. At site i, each spin has N nearest neighbours of type $\mathbf{S}_j$ and vice versa. J is the exchange coupling, where $J > 0$ denotes antiferromagnetic exchange, $\mathbf{H}$ is an external magnetic field in units of energy, and K denotes the anisotropy energy in the $\hat{z}$-direction.

To lowest order in the fields and gradients satisfying all symmetry requirements and conditions from the previous sections, the free energy functional F_{AFM} of the collinear easy-axis chiral AFM with magnetic-field on a centered square lattice is expressed as the integral over the free energy density functional $\mathcal{F}_{AFM}$. It is obtained in app. A as

$$\begin{aligned} &F_{AFM}[\mathbf{m}(\mathbf{r},t),\mathbf{n}(\mathbf{r},t)] \\ &= \frac{1}{V}\int d\mathbf{r}\left\{a\frac{\mathbf{m}^2}{2}+\frac{A}{2}\left[\sum_{i=x,y,z}|\partial_i\mathbf{n}|^2+\frac{1}{2}\sum_{i\neq j}(\partial_i\mathbf{n}\cdot\partial_j\mathbf{n})\right]\right. \\ &\qquad +B\sum_i(\mathbf{m}\cdot\partial_i\mathbf{n}-\mathbf{n}\cdot\partial_i\mathbf{m})-\mathbf{H}\cdot\mathbf{m}-\frac{K_z}{2}(\mathbf{n}_z)^2 \\ &\qquad \left.-\mathcal{D}(\mathbf{r})\Big[\mathbf{n}\cdot(\tilde{\nabla}\times\mathbf{n})-\mathbf{m}\cdot(\nabla\times\mathbf{m})\Big]+\lambda(\mathbf{n}\cdot\mathbf{m})+\frac{\beta}{2}(\mathbf{n}^2-1)\right\} \end{aligned} \tag{2.27}$$

As mentioned, we have neglected Gilbert damping and torques due to spin transfer and external currents. Note the $\sim$ on the ∇s in the DMI-term $\propto\mathcal{D}(\mathbf{r})$, ensuring the direction of the IDMI-interaction is in the xz-plane. We have absorbed the factors $\rho\gamma$ into the definition of the magnetic field $\mathbf{H}$, giving it dimensions of energy. Lastly, remember that $\mathcal{D}(\mathbf{r})$ includes a homogeneous part d_h including the same parameters in its definition as $\mathcal{D}$.

To formally enforce the constraints we imposed on the continuum-fields $\{\mathbf{m},\mathbf{n}\}$ in the exchange approximation, see sec. 2.3, $\mathcal{F}_{AFM}$ contains two Lagrange multipliers $\{\lambda,\beta\}$ for the dynamical restrictions $\mathbf{m}\cdot\mathbf{n}=0$ and $\mathbf{n}\cdot\mathbf{n}=1$. We will show that $\{\lambda,\beta\}$ are functions of $\mathbf{n}$ and $\mathbf{m}$ in a manner that fulfills the constraints on the fields, see app. B.

2.5.1 Discarding anisotropic and parity-breaking terms

This section recapitulate the discussion of the anisotropic terms in [118], which we refer to for more info and relevant references.

The $3^{\text{d}} \propto (\partial_i \mathbf{n} \cdot \partial_j \mathbf{n})$ and 4^{th} term $\propto (\mathbf{m} \cdot \partial_i \mathbf{n} - \mathbf{n} \cdot \partial_i \mathbf{m})$ in the free energy, eq. 2.27, are anisotropic. We can rewrite the 2^{nd} part of the latter term $\propto -\mathbf{n} \cdot \partial_i \mathbf{m}$ with integration by parts and combine it with $\mathbf{m} \cdot \partial_i \mathbf{n}$, resulting in the more compact combined form

$$B \sum_i (\mathbf{m} \cdot \partial_i \mathbf{n} - \mathbf{n} \cdot \partial_i \mathbf{m}) \simeq 2B \sum_i (\mathbf{m} \cdot \partial_i \mathbf{n}) \tag{2.28}$$

where the non-equivalence arises because we have dropped a term $\propto \partial\mathbf{n}\partial\mathbf{m}$ due to the smallness of the field $\mathbf{m}$, which makes its gradient negligible. The term in eq. 2.28 is not invariant under sublattice exchange, which sends $\mathbf{n} \to -\mathbf{n}$, and thus breaks parity. This can seem like an oversight, since one might assume from the relatively simple symmetry of the centered square lattice AFM that the system cannot contain such a term. As argued in [118], the term reflects the intrinsic magnetization of the AFM. Exchanging the spins of the sublattices $\{\alpha, \beta\}$ has a non-zero energy cost if the order parameter is spatially inhomogeneous. This finite energy is the parity-breaking term in the free energy functional.

When deriving the semi-classical EOM's of the Néel AFM in the exchange approximation, we will find that the magnetization $\mathbf{m}$ is expressible in terms of the field $\mathbf{n}$ and its derivatives, allowing us to express the AFM dynamics in terms $\mathbf{n}$ alone. One can then, as will be done in appendix B, express $\mathcal{F}_{AFM}$ in terms of $\{\mathbf{n}, \dot{\mathbf{n}}, \partial_i \mathbf{n}\}$. The only resulting effect of the anisotropic terms in the Lagrangian density $\mathcal{L}$ will be a renormalization of the exchange stiffness A,

$$A \to A^* = A - \frac{B^2}{2} = \frac{A}{2}$$

and the inclusion of a topological term $\propto \partial_i \mathbf{n}(\mathbf{n} \times \dot{\mathbf{n}})_i$. This term can be shown to correspond to a total derivative [28], which drops out of the semi-classical dynamics of the $\mathbf{n}$-field.

The topological term only has consequences when considering quantum effects, and can fundamentally change the ground state and low energy-spectrum of the AFM. These effects can be meaningful even in the thermodynamic limit, with one prominent example being the *Haldane gap* [35] in integer spin chains. This is a whole nother topic outside the scope of this thesis, and the topological term is subsequently dropped.

2.6 Semi-classical equations of motion for the Neél AFM

We will now outline the procedure of obtaining the semi-classical equations of motion in the exchange approximation for the Néel AFM in terms of the order parameters $\{\mathbf{m}, \mathbf{n}\}$. As mentioned earlier, we will be able to eliminate the magnetization $\mathbf{m}$ by expressing it in terms of $\mathbf{n}$, making $\mathbf{m}$ a so-called *slave variable* completely determined by the dynamics of $\mathbf{n}$. The derivation itself is detailed in app. B, with the main steps and intermediate results given in this section.

The *principle of least action* [16, 41] states that for a classical system there exists a quantity $\mathcal{S}$, called the *action*, which has a minimum for the systems actual, real-life motion. This minimum is found by setting the 1st-order variation of $\mathcal{S}$ to zero, meaning that the action is *stationary* for this motion. The paths of the system are paths in a abstract configuration space, or *phase space*, where the coordinates can be given by any set of generalized coordinates $\{\mathbf{q}_i, \dot{\mathbf{q}}_i\}$, which in our case is the fields $\{\mathbf{m}, \mathbf{n}\}$, with $\mathcal{S}$ a functional of these fields. The action is defined as

$$\begin{aligned}\mathcal{S}[\mathbf{m}(\mathbf{r},t),\mathbf{n}(\mathbf{r},t)] &= \int d\mathbf{r}dt\ \mathcal{L}[\mathbf{m}(\mathbf{r},t),\mathbf{n}(\mathbf{r},t)] \\ &= \int d\mathbf{r}dt\ [\mathcal{K}-\mathcal{F}]\end{aligned}$$

$\mathcal{L}$ is the *Lagrangian density*, $\mathcal{K}$ is a kinetic energy (density) contribution of the system, and $\mathcal{F}$ is the free energy density, which we have derived already for the AFM.

$\mathcal{K}$ is acquired from the *Berry phase of a antiferromagnetic spin dimer* [35, 118], a interacting pair of spins with antiferromagnetic exchange. Its origin will be explained in a brief manner [35], glossing over many of the details, but included to give a glimpse of the connection to between QM and semi-classical SW-theory.

The *path intergral formulation* in terms of *coherent states* [70], in contrast to *Fock states*, can often lead to expressions which lends themselves well to approximations and a more "intuitive" understanding of the system than the exact solutions. For spin-path integrals, the spin coherent states depends on the time-history of the spins. Following [35], the *generating functional* [70, 106] in the imaginary time formulation including sources j_i, with the division of the time interval into discrete time steps ϵ is given by

$$\begin{aligned}Z[j_i] &= Tr T_\tau \left[e^{-\int_0^\beta d\tau\ \mathcal{H}(\tau)} \right] \\ &= \lim_{N_\epsilon \to \infty} Tr T_\tau \prod_{n=0}^{N_\epsilon - 1} [1 - \epsilon \mathcal{H}(\tau_n)]\end{aligned} \tag{2.29}$$

where the sources j_i are included in the Hamiltonian $\mathcal{H}$, T_τ is the *time ordering operator* which orders the operators in $\mathcal{H}$ such that they act in order of increasing imaginary time, β is the inverse temperature, and $\tau_n = n\epsilon$. Note that in the imaginary time-formalism, $\epsilon = \beta/N_\epsilon$. The reason for splitting the time integral into discrete chunks is that we wish to formulate the dynamics of the system in terms of smooth, continuous paths, which neglects the quantum behaviour of the system. To rule out these *discontinuous* paths, we wish to in some way impose well-behaved analytical behaviour on the path integral, which we try to achieve by expressing the integral in terms of the spin states parametrized in terms of angles and, crucially, derivatives, which we know how to manipulate.

This is done by inserting the resolution of the identity in terms of the (non-orthogonal) coherent spin states [35]

$$\int \prod_i \left(\frac{2S+1}{4\pi} d\hat{\Omega}_i \right) |\hat{\Omega}\rangle\langle\hat{\Omega}| \;=\; 1 \tag{2.30}$$

between every time-step ϵ in the discretized path integral of eq. 2.29. The coherent spin states $|\hat{\Omega}\rangle$ can be parametrized in terms of three *Euler angles* $\{\phi, \theta, \chi\}$ in some abstract vector space [46], which we will not go further into. It is evident from the identity-resolution that the states are not orthogonal if one compares them to the resolution of the identity in e.g. Fock states in QM [115].

A essential but technically illegal step is performed when the *time differences* in the coherent states are approximated as *time-derivatives* in the limit $N_\epsilon \to \infty$. This assumption implies that the path integral is dominated by *smooth*, *classical paths*, which turns out to be *wrong* [46], but can still give reasonable approximations. The spin-path integral is reobtained if we go ahead and take the limit $N_\epsilon \to \infty$. However, the overcompleteness of the spin coherent states in eq. 2.30 has given us a overlap-term between states separated by the infinitesimally small time step ϵ. This overlap takes the form

$$\langle \hat{\Omega}(\tau+\epsilon) || \hat{\Omega}(\tau) \rangle \;=\; e^{-iS\epsilon \sum_i \dot{\phi}_i \cos\theta_i(\tau) + \chi_i} \tag{2.31}$$

where two of the three Euler angles ϕ and θ are the only degrees of freedom needed to describe the spins, while χ can be set by fixing a arbitrary gauge and is disregarded. The above term becomes an extra term in the classical action $\mathcal{S}_c$ in the path integral, which we won't state. However, the contribution from eq. 2.31 to the path integral can be written as

$$\begin{aligned} \mathcal{S}[\hat{\Omega}]_\omega \;&=\; -iS \sum_i \omega[\hat{\Omega}_i] \\ &= iS \sum_i \int_0^\beta d\tau \dot{\phi}_i \cos\theta_i \\ &= iS \int_{\phi_0}^{\phi_1} d\phi \;\cos\theta_\phi \end{aligned}$$

This shows that ω is dependent on the path taken by the unit spin Ω_i on the unit sphere [35]. This part of the functional is the *Berry phase* of the spin, acquired by the spin as it aligns with a slowly varying external field parallel to Ω. We can introduce a vector potential $\mathbf{A}(\Omega)$ to avoid specifying the coordinates on the unit sphere $\{\phi, \theta\}$, meaning we have a *gauge invariant* form of the Berry phase. We can achieve this if we introduce a vector potential which satisfies

$$\omega \;=\; \int_0^\beta d\tau \; \mathbf{A}(\hat{\Omega}) \cdot \dot{\hat{\Omega}}$$

There are several possible choices for $\mathbf{A}$, which is the vector potential of a *magnetic monopole*. A conventional one is $\mathbf{A} = -\cos\theta/\sin\theta\hat{\phi}$. We now essentially have a dot product between the vector potential and the classical spin, $\mathbf{A}\cdot\dot{\hat{\Omega}}_i$, where the spin Ω_i corresponds to a spin $\mathbf{S}$ belonging to one of the magnetic sublattices $\{\alpha,\beta\}$. We now connect this to the kinetic term $\mathcal{K}$ and straightforwardly state the result, since the rigorous derivation is outside the scope of this thesis: we define a vector potential for each of the two spins in each AFM unit cell $\{\mathbf{A}_\alpha,\mathbf{A}_\beta\}$, where the above choice of vector potential is convenient, and expand the Berry phase in small deviations in the angles $\{\phi,\theta\}$ around their equilibrium Néel configuration [118]. In the basis of the order parameters $\mathbf{n}$ and $\mathbf{m}$, which is readily expressible by the angular dependence of the spins, the kinetic term $\mathcal{K}$ can be identified as

$$\mathcal{K} = \rho\,(\dot{\mathbf{n}}\times\mathbf{n})\cdot\mathbf{m} \tag{2.32}$$

where $\rho = 2S\hbar$ is the magnitude of the angular momentum in the AFM unit cell. The above part constitutes a brief recollection of how to obtain the kinetic term, and we refer to relevant sources for details [35, 46, 70].

We can now obtain the EOMs for the fields $\{\mathbf{n},\mathbf{m}\}$. Per our previous discussion in this section, we demand that the action of the continuum AFM is stationary through the condition $\delta\mathcal{S} = 0$, which we can write as the functional derivative of the Lagrangian density w.r.t. $\mathbf{n}$ and $\mathbf{m}$.

$$\begin{aligned}\frac{\delta\mathcal{L}}{\delta\mathbf{n}} &= \frac{\delta\mathcal{K}}{\delta\mathbf{n}} - \frac{\delta\mathcal{F}}{\delta\mathbf{n}} = 0\\ \frac{\delta\mathcal{L}}{\delta\mathbf{m}} &= \frac{\delta\mathcal{K}}{\delta\mathbf{m}} - \frac{\delta\mathcal{F}}{\delta\mathbf{m}} = 0\end{aligned} \tag{2.33}$$

The resulting coupled equations of motion for the fields, derived in app. B, take the form of torque equations as we remarked at the start of chap. 2

$$\begin{aligned}\dot{\mathbf{n}} &= \mathbf{f}_\mathbf{m}\times\mathbf{n}\\ \dot{\mathbf{m}} &= \mathbf{f}_\mathbf{m}\times\mathbf{m} + \mathbf{f}_\mathbf{n}\times\mathbf{n}\end{aligned} \tag{2.34}$$

These are the coupled *Landau-Lifshitz*-equations of motion for the fields in the absence of Gilbert damping, in the same form as the torque equation 2.1 stated at the start of this chapter. These equations can also be acquired by other procedures, e.g. the *Poisson bracket algebra* [22]. The effective fields $\mathbf{f}_\mathbf{n}$ and $\mathbf{f}_\mathbf{m}$ are given by the functional derivative of the magnetic free energy density $\mathcal{F}$. w.r.t. to the denoted field: $\mathbf{f}_\mathbf{n} = -\frac{\delta\mathcal{F}}{\delta\mathbf{n}}$ and $\mathbf{f}_\mathbf{m} = -\frac{\delta\mathcal{F}}{\delta\mathbf{m}}$.

In the exchange approximation, the equations of motion in eq. 2.34 can be used to reduce the coupled equations to a single 2^{nd}-order equation in time for the field $\mathbf{n}$. A step towards this is to realize that the magnetization, without intrinsic magnetization, can be expressed in terms of $\mathbf{n}$ as

$$\mathbf{m} = \frac{\rho}{a}\dot{\mathbf{n}}\times\mathbf{n} + \frac{1}{a}\mathbf{n}\times(\mathbf{H}\times\mathbf{n})$$

We note that including the intrinsic magnetization, the above equation should have an extra term proportional to the gradient of $\mathbf{n}$ [118]. The term $\dot{\mathbf{n}} \times \mathbf{n}$ implies that the dynamic motion of $\mathbf{n}$ give rise to a finite magnetization. In equilibrium, $\dot{\mathbf{n}} = 0$, and the only magnetization comes from the magnetic field $\mathbf{H}$.

The above expression also implies that one can excite and measure SWs by coupling to magnetic fields, which allows for the use of EM-fields in manipulations of AFM-SWs, e.g. Brillouin light scattering. This has been one of the primary methods of studying AFM-SWs for many years, as commented in [109].

With $\mathbf{m}$ expressed in terms of $\mathbf{n}$, we can express $\mathcal{L}$ in terms of $\mathbf{n}$ and its derivatives. $\mathcal{L}$ then takes the form, with details referred to app. B

$$\begin{aligned}\mathcal{L}[\mathbf{n}, \dot{\mathbf{n}}, \partial_i \mathbf{n}] = \frac{\rho^2}{2a}(\dot{\mathbf{n}} - \gamma \mathbf{H}_{ext} \times \mathbf{n})^2 - \frac{A}{2}|\partial_i \mathbf{n}|^2 + \frac{K_z}{2}(\mathbf{n} \cdot \hat{z})^2 \\ - \mathcal{D}(\mathbf{r})\left[(\mathbf{n} \cdot \hat{\mathbf{y}})(\nabla \cdot \mathbf{n}) - (\mathbf{n} \cdot \nabla)(\mathbf{n} \cdot \hat{\mathbf{y}})\right]\end{aligned} \tag{2.35}$$

with $\mathbf{H}_{ext}$ a external magnetic field with units of a field. Neglecting the DMI and magnetic field, this effective Lagrangian density corresponds to the well known *non-linear σ-model* (NLSM) with anisotropy [22, 28, 70], connecting the quantum Heisenberg antiferromagnet in D dimensions to a $D+1$-dimensional classical model. The non-linearity of the NLSM is due to the previously defined unimodularity constraint on the Néel field $|\mathbf{n}| = 1$. In the absence of anisotropy, the NLSM is $O(3)$-rotationally symmetric.

In the absence of *topological* Berry phases, the NLSM represents the ground state of the quantum Heisenberg AFM. However, if one considers additional topological Berry phases, the ground state of the AFM might differ drastically from the classical case [35]. The NLSM has many interesting topological properties such as *soliton solutions* in the form of movable domain walls separating different ground states. These properties of the NLSM is outside the scope of this thesis, and will not be commented on further.

One can infer some basic properties of the spectrum by just the fact that we have obtained the NLSM: the spin waves are the *Goldstone-modes* [70] of the collinear AFM. When the ground state breaks the continuous O(3)-rotational symmetry of the NLSM, or the Heisenberg Hamiltonian for that matter, Goldstone's theorem [70, 71] states that there should be gapless excitations of zero mass in the SW-spectrum. However, introducing anisotropies into the system (e.g. the easy-axis anisotropy in our model), Goldstone's theorem is no longer applicable as it is only valid for spontaneous symmetry breaking, while we explicitly break the symmetry of the system with the introduction of anisotropies.

Introducing anisotropy, the spectrum becomes gapped, requiring a minimum resonance frequency to excite modes in the AFM. This frequency defines the *antiferromagnetic resonance frequency* of the system, the lowest frequency needed to make the spins oscillate. The gap in the SW-spectrum are due to localized standing SW-modes interfering destructively, and has been studied in both FM- and AFM-magnonic crystals [74, 90].

2.7 Klein-Gordon-equation of in-plane SW-fluctuations

We have adapted a semi-classical model in the $T << T_N$ -regime with the assumption that we will be able to obtain qualitative information about the low-frequency SW-spectrum of the thin-film insulating AFM-system subject to IDMI. In the last section, we showed that the continuum description of the order parameter $\mathbf{n}$ corresponded to the anisotropic NLSM [22].

Before proceeding, we comment on the effects of *magnon-magnon*-interactions. In this thesis, we take the SWs to be non-interacting. The first calculations done on SW/magnon-interactions was performed by Dyson [8, 9]. A arguably more intuitive treatment can be performed with the Holstein-Primakoff-formalism [68, 70]: to 2^{nd} order in the bosonic magnon creation and annihilation operators a and $a^\dagger$, the Holstein-Primakoff-approach results in a theory of *non-interacting Bloch-waves*, which is the assumption used in this thesis. However, including higher order terms in the a, $a^\dagger$-operators corresponds to including magnon-magnon-interactions. However, Dyson showed that many of the complicated interactions between the magnons cancel each other. The conclusion is that for low temperatures $T << T_N$, the simple model of non-interacting SWs is well justified. Approximately non-interacting SWs means that we can safely apply a Bloch-wave-treatment. We also take the two SW precessional modes of the easy-axis collinear AFM to be independent of each other. They can thus be treated separately, and the effective wave equations for the SWs decouple.

We now turn to the study of low-frequency SW-oscillations around some equilibrium direction in the AFM, which we take to be the $\hat{z}$-direction. We introduce a easy-axis anisotropy along this direction, such that the spins in each AFM-unit cell thus points along $\pm\hat{z}$. We separate the Néel field into a static equilibrium part $\mathbf{n}_0$ and a dynamical part $\delta\mathbf{n}$. The SWs $\delta\mathbf{n}$ are fluctuations of $\boldsymbol{n}$ in a plane transverse to $\mathbf{n}_0$, in this case the xy-plane.

$$\mathbf{n}(\mathbf{r},t) = \mathbf{n}_0\hat{Z} + \delta\mathbf{n}(\mathbf{r},t) \tag{2.36}$$

$$\delta\mathbf{n}(\mathbf{r},t) = \delta n_X(x,z;t)\hat{X} + \delta n_Y(x,z;t)\hat{Y} \tag{2.37}$$

The coordinates $\{x,y,z\}$ are the usual cartesian coordinates, $\{\hat{X},\hat{Y},\hat{Z}\}$ are arbitrary mutual orthogonal axes. The need for defining a new coordinate system comes from the fact that we often wish to describe the dynamics of the system in relation to some arbitrary direction of e.g. applied field $\mathbf{H}$ or magnetization (or Néel order). These are often not parallel to one of the cartesian axes. Defining new axes is also convenient in the studies of optical excitations of magnons, such as with Brillouin light scattering, where the photon can come in from a direction ofset by some angle from one of the axes. Thus, it is convenient to relate these directions to the propagation direction of spin waves in the system. In this thesis, we will take $\boldsymbol{n}_0 \| \hat{z}$, and apply $\mathbf{H} \parallel \hat{z}$. Thus, the dynamics in relation to the separate coordinate system $\{\hat{X},\hat{Y},\hat{Z}\}$ can be dropped, and we continue to use cartesian axes. We then

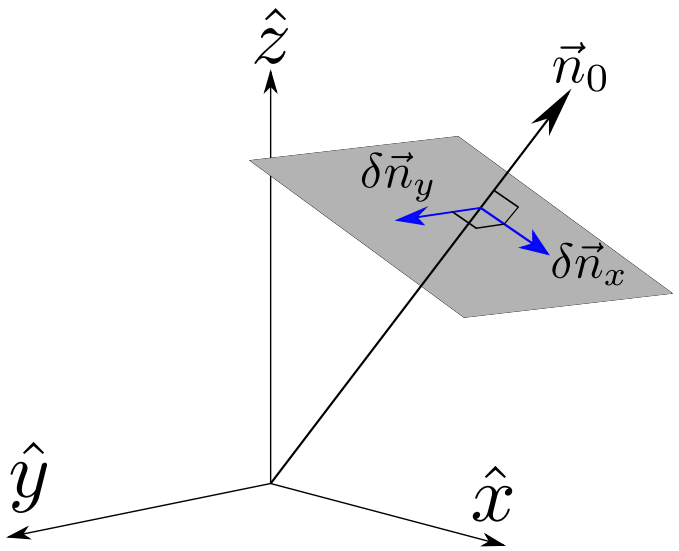

Figure 2.3: SW-fluctuations in a plane perpendicular to the equilibrium $\mathbf{n}_0$. One can define a set of axes $\hat{X}, \hat{Y}, \hat{Z}$ for convenience (not shown) if one works with fields and optical excitation from arbitrary directions.

have

$$\delta\mathbf{n}(\mathbf{r}, t) = \delta n_x(x, z; t)\hat{x} + \delta n_y(x, z; t)\hat{y} \tag{2.38}$$

Note that the label y on δn_y does not imply that it is a function of the y-coordinate: it is still a function of the cartesian coordinates in the plane of the thin film, $\{x, z\}$. Due to the thin film geometry, we assume that the y-direction has no impact on the dynamics of the system, meaning that the SWs cannot depend on this coordinate. We remember that for this to hold, we have to be in the regime $\mathbf{k}_{\parallel} c \ll 1$ [58], with c the film thickness. Regarding thin films and DMI, the strength of the IDMI in FM-thin films has been found to vary as $\sim 1/c$ [105, 108], which is expected due to IDMI being an interface-effect.

Assuming $|\delta n_x|^2, |\delta n_y|^2 \ll 1$, we will only consider dynamics up to 1^{st} order in these small parameters, effectively ignoring scattering effects. Here, δn_x, δn_y are taken to be complex, allowing for the notion of a phase shift between different SW-modes. This will be a central part of the application of interfacial DMI as a spin wave filter. Expanding on this, we can define the spin wave as a complex field [130] via the *spin wave function* $\psi(\mathbf{r}, t)$.

$$\psi(\mathbf{r}, t) = \delta n_x \pm i\delta n_y \tag{2.39}$$

where we have included the $\pm$ to denote the *helicity* or *handedness* of the SW. We will make use of the notation $\psi_+ = \delta n_x + i\delta n_y$ and $\psi_- = \bar{\psi} = \delta n_x - i\delta n_y$, which denotes *right-handed* (RH) and *left-handed* (LH) SWs respectively.

Using polar coordinates $\{x, z\} \to \{r, \phi\}$, we can write $\psi(\mathbf{r}, t) = |\psi| e^{i\phi}$. The phase shift between the modes is then $e^{i\phi}$, where ϕ is the phase angle between the precessional modes of the spins in a unit cell. The phase shift is analogous to the polarization angle of EM-waves, and represents a new degree of freedom for the magnonic system. This degree of freedom is unique to the AFM, with all spin waves in FMs being right-handed [35, 68].

The angle $\phi = 0$ corresponds to *linear polarization*. The cone angles of the spins $\mathbf{S}_\alpha$ and $\mathbf{S}_\beta$ at each lattice site is equal, with the spins pointing in opposite directions of one another with no relative canting, see fig 1.3. Thus, the oscillations of the Néel field at a given lattice site $\mathbf{n} = (\mathbf{S}_\alpha - \mathbf{S}_\beta)/2S$ is purely linear.

From the polar-notation, we see that the two SW-modes are related by $\phi \to \phi - \pi$, and that the components δn_x and δn_y are related as $\delta n_x = e^{\mp i\pi/2} \delta n_y$, i.e. $\phi = \pm\pi/2$. This corresponds to *circular polarization*. Circularly polarized RH/LH-modes preccess around some equilibrium direction, i.e. $\hat{z}$, with different amplitudes, with the spins tracing out different cone angles. In this case, the components of the spin wave lead or lag behind each other by an angle of $\pm\pi/2$ depending on the SW-chirality. As a consequence of this perpendicularity of the components, the cone angles of the spins in each unit cell, see fig. 1.3, have opposite ratios.

Interestingly, the magnon chirality is connected to the polarization of photons, which admits the possibility of exciting the degenerate modes through optical methods [76]. The degeneracy of the modes can be lifted by applying a magnetic field along the equilibrium direction, which will consequently increase and decrease the frequency of the RH/LH-modes depending on if the field points along $\pm\mathbf{z}$.

To solve the equations of motion, we will take $\delta\mathbf{n}$ to be in the form of *monochromatic plane waves* [68, 113, 130]

$$\delta \boldsymbol{n}(\mathbf{r}, t) = (\delta n_x \hat{x} + \delta n_y \hat{y}) e^{i\boldsymbol{k}\cdot\boldsymbol{r} - i\omega t} \tag{2.40}$$

with spin wave vector $\mathbf{k}$, frequency ω, and $\mathbf{r} = (x, 0, z)$. $\{\delta n_x, \delta n_y\}$ are taken to be complex coefficients. Thus, the SW-function $\psi_\pm$ take the same form

$$\psi_\pm = \tilde{\psi}_\pm e^{i\boldsymbol{k}\cdot\boldsymbol{r} - i\omega t} \tag{2.41}$$

where $\tilde{\psi}_\pm$ are SW-amplitudes which can be used when boundary conditions on the SWs are considered. We will not use this, and the notation is dropped.

Before presenting the effective SW-equation for the AFM spin waves acquired in app. B, we list the parameters acquired in the continuum limit of the complete micromagnetic Hamiltonian of eq. 2.26, which is found in app. A.

		1D	2D
a	Homogeneous exchange energy	$8JS^2$	$4N_nJS^2$
A	Exchange stiffness	$J\Delta^2S^2$	$N_n\Delta^2JS^2/2$
B	Anisotropic exchange stiffness	$2\Delta JS^2$	$N_n\Delta^2JS^2$
K_z	Easy-axis anisotropy	$2KS^2$	$2KS^2$
ρ	Angular momentum per unit cell	$2S\hbar$	$2S\hbar$
c	Spin wave phase velocity	$SJ\Delta/\hbar$	$N_nSJ\Delta/2\hbar$
$\mathcal{D}$	DMI strength	ΔDS^2	ΔDS^2

N_n is the number of nearest neighbours, which for the square lattice is $N_n = 4$. Δ is the width of the AFM unit cell, which in the centered square lattice is $\Delta = 2d/\sqrt{2} = \sqrt{2}d$, with d being the nearest neighbour distance, see fig. 2.1. In general, $\Delta = 2d/\sqrt{N_D}$, where N_D is the number of dimensions.

This thesis is primarily concerned with the phenomenology of the AFM system, and thus a thorough investigation of any explicit materials with experimental parameters is not performed. Instead, parameters in sensible ranges of AFM materials will be chosen. We will also denote the energies of the fields in terms of frequencies, i.e. $\omega_J = J/\hbar$ etc.

In app. B, we obtain the EOMs for the coupled $\{\mathbf{n}, \mathbf{m}\}$-fields, and reduce the AFM-SW-dynamics to a single differential equation in $\mathbf{n}$, which is the Lagrangian density $\mathcal{L}$ in eq. B.17. The effective K.G.-equation is obtained as $\delta\mathcal{S}/\delta\psi_\pm$. Applying Euler-Lagrange's equations B.5 [41] to $\mathcal{L}$ to linear order in the fields $\{\psi, \bar{\psi}\}$, and expressing the result as a matrix equation acting on a vector consisting of the two decoupled SW-modes $\psi_\pm$, we can now write the effective K.G.-equation for both SW-modes.

$$\rho^2\frac{\partial^2\Psi}{\partial t^2} = a\left[A\nabla^2 - K_z + (\gamma\rho H_{ext})^2\frac{1}{a} + \sigma_3\frac{2i\gamma\rho^2 H_{ext}}{a}\partial_t - \sigma_3\frac{i}{2}\left(D(\mathbf{r})\partial_x - \partial_x D(\mathbf{r})\right)\right]\Psi \tag{2.42}$$

We note that the DMI-operator has the form of a commutator, which is necessary to ensure hermicity [41]. Also, remember that $D(\mathbf{r}) = d_h + D(\mathbf{r})$. We have expressed the two SW-modes as

$$\Psi = \Psi_{\mathbf{k}}(\mathbf{r}, t) = \begin{bmatrix}\psi_+ \\ \psi_-\end{bmatrix} = \begin{bmatrix}\tilde{\psi}_+ \\ \tilde{\psi}_-\end{bmatrix} e^{i(\omega t - \mathbf{k}\cdot\mathbf{r})} \tag{2.43}$$

We will use redefined parameters instead of the ones in eq. 2.42. The effective K.G.-equation can be stated as

$$\frac{\partial^2\psi}{\partial t^2} = c^2\left[\nabla^2 - \bar{\mathcal{K}}_z + \bar{H}^2 + 2i\sigma_3\frac{\bar{H}}{c}\partial_t - \frac{i\sigma_3}{2}\left(\bar{\mathcal{D}}(\mathbf{r})\partial_x - \partial_x\bar{\mathcal{D}}(\mathbf{r})\right)\right]\begin{bmatrix}\tilde{\psi}_+ \\ \tilde{\psi}_-\end{bmatrix} \tag{2.44}$$

where we have defined the *spin wave phase velocity* $c^2 = \mathcal{A}/\rho^2 \equiv N_n\Delta JS/2\hbar$, with $\mathcal{A} = aA$, $\bar{\mathcal{K}} \equiv \mathcal{K}_z/\mathcal{A}$ with $\mathcal{K}_z = aK_z = 2aKS^2$, $\bar{H} \equiv H^*/\sqrt{\mathcal{A}}$ with $H^* = \gamma\rho H_{ext}$, and

the DMI parameter $\bar{\mathcal{D}} \equiv \mathcal{D}^*/\mathcal{A}$. $\mathcal{D}^*$ is redefined according to the value found in the continuum limit, app. A: $\mathcal{D}^*(\mathbf{r}) = a\Delta D(\mathbf{r})S^2$. We have scaled $\mathcal{A} \to aA^* = aA/2$ according to the discussion in section 2.5.1. In this notation, terms without σ_3 is multiplied by the 2D identity matrix $\mathbb{I}_2$. The quantity inside the square bracket now have units $[m^{-2}]$.

We will call the SW equation 2.44 a effective *Klein-Gordon*-equation (KGE). The name is chosen because of a parallel between the modes of the AFM-SWs and the KGE equation in special relativity. KGE (in special relativity) is a relativistic spin-zero wave equation [77]. It is the relativistic generalization of the *Schrödinger-equation* [115], and in the same manner as non-interacting AFM-SWs, it can be treated and solved as two separate components, which yields positive- and negative-energy solutions. This is reflected in the eigenvalues obtained in the KGE, as they are quadratic, admitting two solutions for the energies.

However, in special relativity, several peculiar phenomena arise when the solutions of positive and negative frequencies ω is used for calculating e.g. the probability current or time evolution of the expectation value of the position operator $\hat{\mathbf{r}}$. These effects include the oscillatory *zitterbewegung* phenomenon, where the interference of positive- and negative-energy energy states of a propagating particle in the form of a wave packet causes large fluctuations around the expected position, and the *Klein paradox* [77], in which the transmission and reflection coefficients of relativistic particles at a potential barrier goes to infinity. This urges caution about thinking of the solutions to the KGE-equation as "particles" in the traditional sense. In addition, the KG-equation has several problems which make it impractical to work with, which includes *nonlocality*, violation of *causality*, and no obvious way of incorporating EM-fields in the theory [47]. Instead, one often reformulates the KGE in the form of the *Dirac equation* [106]. This fomalism has been used to demonstrate a magnonic analogue of zitterbewegung and the Klein-paradox in AFM spin chains [127]

CHAPTER 3

1D MAGNONIC CRYSTAL

Having arrived at a effective KGE, eq. 2.44, for the SWs in the previous chapter, before investigating the case of modulated DMI, we highlight characteristic features of the SW-spectrum in the presence of homogeneous DMI d_h in a thin film system, with the xz-plane as the basal plane. We choose to use the notation $d_h = D$ for the homogeneous DMI until stated otherwise.

Assuming plane wave solutions as in eq. 2.41, $\psi \sim e^{i\mathbf{k}\cdot\mathbf{r}-i\omega t}$, we can obtain the dispersion relation $\omega(\mathbf{k})$ of the RH/LH SWs. We will see that the degeneracy of the modes will be completely lifted for $D \neq 0$ and $\mathbf{H} \neq 0$, with a resulting decoupling of the SW-modes.

The DMI can be shown to only depend on the spatial derivative with respect to x, see app. B, so we must first specify directions in the film. We define the angles as in figure 3.4. A general radial unit vector $\hat{\rho}$ can be given by $\hat{\rho} = (\cos\theta\sin\phi, \sin\theta\sin\phi, \cos\phi)$. If we take the direction of propagation of $\mathbf{k}$ to lie in the xz-plane, we have $\theta = 0$, such that the in-plane-wavevector can be written as $(k_x, 0, k_z) \equiv \mathbf{k}_\perp = k(\sin\phi, 0, \cos\phi)$, where $k = |\mathbf{k}|$.

Since the SW modes ω_R and ω_L are connected by a phase shift of π and the symmetry $H \to -H$, we can choose to work with just one of them; the results for the other mode can be acquired identically with a sign change in front of the linear magnetic field term $\propto \partial_t$ and the DMI-term. For now, we keep both modes in mind with a unified sign notation, e.g. $(\pm)_{R/L}$.

Assuming SWs in the form of monochromatic plane waves $\psi \sim e^{i(\omega t - \mathbf{k}\cdot\mathbf{r})}$ of frequency ω, we obtain the spin wave dispersion of the from eq. 2.44 as

$$\begin{aligned} -\omega^2 &= c^2\left\{-k^2 - \bar{\mathcal{K}}_z + \bar{H}^2(\mp)_{R/L}2\frac{\bar{H}}{c}\omega(\pm)_{R/L}\bar{\mathcal{D}}k_x\right\} \\ \implies 0 &= \frac{\omega^2}{c^2}(\mp)_{R/L}2\frac{\bar{H}}{c}\omega - k^2 - \bar{\mathcal{K}}_z + \bar{H}^2(\pm)_{R/L}\bar{\mathcal{D}}k_x \end{aligned} \tag{3.1}$$

where k_x is the projection of $\mathbf{k}$ onto the x-axis in the xz-plane, given by $k\sin\phi$, where ϕ is the polar angle w.r.t. the z-axis and $k \equiv |\mathbf{k}|$. Note that for $\phi = 0$, the effect of the DMI disappears. In the 1D magnonic crystal, the spin waves propagating perpendicular to the direction of the DMI modulation will not sense the presence of the DMI at all, and will be ungapped except for the lowest energy gap from the easy-axis anisotropy and the magnetic field. Solving eq. 3.1 for ω, we obtain

$$\omega_{\pm,R/L} = (\pm)_{R/L}c\bar{H} \pm c\sqrt{k^2 + \bar{\mathcal{K}}_z(\mp)_{R/L}\bar{\mathcal{D}}k\sin\phi} \tag{3.2}$$

The solution in eq. 3.2 admits RH/LH precessional modes, connected to our two

solutions ψ and $\bar{\psi}$. As discussed earlier, the modes are circularly polarized, and can be thought of as if the in-plane fluctuations $\delta\mathbf{n}$ and the magnetization $\mathbf{m}$ precess anti-clockwise (RH) or clockwise (LH) around the equilibrium ground state configuration $\mathbf{n}_0$. This can also be seen from substituting ω back into the equation of motion in eq. 2.44 and look at each of the two components of the wavefunction $\psi_\pm = \delta n_x \pm i\delta n_y$ and compare with the real and imaginary part of eq. 2.41. One finds that the components are connected by a phase shift of $\pi/2$: $\delta n_x = e^{\mp i\pi/2}\delta n_y$, revealing the right-circularly polarized wave with phase shift $-\pi/2$ to gain energy from a applied magnetic field, thus being the mode of highest energy. The lowest energy mode is thus the left-handed mode with phase shift $\pi/2$.

The $\pm$ from the solution of the polynomial in ω implies two SW-branches, representing the excitations of the two sublattices $\{\alpha, \beta\}$. The lowest-energy bands in the two branches, neglecting homogeneous/inhomogeneous DMI and magnetic field, are separated by a frequency gap of width $2c\sqrt{\bar{\mathcal{K}}_z}$. At zero wavevector $\mathbf{k} = 0$ and in the absence of external magnetic field, this is the threshold value of the homogeneous DMI for the ground state to twist into a spiral, destroying the uniform Néel order. We will keep to the regime $D < c\sqrt{\bar{\mathcal{K}}_z}$, such that the bottom of the lowest positive SW-branch do not drop below 0.

3.0.1 Effects of DMI on spin wave spectrum

In this section, we will restrict ourselves to the positive frequency branch of eq. 3.2

$$\omega_{+,R/L} \equiv \omega_{R/L} = (\pm)_{R/L} c\bar{H} \pm c\sqrt{k^2 + \bar{\mathcal{K}}_z (\mp)_{R/L} \bar{\mathcal{D}} k \sin\phi} \tag{3.3}$$

To keep the notation simple when showing the effects of the magnetic field, anisotropy and homogeneous DMI on the SW-dispersion, we rewrite eq. 3.3 in dimensionless form

$$\omega'_{R/L} = (\pm)_{R/L} 1 + \sqrt{k'^2 (\mp)_{R/L} \mathcal{D}' k' \sin\phi + \mathcal{K}'_z}$$

with $\omega' = \omega/\omega_H$, $k' = k/\bar{H}$, $\mathcal{K}'_z = \bar{\mathcal{K}}_z/\bar{H}^2$, $\mathcal{D}' = \bar{\mathcal{D}}/\bar{H}$ and the characteristic frequency $\omega_H = c\bar{H}$. The dispersion solved for the dimensionless wave vector k', which we will need in our discussion on the 1D MC, reads

$$k'_\pm = (\pm)_{R/L} \frac{\mathcal{D}' \sin\phi}{2} \pm \sqrt{\left(\frac{\mathcal{D}' \sin\phi}{2}\right)^2 + (\omega' \ (\mp)_{R/L} \ 1)^2 - \mathcal{K}'_z} \tag{3.4}$$

As noted earlier, the interfacial DMI lifts the k-degeneracy of the precessional modes, as is evident from fig. 3.2 and 3.3. In the absence of magnetic field (necessarily with other definitions of the parameters than we have applied since we divide by the magnetic field), for frequencies ω above the antiferromagnetic resonance frequency $\omega_R = \sqrt{\mathcal{K}'_z}$, the k-splitting is independent of ω [113]: $\Delta k = k_R - k_L$,

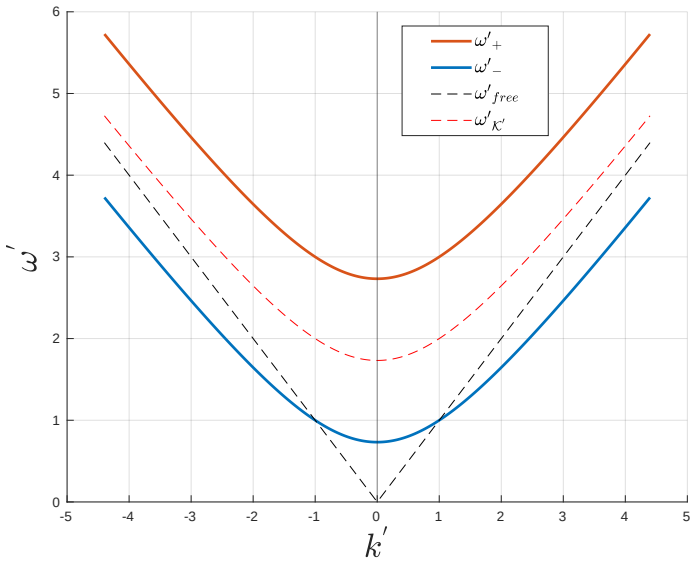

Figure 3.1: Spin wave dispersion relation for the lowest band with applied magnetic field $H/J = 1/100$ and easy axis anisotropy $K/J = 1/10$. The magnetic field lifts the degeneracy of the two degenerate right-handed +-mode and left handed −-mode. The anisotropy gaps the lowest band.

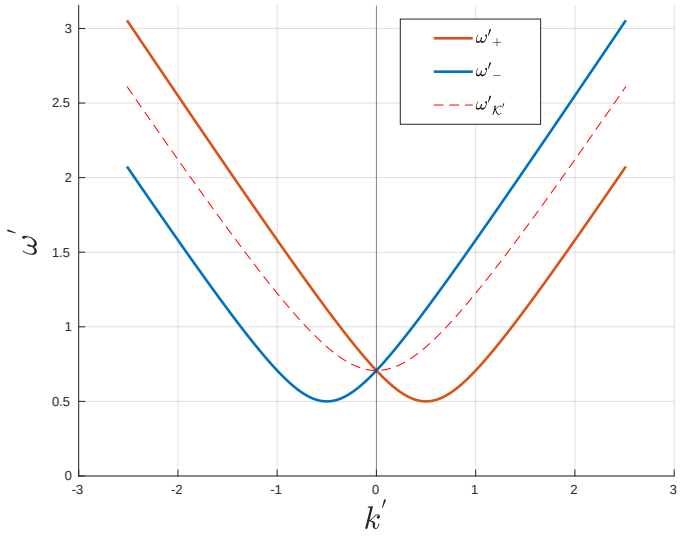

Figure 3.2: RH/LH-dispersion with anisotropy $K/J = 1/10$ and homogeneous DMI $D/J = 1/10$. The DMI reduces the frequency of the SW-modes equally.

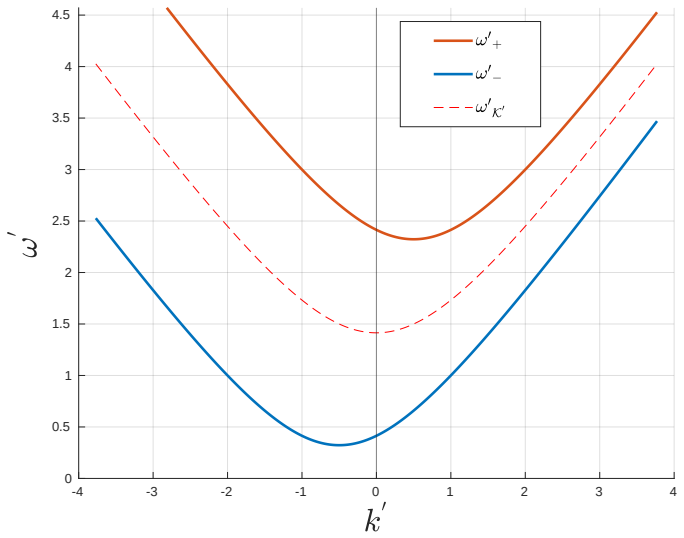

Figure 3.3: RH/LH-dispersion in the presence of magnetic field $H/J = 1/100$, anisotropy $K/J = 1/10$ and homogeneous DMI $D/J = 1/10$. As remarked earlier, the RH-mode is increased in frequency, while the LH-mode is decreases for application of a H-field along $+\hat{z}$.

where k_R and k_L are the wavevectors of the LH/RH-modes at the same frequency ω. The DMI reduces the frequency of both modes, which can be thought of as a energy cost of splitting the modes.

We briefly mention the analogy of the DMI as a "effective magnetic field" directed perpendicular to the xz-plane of the thin film [75, 103]. In a effective theory, the in-plane IDMI can be represented as a vector potential which can alter the propagation of magnons. The vector potential $\mathbf{A}_{DMI}$ is defined such that the resulting effective field acts in the plane of the film, according to $\mathbf{H}_{eff} = \nabla \times \mathbf{A}_{DMI}$. The behaviour of the SWs in this effective field is thus analogous to the motion of a charged particle in a magnetic field perpendicular to the film. The subsequent bending of the charged particles trajectory in the plane of the film is the *Hall effect*. In the same manner as the conventional Hall effect, the SWs in the film are deflected due to the DMI-induced effective "magnetic" field. This is dubbed the *magnon hall effect*, one of many types of similar Hall-type phenomena, and has been expreimentally observed [75].

3.0.2 1D modulation and the DMI Kronig-Penney model

To model a simple magnonic crystal, we consider a periodically varying DMI $D(\mathbf{x})$ in the x-direction of a thin film, and disregard the homogeneous DMI d. The modulation has periodicity l, denoted the *DMI lattice constant*, and consists in one

period of two regions of different DMI-strength, D_1, D_2, as shown in fig. 3.4.

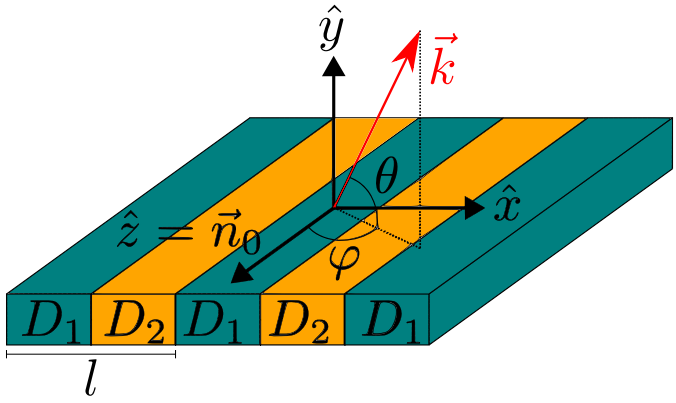

Figure 3.4: Sketch of the magnonic crystal with alternating DMI strengths

We model these regions of varying DMI as square potential steps of finite length $l/2$. This problem can be solved in the same way as a particle in a QM-potential well-problem [115]. The model is a variant of the Kronig-Penney model [45], which is exactly solvable for our simple case.

The periodic DMI is defined as

$$\begin{cases} I: \quad D(x) = D_1, & nl < x \leq (n+\frac{1}{2})l \\ II: \quad D(x) = D_2, & (n+\frac{1}{2})l < x \leq (n+1)l \end{cases} \quad \text{where n =...-2,-1,0,1,2,...}$$

The form of the solution is given by the same procedure as outlined in [45]. We choose to work with RH-modes only. We are thus looking for the solutions of the wave equation

$$\frac{\partial^2 \psi_+}{\partial t^2} = c^2 \left[\nabla^2 - \bar{\mathcal{K}}_z + \bar{H}^2 + 2i\frac{\bar{H}}{c}\partial_t - \frac{i}{2}\left(\bar{\mathcal{D}}(x)\partial_x - \partial_x \bar{\mathcal{D}}(x)\right) \right] \psi_+ \tag{3.5}$$

where, we have dropped a x-sign on ψ. In treating the DMI as a periodic step-potential, we expect to be able to control the band gaps of the spin waves by changing the properties of the modulation, i.e. the square potential profile and amplitude.

To find the RH-dispersion $\omega_+(\mathbf{k})$ for the SW in a periodic potential, we apply *Blochs theorem* [24, 45]. The theorem states that the complete solution ψ of a particle in a periodic potential must consist of a *envelope function* with the periodicity of the potential and a phase depending on the *crystal wave vector* $\mathbf{k}$:

$$\psi_{\mathbf{k}}(\mathbf{r}) = u_{\mathbf{k}}(\mathbf{r}) e^{i\mathbf{k}\cdot\mathbf{r}}$$

For this simple 1D potential, we can use Blochs theorem to match the wavefunctions at specific points in the potential. We can then obtain a analytical solution for the gaps in the frequency spectrum of the spin waves.

For simplicity, consider the 1st period of the inhomogeneous potential, $n = 0$. The solution ansatz for the two regions of DMI is

$$\begin{aligned}\psi(x) &= Ae^{iKx} + Be^{-iKx}\ ;\ 0 < x < l/2,\ D(x) \equiv D_1 \\ \psi(x) &= Ce^{iQx} + De^{-iQx}\ ;\ l/2 < x < l,\ D(x) \equiv D_2\end{aligned} \tag{3.6}$$

The wave vectors $\{K, Q\}$ are the momenta in region I and II respectively. They are found from the RH-version of eq. 3.4, with $K \equiv K(D_1)$ and $Q \equiv Q(D_2)$. We use the definitions from eq. 3.5 in eq. 3.4, so that the expressions for $\{K, Q\}$ reads

$$\{K, Q\} = \{k_1, k_2\} = k_i\ ;\ i = 1, 2$$
$$k_i = \frac{\bar{\mathcal{D}}_i \sin\phi}{2} + \sqrt{\left(\frac{\bar{\mathcal{D}}_i \sin\phi}{2}\right)^2 + (\omega/c - \bar{H})^2 - \bar{\mathcal{K}}_z}$$

where the index i denotes the DMI in region I and II respectively. Thus, $D(x) \equiv D_1$ when $0 < x < l/2$, we have $k_{\pm,i} \equiv K$. Similarly, $D(x) \equiv D_2$ when $l/2 < x < l$, we have $k_{\pm,i} \equiv Q$.

By Blochs theorem, the solutions in the two regions of DMI (eqs. 3.6) has to be related to each other by a phase shift.

$$\psi(l/2 < x < l) = \psi(-l/2 < x < 0)e^{ikl} \tag{3.7}$$

At the DMI step, $x = l/2$, the wavefunctions in each region has to match. The commutator $[D(x), \partial_x] = D(x)\partial_x - \partial_x D(x)$ in the EOM, eq. 3.5, results in a finite difference in the derivatives of the wavefunctions in the regions

$$\begin{aligned}\psi_1(l/2) &= \psi_2(l/2) \\ \left.\frac{d\psi_1}{dx}\right|_{x=l/2} - \left.\frac{d\psi_2}{dx}\right|_{x=l/2} &= \frac{i}{2}\Delta\bar{\mathcal{D}}\sin(\phi)\psi(l/2)\end{aligned} \tag{3.8}$$

where the 2nd condition implies the existence of a accumulated phase due to the effect of the DMI. We have defined $\Delta\bar{\mathcal{D}} = \bar{\mathcal{D}}_2 - \bar{\mathcal{D}}_1$. We note that our definition of $\bar{\mathcal{D}}$ was $\bar{\mathcal{D}} = 2\hbar a \Delta D/N_n J$, where Δ here is the nearest neighbour distance $\Delta = d$.

The constants A, B, C and D in eqs.3.6 is chosen such that the wave function ψ_i and its derivative $\frac{\partial\psi_i}{\partial x}$ is continuous at $x = 0$ and $x = l/2$. We note that these coefficients and their ratios give the transmission and reflection ratios of the spin waves at the potential step,

$$\begin{aligned}\psi_I &= Ie^{ik_1 x}\text{; Incident waves} \\ \psi_R &= A_0 e^{-ik_2 x}\text{; Reflected waves} \\ \psi_T &= B_0 e^{ik_3 x}\text{; Transmitted waves}\end{aligned}$$

with I, A_0, B_0 the wave amplitudes. We will not go further into detail on this. For a simple treatment of reflection and transmission of AFM spin waves for a DMI potential step, we refer to e.g. the supplementary material of [113].

At the point $x = l/2$, we use Bloch's theorem to relate $\psi(l/2)$ to the solution at $\psi(-l/2)$. Including the DMI phase required by the 2$^{\text{nd}}$ condition of eqs. 3.8, we must account for the phase from the DMI in the regions. We thus have that at $x = l/2$, ψ have acquired a phase $e^{i(\bar{\mathcal{D}}_1/2)l/2}$. Using Bloch's theorem to relate $\psi(l/2)$ to $\psi(-l/2)$ with eq. 3.7, we have that the accumulated DMI phase must be $e^{i(\bar{\mathcal{D}}_2/2)(-l/2)}$.

$$x = 0: \quad \begin{Bmatrix} A + B & = C + D \\ iK(A - B) & = iQ(C - D) \end{Bmatrix} \tag{3.9}$$

$$x = l/2: \quad \begin{Bmatrix} (Ae^{iKl/2} + Be^{-iKl/2})e^{i(\bar{\mathcal{D}}_1/2)(l/2)} & = (Ce^{-iQl/2} + De^{iQl/2})e^{ikl}e^{i(\frac{\Delta l}{4})}e^{i(\bar{\mathcal{D}}_2/2)(-l/2)} \\ iK(Ae^{iKl/2} - Be^{-iKl/2})e^{i(\bar{\mathcal{D}}_1/2)l/2} & = iQ(Ce^{-iQl/2} - De^{iQl/2})e^{ikl}e^{i(\bar{\mathcal{D}}_2/2)(-l/2)} \end{Bmatrix} \tag{3.10}$$

We see that we can collect the DMI phases on both sides of eqs. 3.10 in a total phase $e^{-i((\bar{\mathcal{D}}_1+\bar{\mathcal{D}}_2)/4)l}$ at the left side, and define $\sin\phi(\bar{\mathcal{D}}_1 + \bar{\mathcal{D}}_2)/4 \equiv \bar{\mathcal{D}}^*$ for convenience.

We solve the four simultaneous equations of eqs. 3.9 and 3.10 by setting the matrix determinant of the set of equations to zero, which has the form

$$\begin{vmatrix} 1 & 1 & -1 & -1 \\ iK & -iK & -iQ & iQ \\ e^{iKl/2} & e^{-iKl/2} & -e^{-iQl/2}e^{i(k-\bar{\mathcal{D}}^*)l} & -e^{iQl/2}e^{i(k-\bar{\mathcal{D}}^*)l} \\ iKe^{iKl/2} & -iKe^{-iKl/2} & -iQe^{-iQl/2}e^{i(k-\bar{\mathcal{D}}^*)l} & iQe^{iQl/2}e^{i(k-\bar{\mathcal{D}}^*)l} \end{vmatrix} = 0 \tag{3.11}$$

Computing the above determinant and simplifying the exponentials with trigonometric functions, we acquire the result

$$-4\Big[2K\cos(kl + (l\Delta/4A))Q + \sin(Ql/2)\sin(Kl/2)(Q^2 + K^2) \\ -2K\cos(Ql/2)\cos(Kl/2)Q\Big](\cos(kl) + i\sin(kl)) = 0$$

This is equivalent to

$$\cos\left(kl - \frac{\bar{\mathcal{D}}_1 + \bar{\mathcal{D}}_2}{4} l\sin(\phi)\right) = \cos(Ql/2)\cos(Kl/2) - \frac{K^2 + Q^2}{2KQ}\sin(Ql/2)\sin(Kl/2) \tag{3.12}$$

where we have reinserted the definition of $\bar{\mathcal{D}}^*$. Eq. 3.12 is a analytical solution for the band gaps due to the periodic modulation of DMI. The right side (RHS)

is bounded |RHS| ≤ 1, while the left side (LHS) can take on any value if we allow $\{K, Q\}$ to be complex, which is what defines the SW bandgaps. All the spin wave information is encoded in the wavevectors $\{K, Q\}$.

The band gaps occur in the regions where the absolute value of the LHS is greater than 1, implying that the allowed energies of the spin wave must be imaginary. These solutions are "forbidden" for the SW, which is exponentially suppressed in the corresponding regions. This is seen by inserting the complex wavevectors into the solution ansatz in eq. 3.6, which yields exponentially decaying solutions. The properties of the gaps can be modified through the energy/frequency-parameters of the model, and as expected for particle in a periodiv potential, we obtain several bands as we go to higher frequencies ω. For $\phi = 0$, the SWs do not feel the DMI, resulting in $K = Q$. Thus, the LHS of eq. 3.12 reduces to $\cos Ql/2$, or equivalently $\cos Kl/2$. Both sides are now bounded $\in [-1, 1]$, meaning that there can be no complex solutions corresponding to forbidden frequencies via the relation $k(\omega)$, and we expect no band gap except for the one caused by the magnetic field or easy-axis anisotropy.

We again note that we do not consider the transmission and reflection of spin waves with different helicities at the boundary, which is necessary to consider if one wants to examine how the SW polarization changes at e.g. electrical gate [113].

3.1 1D magnonic crystal results

In order to obtain the SW-dispersion for the 1D MC, eq. 3.12 was solved implicitly for the wave vector k: the LHS of the equation was evaluated for a range of frequencies $\omega \in [0, 100]$, and if the frequency yielded a LHS-value $\in [-1, 1]$, the k-value was accepted as a allowed momentum. In all the plots we set $\omega_J = 100$ THz, $\omega_{D_1} = 0$ and $d = 5$ Å. The length of the 1D BZ is $k_b \equiv 2\pi/d$. We will see that the SW-behaviour predicted in sec. 3.0.1 is recreated by the analytical solutions, in addition to the bands gaps due to modulated DMI.

To further investigate the properties of the bandgaps in 1D, we computed gap diagrams in a similar manner as done for FMs [124], see fig. 3.9, 3.10 and 3.11. The band gaps are found by implicit solution of eq. 3.12. We can choose a range of spin wave frequencies ω, insert into the LHS of eq. 3.12, and see if the obtained value is contained in the interval $[-1, 1]$, corresponding to a allowed propagation mode for the SW. If the value is not in the interval, spin wave propagation is exponentially suppressed, and the combinations of parameters and momenta $\{K, Q\}$ constitutes a forbidden SW mode, signalling a gap in the spectrum, which are the black areas of the plots. The gaps are calculated as functions of the angle between $\mathbf{k}$ and the direction of DMI modulation ($\hat{x}$) ϕ, the DMI lattice constant l and DMI strength in one of the regions, D_2. In all the calculations, we take $D_1 = 0$, since the gaps only depend on $\Delta D \equiv |D_2 - D_1|$. We only plot the gap-diagrams for the RH-mode, since the ones for the LH-mode are similar. In the absence of magnetic field H, both modes are equal in terms of the size of the

gaps, with the same gap width for the same values of ΔD, l and K. However, when including a magnetic field, the RH-modes will increase in frequency, while the LH-modes will decrease. Thus, the only difference in the gap-plots, figs. 3.9, 3.10 and 3.11, will be when $H \neq 0$. For example, when $H > 0$ the lowest gap in all the gap-plots for the RH-mode will increase in bandwidth. Since all the bands are increased an equal amount in frequency, the gaps between the higher gaps stay the same, and only the lowest gap will become larger. For LH-modes, the lowest gap will decrease, while all higher gaps will stay the same.

In the calculation, approximate parameters in sensible ranges for AFM materials have been chosen to make the gaps clear, with the definitions of the parameters according to the 1D-column in table 2.7. We will give the frequencies and energies as a fraction of J, since the relevant parameters are the ratios of the interaction strengths.

In fig. 3.5, we observe that the 1^{st} gap has the largest bandwidth, with the 2^{nd} one being narrower, and the 3^{d} being wider than the 2^{nd} one. The frequency bandwidth of the bands are determined by the DMI lattice spacing l, which can be seen by fig. 3.10. For a single value of l, we see that the bandwidth of the gap can increase as we go to higher frequencies. The frequency gaps get asymptotically vertical for higher and higher frequencies.

The analytical 1D result in fig. 3.6 clearly show the effect of the DMI on the low frequency spectrum of the AFM. The spectrum is shifted in k for $D_2 \neq 0$, RH-SWs being shifted towards positive k and opposite for LH-SWs. A in-plane magnetic field $H \neq 0$ in the equilibrium direction $\mathbf{n}_0 \sim \hat{z}$ lifts the degeneracy of the circularly-polarized modes, increasing the frequency of ω_+ and decreasing the frequency for ω_-. The bandgaps are shifted away from the edges of the BZ due to the nonreciprociy-inducing DMI. We stated earlier that the reason for this is that counterpropagating waves of the same frequency no longer have the same quasimomenta $\mathbf{k}$. As a result, the standing spin waves do not necessarily occur at the BZ edge. We can see that the nonreciprocity increases and the frequency of the SWs decreases as D gets larger, in addition to increasing the gap width, in fig. 3.7.

In fig. 3.8, the dispersion is plotted in the absence of easy-axis-anisotropy, magnetic field and DMI. The lowest band is gapless, with the expected linear dispersion for AFM-SWs in the absence of anisotropy. The model for the SWs is built on the assumption that we are working in the long-wavelength limit, meaning small wavenumbers k. In this regime, the SW-dispersion is linear in k right up to the BZ-edge.

Fig. 3.9 shows that the width of the bandgaps increases as the direction of propagation is directed in x-direction, with the full effect of the modulation on the SWs when $\theta = \pi/2$, meaning $\mathbf{k} = (k_x, 0)$. The lowest gap comes from the easy-axis anisotropy of the system. The result in fig. 3.10 is similar to the one obtained for periodic variation of DMI in FMs [124]. As argued in the reference, as the lattice spacing increases, the domain where spin waves are exposed to the DMI increases. This amounts to a larger potential barrier for the spin waves, in turn making the allowed bands narrower. The behaviour of the band gaps exhibited in fig. 3.11 is

also as expected. As the DMI energy increases, we see that the lowest spin wave band gap approaches 0, signalling the transition to a spiral state, in which our assumption of harmonic, low energy excitations are invalid. This threshold value in the absence of magnetic field is given by $D_{th} = \sqrt{JK_z}$.

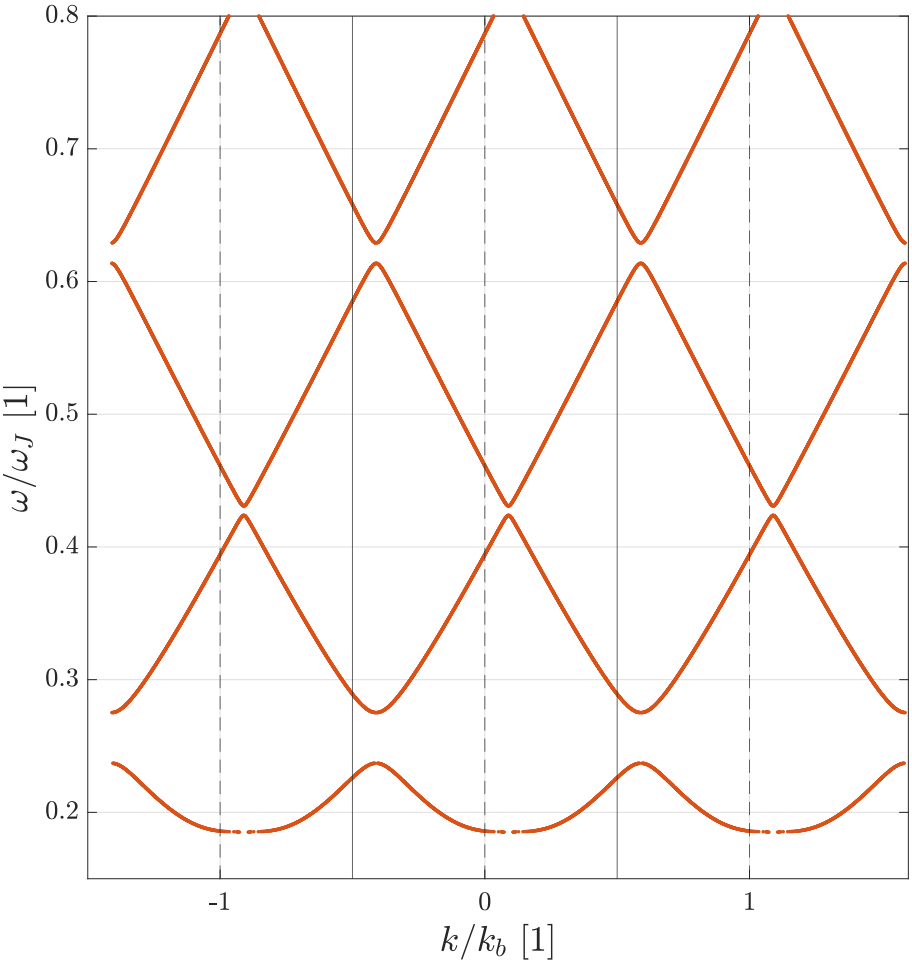

Figure 3.5: 1D dispersion relation for the RH-mode, with $D_2/J = 1/10$, $K/J = 1/10$, $H = 0$ and $l = 10$ nm. The solid lines represent the edges of the BZ, $k_b/2$, and the perforated lines are the center of the neighbouring BZs. The gap between the 1. and 2. band is of the order ~ 0.5 THz. As l is increased, the bands flatten and the bandgaps decreases. We will come back to this in chap. 4.

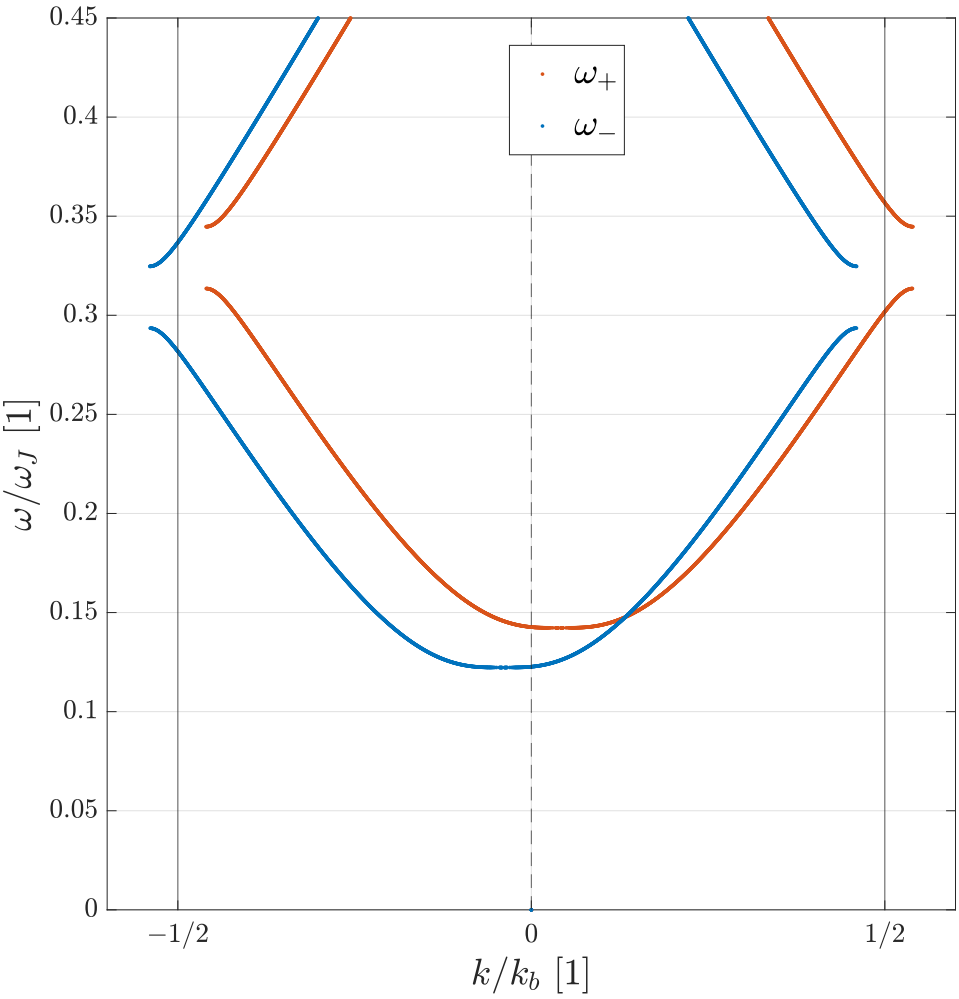

Figure 3.6: Right- (ω_+) and left-handed (ω_-) spin waves where the degeneracy in ω is split by a magnetic field $\omega_H = 1.5$ THz ($H/J = 0.015$), and the k-degeneracy is lifted by the modulated DMI. We set $K/J = 1/20$ and $D_2/J = 1/10$. The dispersion relation is nonreciprocal in both modes, which is evident from the "tilt" away from $k = 0$.

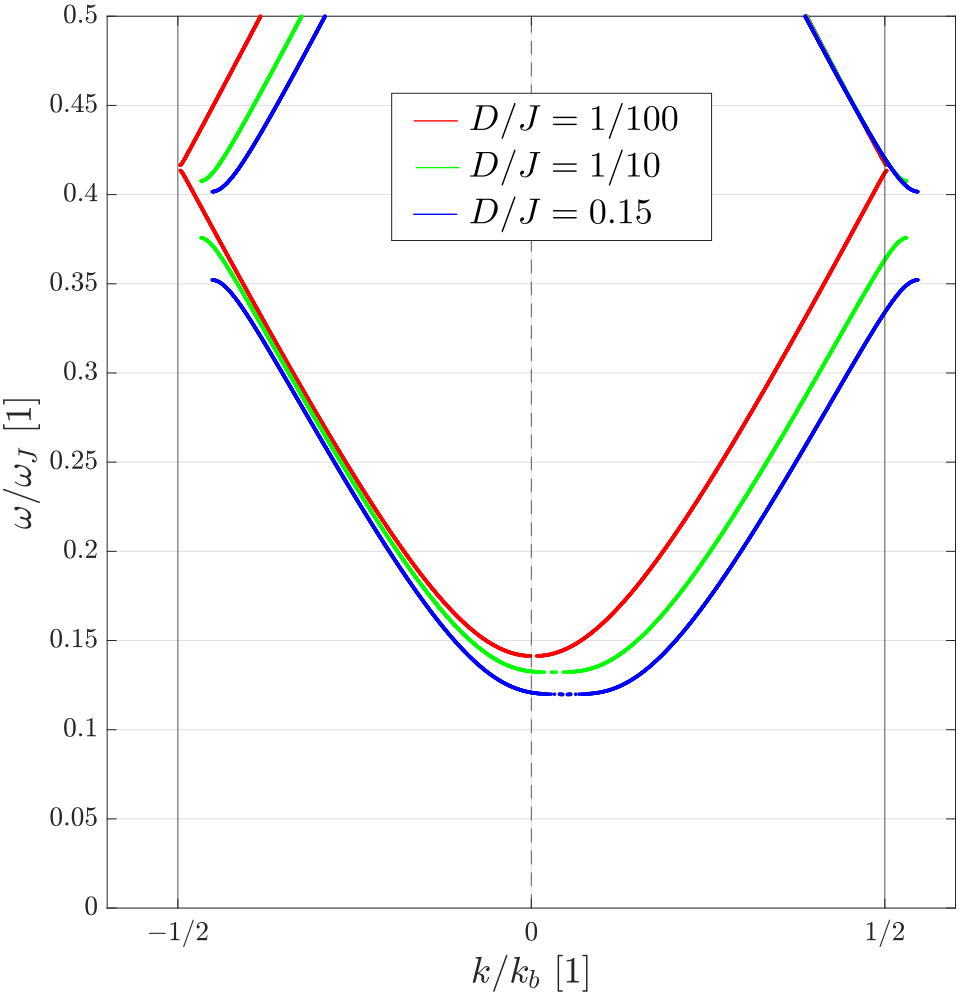

Figure 3.7: ω_+-mode plotted for different values of ω_{D_2}. We set l = 8 nm and K/J = 1/20, the rest of the parameters are as in fig. 3.5.

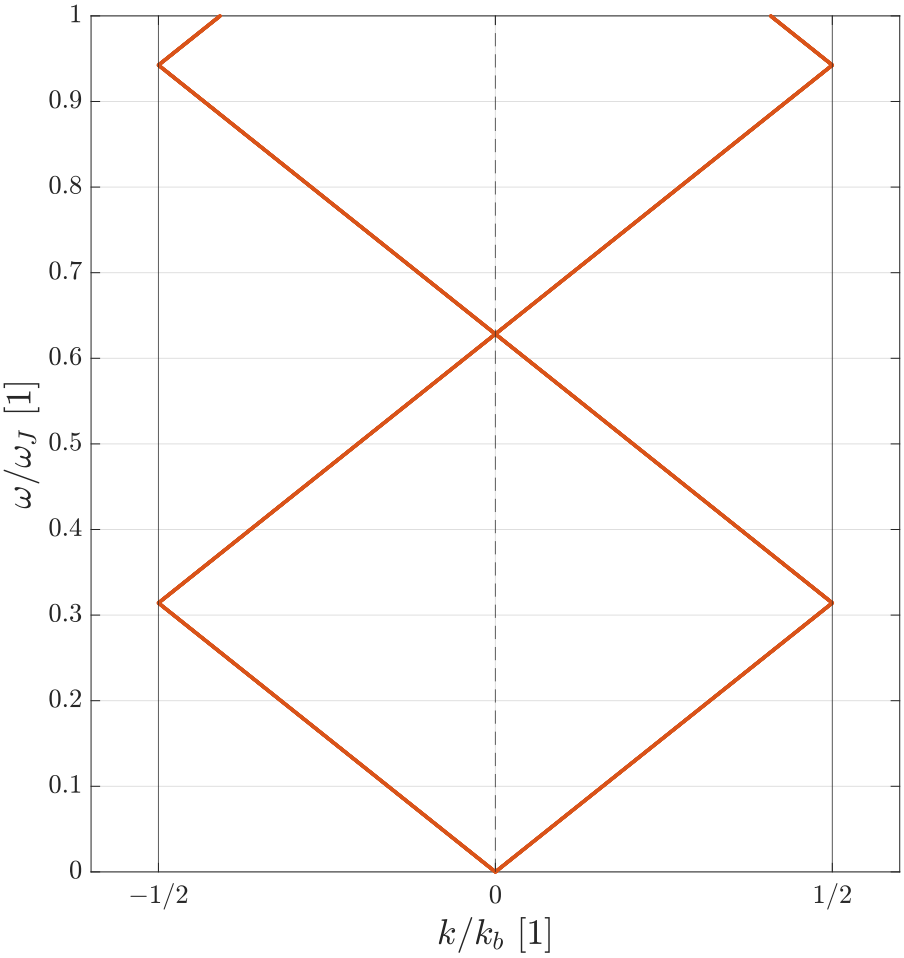

Figure 3.8: The ω_+-mode with $K = D_2 = H = 0$, and the rest of the parameters as in fig. 3.5.

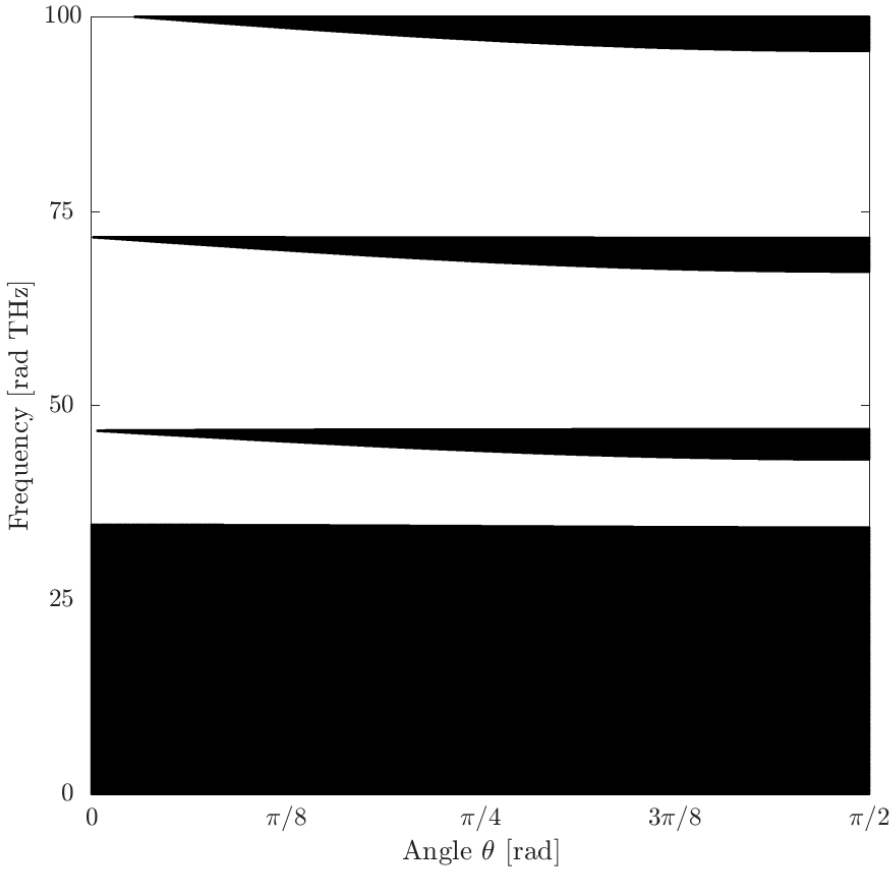

Figure 3.9: AFM spin wave frequency gaps for a 1D magnonic crystal as a function of the angle $\theta \in [0, \pi/2]$. The parameters are $l = 10$ nm, $K/J = 3/100$ and $D_2/J = 1/10$. As the momentum-component in the direction of DMI-modulation increases, the effect of the periodic potential increases up to a maximum value at $\pi/2$. As is confirmed by fig. 3.9, when $\theta = 0$, the propagation direction is perpendicular to the periodic DMI, and the potential felt by the spin waves is constant. This does not give rise to magnonic band gaps.

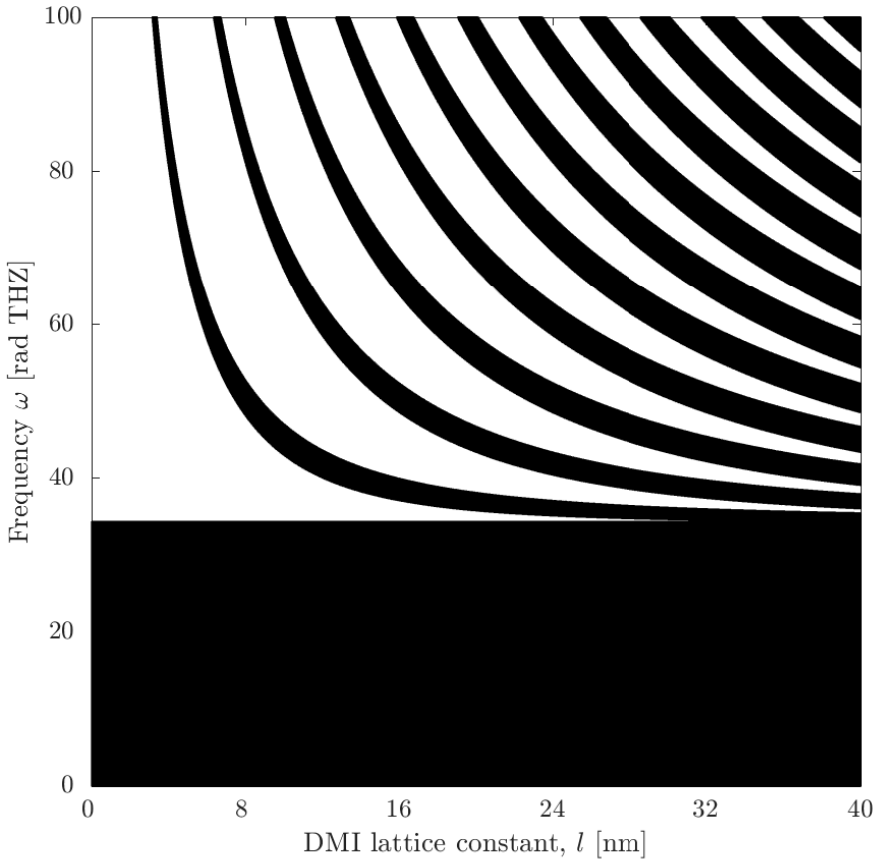

Figure 3.10: Frequency gaps as a function of the DMI lattice parameter $l \in [0, 40]$ nm, with each consecutive region of DMI $D1$, $D2$ having the length $l/2$. The parameters are $\theta = \pi/2$, and $K/J = 3/100$ and $D_2/J = 1/10$. The lowest gap between $\omega_0 \sim 0 - 35$ THz. We see that there is a range of $l \sim 0 - 4$ nm where there no bandgaps allowed. Increasing D_2 makes the "thin" band-gap-lines thicker, meaning larger bandgaps.

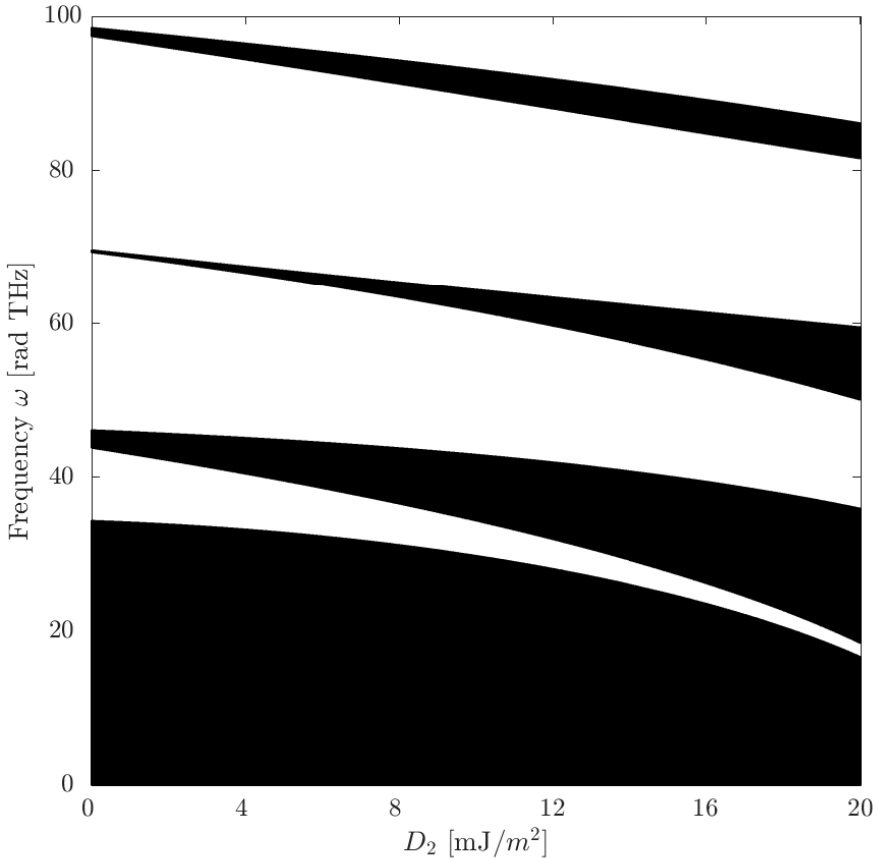

Figure 3.11: Frequency gaps as a function of the DMI strength $\omega_{D_2} \in [5, 30]$ THz. The parameters are $\theta = \pi/2$, $l = 10$ nm and and $K/J = 3/100$. We have plotted the DMI in units of energy averaged of a area d^2.

CHAPTER 4

2D MAGNONIC CRYSTAL AND THE PLANE WAVE EXPANSION

In this chapter, we will construct a 2D MC-model, and investigate the associated dispersion of spin waves subject to spatially modulated inhomogeneous DMI. In chap. 3, we considered a particularly simple potential, which allowed us to solve the problem analytically. In general, there are several methods to obtain the dispersion of the spin waves in such a periodic system. A especially popular routine for obtaining band structures for MCs which, we will utilize a version of, is the so-called *plane wave method* (PWM) [57]. We will use the similar *plane wave expansion* (PWE), or *multiband envelope function method* [40]. Simulation methods like the *Dormand-Prince method*, which solves the differential equation by e.g. Runge-Kutta-methods, can also be used to obtain the dynamics and frequency spectrum of the system. However, we are interested in the dispersion of the spin waves of a continuum model, with the assumption of dissipationless dynamics. In this "free" spin wave regime, a suitable number of plane waves is expected to yield good results.

PWM and PWE uses the same principle when obtaining the frequency-momentum-relations of a system: the periodic parameters of the problem, e.g. magnetization or exchange stiffness (in our case the IDMI), are described by a plane wave expansion in reciprocal lattice vectors by virtue of Blochs theorem [40]. One calculates the Fourier components, insert the expansions into the EOMs, and formulate a eigenvalue problem which is readily solvable by numerical methods. The advantage of the PWE is its ability to describe arbitrarily shaped scattering-centers [57], and the effects of crystal strain and electric fields can be included analytically through the Fourier coefficients [40]. PWE forgoes the calculation full spatial distribution of the potential, which means lower computational expense.

4.1 General formulation of PWM

We start out with a review of some concepts from solid state theory, and a bit more thorough review of Bloch's theorem than in chapter 3.

Bloch's theorem states that the wavefunction of a particle $\mathbf{\Psi}(\mathbf{r})$ in a periodic potential can be written as the product of a function with the periodicity of the real space potential and a phase factor

$$\mathbf{\Psi}_{\mathbf{k}}(\mathbf{r}) = u_{\mathbf{k}}(\mathbf{r})e^{i\mathbf{k}\cdot\mathbf{r}} \tag{4.1}$$

where the *envelope function* $u(\mathbf{r})$ has the periodicity of the lattice, and $e^{i\mathbf{k}\cdot\mathbf{r}}$ is a

momentum-dependent phase. These *Bloch waves* satisfy the condition

$$\mathbf{\Psi}_{\mathbf{k}}(\mathbf{r}+\mathbf{R}) \;=\; \mathbf{\Psi}_{\mathbf{k}}(\mathbf{r}) \tag{4.2}$$

which can readily be proven [45]. Here, $\mathbf{R} = h\mathbf{a}_1 + k\mathbf{a}_2 + l\mathbf{a}_3$ is a arbitrary lattice vector, $\{h,k,l\}$ are integers and $\{\mathbf{a}_i\}$ is a set of basis vectors or *primitive lattice vectors*. $\mathbf{k}$ is a wave vector defined in 1$^{\text{st}}$ Brillouin zone (1BZ), where $\mathbf{k}$ is a quasi-momentum, or crystal momentum. We label every function $u(\mathbf{r})$ with a unique $\mathbf{k}$-vector, since all $\mathbf{k}$ can be translated back to the 1BZ by a suitable reciprocal lattice vector $\mathbf{G}$.

The envelope functions $u_{\mathbf{k}}$ with the periodicity of the real lattice can be expanded in a (formally) infinite Fourier series in $\mathbf{G}$.

$$\mathbf{\Psi}_{\mathbf{k}}(\mathbf{r}) \;=\; u_{\mathbf{k}}(\mathbf{r})e^{i\mathbf{k}\cdot\mathbf{r}} = \sum_{\mathbf{G}} c_{\mathbf{k}}(\mathbf{G})e^{i\mathbf{G}\cdot\mathbf{r}}e^{i\mathbf{k}\cdot\mathbf{r}} = \sum_{\mathbf{G}} c_{\mathbf{k}}(\mathbf{G})e^{i(\mathbf{G}+\mathbf{k})\cdot\mathbf{r}} \tag{4.3}$$

where $a_{\mathbf{k}}(\mathbf{G})$ are expansion coefficients and $e^{i\mathbf{G}\cdot\mathbf{r}}$ a phase factor.

In practice, one imposes a cutoff on the number of lattice vectors $\mathbf{G}$ considered in the calculation, which we will return to later in this chapter. Blochs theorem and the expansion of periodic functions in reciprocal space are essential parts of the PWE. In our case, the expression will be simpler than for the treatment of e.g. quantum dot-lattices or band structures of complicated compounds like e.g. germanium or gallium arsenide [114], which the PWE can be very well suited for. We will follow [40] in this section.

The PWE-method solves the eigenvalue problem $\hat{\mathbf{H}}\mathbf{\Psi} = E\mathbf{\Psi}$, where $\hat{\mathbf{H}}$ is some effective Hamiltonian depending on the bands N. We split the effective Hamiltonian into two parts

$$\hat{\mathbf{H}} \;=\; \hat{\mathbf{H}}_0 + \hat{\mathbf{V}}$$

where $\hat{\mathbf{H}}_0$ is the "unperturbed" Hamiltonian without modulation. The diagonalization of the matrix representation of $\hat{\mathbf{H}}_0$ with a suitable basis set yield the eigenvalues of the non-modulated system when acting on the states ψ. $\hat{\mathbf{V}}$ is the "perturbation" of the effective Hamiltonian. The matrix elements of $\hat{\mathbf{V}}$ describes the effect of the periodic modulation of parameters on the particles. In PWE, the eigenstates of $\hat{\mathbf{H}}_0$ are chosen as the basis states of the expansion.

A general set of such eigenstates can be given in a general Bloch-form as

$$\psi_{\mathbf{k},l,s}(\mathbf{r}) \;=\; \sum_{i=1}^{N} A_i^s(\mathbf{k},l)u_{\mathbf{k},i}(\mathbf{r})e^{i(\mathbf{k}+\mathbf{G}_l)\cdot\mathbf{r}} \tag{4.4}$$

$A_i^s(\mathbf{k},l)$ is a function which depends on the type of state s we treat (e.g. degenerate electron, holes etc.). $u_i(\mathbf{r})$ are the envelope functions describing the periodicity of the lattice potential, $\mathbf{k}$ is the crystal/quasi-momentum and $\mathbf{G}_l$ is some reciprocal lattice vector labeled by the index l. The set $\{\mathbf{G}_l\}$ describes the superlattice of scattering centers, with the label l denoting their locations in k-space in one, two or

three dimensions according to some arbitrary sorting scheme. The index i labels the Bloch-functions, and thus also labels the energy bands.

A wavefunction $\mathbf{\Psi_k}$ for each value of the quasimomentum $\mathbf{k}$ allowed by the Born-von-Karman boundary condition [24] satisfying the full eigenvalue problem is given by a linear combination of the basis states $\psi_{\mathbf{k},l,s}$

$$\mathbf{\Psi_k}(\mathbf{r}) = \sum_S \sum_l C_{\mathbf{k},l,s}\psi_{\mathbf{k},l,s}(\mathbf{r}) \tag{4.5}$$

With the eigenstates of the above form and some operator $\hat{\mathbf{H}}$, one seeks a matrix $\mathbf{M}$ which is subsequently diagonalized. The eigenvalues are the energies of the system, and the obtained coefficients $C_{\mathbf{k},l,s}$ are the eigenvectors of $\mathbf{M}$. The matrix $\mathbf{M}$ can be stated in general form as

$$\mathbf{M}_{\mathbf{k},l,l'} = \langle \mathbf{\Psi}_{\mathbf{k}}^{l',s'} | \hat{\mathbf{H}} | \mathbf{\Psi}_{\mathbf{k}}^{l,s} \rangle = E_l(\mathbf{k}-\mathbf{G}_l)\delta_{S,S'}\delta_{l,l'} + \sum_{i,i'}^{N} (u^{\mathbf{k}}_{i',S',l'})^* u^{\mathbf{k}}_{i,S,l} V'_{S,S',i,i'}{}^{\mathbf{k}}(l,l') \tag{4.6}$$

where the set of quantum numbers $\{\mathbf{k}, l, l'\}$ denote the quasimomentum $\mathbf{k}$ and the plane wave states l and l', and N is the number of Bloch/envelope functions. In the PW-basis, $\mathbf{M}$ is diagonal in the quantum numbers $\{\mathbf{k}, l, l'\}$ in the absence of periodic modulation, since the scattering centers located at $\{\mathbf{G}_l\}$ disappear from the problem. E_l are the eigenvalues of the unmodulated operator $\hat{\mathbf{H}}$, with l denoting the set of energy bands generated by translations of $\mathbf{G}$ in the reciprocal lattice of the potential. The matrix elements of the potential $V'_{S,S',i,i'}{}^{\mathbf{k}}(l,l')$ are given by

$$V'_{S,S',i,i'}{}^{\mathbf{k}}(l,l') = \frac{1}{V_C}\int_\Omega d\mathbf{r}\; e^{i(\mathbf{G}_{l'}\cdot\mathbf{r})}\,\hat{\mathbf{V}}\,e^{-i(\mathbf{G}_l\cdot\mathbf{r})} \tag{4.7}$$

In summary, the method is very similar to solving the Schrödinger-equation for a electron in a periodic potential [45]: the PWE-method can simply be seen as representing an operator in a plane wave basis set, where the information about the scattering centers of the potential are encoded in reciprocal lattice vectors. In section 4.2, we will greatly simplify the general equations above. As mentioned, a essential part of the PWE is to be expand the periodic crystal potential in a Fourier series, which in our case will be an expansion of the modulated DMI $D(\mathbf{r})$.

$$D(\mathbf{r}) = \sum_{\mathbf{G}} D_{\mathbf{G}} e^{i\mathbf{G}\cdot\mathbf{r}} \tag{4.8}$$

We will return to this shortly.

4.2 PWE for AFM spin waves

In the case of non-interacting AFM spin waves in the continuum, the representation of the system is reducible, and the R/L-handed SW precessional modes

decouple. Since the states do not mix, we can diagonalize the matrix representations of the effective KG-operator, the bracket in eq. 2.44, acting on the two helicities separately. Spin s is not part of our continuum approach, and is disregarded. Denoting the effective KG-operator for right- and left-handed spin waves as $\hat{\mathcal{H}}$ and $\hat{\mathcal{H}}^\dagger$ respectively, we can express eq. 2.44 as a matrix equation with the matrix operator $\hat{\mathbb{H}}$ as

$$\hat{\mathbb{H}}\Psi_{\mathbf{k}}(\mathbf{r}) = \begin{bmatrix} \hat{\mathcal{H}} & 0 \\ 0 & \hat{\mathcal{H}}^\dagger \end{bmatrix} \begin{bmatrix} \psi^+_{\mathbf{k}}(\mathbf{r}) \\ \psi^-_{\mathbf{k}}(\mathbf{r}) \end{bmatrix} = \omega^2 \Psi_{\mathbf{k}}(\mathbf{r}) \tag{4.9}$$

In applying the PWE-method as described in the previous section, the operators $\hat{\mathcal{H}}$, $\hat{\mathcal{H}}^\dagger$ are represented as part of the matrix in eq. 4.6.

We now formulate the general eigenvalue problem for spin waves in a 2D AFM thin film. The equation of motion for the spin waves from chapter 2 is

$$\frac{\partial^2 \psi}{\partial t^2} = c^2 \left[\nabla^2 - \bar{\mathcal{K}}_z + \bar{H}^2 + 2i\sigma_3 \frac{\bar{H}}{c}\partial_t - \frac{i\sigma_3}{2}\left(\bar{\mathcal{D}}(\mathbf{r})\partial_i - \partial_i \bar{\mathcal{D}}(\mathbf{r})\right) \right] \begin{bmatrix} \psi_+ \\ \psi_- \end{bmatrix} \tag{4.10}$$

where as earlier, we take $\bar{\mathcal{D}}(\mathbf{r})$ to consist of a homogeneous background and spatially modulated part: $\bar{\mathcal{D}}(\mathbf{r}) = d_h + \bar{\mathcal{D}}(\mathbf{r})$. We again remind that the homogeneous DMI d_h is redefined in the same manner as $D(\mathbf{r}) \to \bar{\mathcal{D}}(\mathbf{r})$, see the discussion after eq. 2.44.

For simplicity, we drop the spin-wave phase velocity c^2 from the notation, and leave out the easy-axis anisotropy $\bar{\mathcal{K}}$, since it will only amount to a additive constant on the diagonal of $\mathbf{M}$. We also set the magnetic field parameter $\bar{H}$ to zero for now. We choose to work with the RH-mode ψ_+ for now, since the expressions for the LH-mode are similar. We change notation $\psi_+ \to \Psi_+$ to separate the Bloch eigenstates ψ_+ and the complete solution Ψ_+ in a periodic potential.

To keep the notation simple, we define the "simplified" operator $c^2\hat{\mathcal{H}} \equiv \hat{\mathcal{H}}$. We choose to keep the +-label in Ψ. We thus work with the operator

$$\begin{aligned} \hat{\mathcal{H}}\Psi_+(\mathbf{r}) &= \left[\nabla^2 - \frac{i}{2}(\bar{\mathcal{D}}(\mathbf{r})\partial_x - \partial_x \bar{\mathcal{D}}(\mathbf{r})) \right] \Psi_+(\mathbf{r}) \\ &= \left[\hat{\mathcal{H}}_0 + \hat{\mathcal{H}}_1 \right] \Psi_+(\mathbf{r}) \\ &= \omega_+^2 \Psi_+(\mathbf{r}) \end{aligned} \tag{4.11}$$

where we have split the operator $\hat{\mathcal{H}}$ into a unmodulated part $\hat{\mathcal{H}}_0$ and a part $\hat{\mathcal{H}}_1$ containing the modulation of the DMI

$$\begin{aligned} \hat{\mathcal{H}}_0 &= \nabla^2 - \frac{i}{2} d_h \partial_x \\ \hat{\mathcal{H}}_1 &= -\frac{i}{2}\left[\bar{\mathcal{D}}(\mathbf{r})\partial_x - \partial_x \bar{\mathcal{D}}(\mathbf{r}) \right] \end{aligned}$$

Note that now, $\bar{\mathcal{D}}(\mathbf{r})$ includes only the spatially modulated DMI, since we included d_h in the operator $\hat{\mathcal{H}}$. We assume that all states are of the same type in all of

the bands, so we ignore the state-specific function $A_i^S(\mathbf{k}, l)$ and only consider the envelope function and the phase factor. This approximation would be a clear point of improvement for the model, since the spin wave bands will in many cases be degenerate or closely spaced. We will return to them later in the thesis, but not for a especially rigorous treatment.

In the presence of a 2D magnonic superlattice described by the modulation part $\hat{\mathcal{H}}$, the complete eigenstates is taken to be a linear superposition of Bloch eigenstates

$$\Psi(\mathbf{r})^+_{\mathbf{k}_{nm}} = \sum_{nm} \psi^+_{nm}(\mathbf{r}) = \sum_{nm} c_{nm}(\mathbf{k}_{nm}) e^{i\mathbf{k}_{nm}\cdot\mathbf{r}} \tag{4.12}$$

We denote $\mathbf{k}_{nm} = \mathbf{k} - \mathbf{G}_{nm} = (k_x - G_n, k_z - G_m)$. $\{G_n, G_m\}$ describes the periodic lattice, giving the location of equivalent k-points in the magnonic superlattice potential in k-space. For simplicity, we will refer to the x- and z-components of $\mathbf{k}_{nm}$ as k_n and k_m respectively.

We now introduce new labels and a sorting scheme, see e.g. [117], for the PW-states labeled by different combinations of n and m to reduce notational clutter. In 2D, each state is labeled by two integers $\{n, m\}$, where the indices represent the number of translations by $2\pi n/l_x = b_n$ and $2\pi m/l_z = b_m$ in the potential. Here, l_x and l_z are the lattice spacing in the two directions. We will take this spacing to be equal in all directions, $l_x = l_z = l$.

We choose to sort the states using a single index $l \sim (n, m)$, not to be confused with the lattice spacing l (which one we refer to will be clear by the context). With $n, m = 0, \pm 1, \pm 2, ...$, we write a state as (n, m), referring to the b_n, b_m lattice-vector translations in the modulation. To obtain the set of states, we let one of the indices, say n, take a value, and let the index m run over all possible values $\{-N, -N+1, ...N-1, N\}$. The number of values N is fixed by the number of reciprocal lattice vectors needed for a adequate description of the periodic crystal potential, since we need to impose a cutoff on the formally infinite Fourier expansion of the periodic modulation $D(\mathbf{r})$.

In 1D, sorting from the lowest energy states to the highest , it would suffice to convert from the $(0, 1, 2, 3, ..., N)$ to the sorted values $(0, 1, -1, 2, -2, ..., N)$ with the formula

$$n = \frac{1 + (-1)^n (2n - 1)}{4} \tag{4.13}$$

In 2D, we choose the sorting integer l to sort after increasing magnitude of $\mathbf{G}_{nm}$. Thus, we choose $l^2 = n^2 + m^2$ as single label for the states. $\{n, m\}$ can take on $2N+1$ values $[-N, \ldots, N]$, meaning that in 2D, we have $(2N+1)^2$ states denoted by the index l. Sorting by the integer l^2 in increasing magnitude, we obtain the sequence

$$\begin{aligned}(n, m) &= (0,0), (0,1), (0,-1), (1,0), (-1,0), (1,1), ... \\ &\rightarrow l = 1, 2, 3, 4, ...\end{aligned} \tag{4.14}$$

For example, the state $l = 3$ represents $(0, -1)$. This ordering scheme is convenient for the numerical calculation. These l's will serve as a label the different spin wave

energy bands. We thus alter our notation $(n,m) \to l$, with the same substitution for the primed labels. This means $\mathbf{k}_{nm} \to \mathbf{k}_l = \mathbf{k} - \mathbf{G}_l$, where each l labels some pair (n,m), denoting the number of translations by the primitive reciprocal lattice vectors $\{\mathbf{b}_1, \mathbf{b}_2\}$ (which we will return to shortly), since every $\mathbf{G}$ is a combination of a these two vectors.

To obtain a algebraic expression, commonly called the *central equation*, for the coefficients $c_{nm}(\mathbf{k}_{nm}) \to c_l(\mathbf{k}_l)$ of the expansion in eq. 4.12, we multiply the operator acting on the states $\hat{\mathcal{H}}'\Psi^+_{\mathbf{k}_l}$ from the left by the adjoint wavefunction $\left(\Psi^+_{\mathbf{k}_{l'}}\right)^*$ and integrate over all space. The result is an algebraic equation for the coefficients c_l

$$\sum_l \Big[(E^0_l(\mathbf{k}_l) - \lambda(\mathbf{k}))\delta_{ll'} + \hat{\mathcal{H}}^1_{ll'}\Big] c_l(\mathbf{k}_l) \;=\; 0 \tag{4.15}$$

where, as mentioned earlier, the spin has been dropped from the problem. E^0_l are the eigenvalues of the operator $\hat{\mathcal{H}}_0$ with $\mathbf{k} \to \mathbf{k}_l$, λ are the eigenvalues of the complete system which we seek, and $\hat{\mathcal{H}}^1_{ll'}$ is given by the matrix elements $\langle\psi^+_{l'}|\hat{\mathcal{H}}^1|\psi^+_l\rangle$. Computing the diagonal elements $E^0_l\delta_{ll'}$, we simply get

$$\begin{aligned}
\langle\psi^+_{l'}|\hat{\mathcal{H}}_0|\psi^+_l\rangle &= \sum_{ll'}\int_{V_c} d\mathbf{r}\; e^{-ik_{l'}\cdot\mathbf{r}}[\nabla^2 - \frac{i}{2}d_h\partial_x]e^{i\mathbf{k}_l\cdot\mathbf{r}} \\
&= \sum_{ll'}\Big[-k_l^2 + d_h(k_l)_x\Big]\int dxdy\; e^{i(\mathbf{G}_l - \mathbf{G}_{l'})\cdot\mathbf{r}} \\
&= \Big[-k_l^2 + d_h(k_l)_x\Big]\delta_{ll'}
\end{aligned}$$

The matrix elements of the periodic DMI modulation is given by

$$\begin{aligned}
\langle\psi^+_{l'}|\hat{\mathcal{H}}_1|\psi^+_l\rangle &= \sum_{ll'}\int d\mathbf{r}\; e^{-i\mathbf{k}_{l'}\cdot\mathbf{r}}\left[-\frac{i}{2}\Big(\bar{\mathcal{D}}(\mathbf{r})\partial_x - \partial_x\bar{\mathcal{D}}(\mathbf{r})\Big)\right]e^{i\mathbf{k}_l\cdot\mathbf{r}} \\
&= \frac{1}{2}\Big\{\bar{\mathcal{D}}_{ll'}(\mathbf{k}_l)_x + i(\partial_x\bar{\mathcal{D}})_{ll'}\Big\}
\end{aligned} \tag{4.16}$$

where the matrix elements of the DMI $\bar{\mathcal{D}}(\mathbf{r})$ and the derivative of the DMI $\partial_x\bar{\mathcal{D}}(\mathbf{r})$ depends on the form of the modulation. Thus, with the sorting order described

above, we can restate the algebraic equation 4.15 for the coefficients c_l as

$$\mathbf{M}_{ll'}c_l(\mathbf{k}_l) = \begin{pmatrix} (\mathbf{k}-\mathbf{G}_1)^2+\sigma_1 & \bar{\mathcal{D}}_{12} & \cdots & \bar{\mathcal{D}}_{1N} \\ \bar{\mathcal{D}}_{21} & (\mathbf{k}-\mathbf{G}_2)^2+\sigma_2 & \cdots & \bar{\mathcal{D}}_{2N} \\ \vdots & \vdots & \ddots & \vdots \\ \bar{\mathcal{D}}_{N1} & \bar{\mathcal{D}}_{22} & \cdots & (\mathbf{k}-\mathbf{G}_N)^2+\sigma_N \end{pmatrix} \begin{pmatrix} c_1(\mathbf{k}_1) \\ c_2(\mathbf{k}_2) \\ \vdots \\ c_N(\mathbf{k}_N) \end{pmatrix} \tag{4.17}$$

$$= \omega^{*2} \begin{pmatrix} c_1(\mathbf{k}_1) \\ c_2(\mathbf{k}_2) \\ \vdots \\ c_N(\mathbf{k}_N) \end{pmatrix} \tag{4.18}$$

where $\{l, l'\} = 1, 2, 3 \ldots, N$ are the PW-state labels. Consequentially, N marks the cutoff for the number of PW-states included in the calculation.

We follow [40] for a discussion on this cutoff: the maximal number of PWs that can be included in the calculation is physically restricted by the number of crystal layers in a given direction in the magnonic crystal. This is the case since we cannot have scattering contributions from more points than there are lattice sites. Thus, we have condition $N_i^{max} < l_i/d_i$ along the direction i, with l the DMI lattice spacing and d the nearest neighbour distance. The PWE-method is in general only valid when the envelope function of the Bloch-solution, the u in eq. 4.4 which is periodic in the lattice potential, varies smoothly over distances comparable to the nearest neighbour lattice constant d_i. A more rapidly varying crystal potential, corresponding to a more rapid variation in u, needs more Fourier components to adequately describe, meaning more plane waves are required.

As a result, wavevectors with magnitude $k_i > 2\pi/d_i$ should be neglected, since they are deemed very large, and should only make a small contribution to the effective SW-equation. We can thus formulate a condition of validity for the PWE: if the number of PWs needed to calculate the wave function along a specific direction in the crystal (with respect to some tolerance level) is less than N_i^{max}, then the PWE-method is well suited for the problem. For the parameters used in this thesis, $l/d \sim 40$. We use $\sim 25-50$ plane waves corresponding to the nearest neighbouring reciprocal lattice points, meaning a cutoff $|\mathbf{G}_{cutoff}| \sim 2-3k_b$, with $k_b = 2\pi/l$.

Convergence is not checked in this thesis. However, the potential we will use to describe the lattice, a 2D cosine potential, only has one Fourier component. Since the number of PWs needed is determined by the number of Fourier components, we can safely assume that our relatively low-cutoff is sufficient for showing the effects of the modulation on the lowest bands.

With eq. 4.17, we have obtained $\mathbf{M}$, which was stated in general form in eq. 4.6, and the arbitrary state labels l has been defined and connected to the labels

of our potential problem. We have also defined the matrix elements

$$\begin{aligned} \sigma_l &\equiv \bar{\mathcal{K}} - d_h(\mathbf{k}_l \cdot \hat{x}) \\ \bar{\mathcal{D}}_{ll'} &\equiv \frac{1}{2}\left[\bar{\mathcal{D}}_{ll'}(\mathbf{k}_l \cdot \hat{x}) + i(\partial_x \bar{\mathcal{D}})_{ll'}\right] \end{aligned} \tag{4.19}$$

where we also reintroduced the anisotropy parameter $\bar{\mathcal{K}}$ along the diagonal. Remember that we left out a factor c^2 which should be multiply all the matrix elements. The set of coefficients c_l are found by the diagonalization of the matrix $\mathbf{M}_{ll'}$, which yields the eigenvectors and energy spectrum of the system. We note that one can use any sorting order of the states when diagonalizing the matrix $\mathbf{M}_{ll'}$, as long as the sorting along the diagonal is consistent with the off-diagonal elements. The matrix elements of the potential $\bar{\mathcal{D}}_{ll'}$ can be found by considering eq. 4.7. We obtain the matrix elements for a specified potential in app. D by directly taking the Fourier transform of the DMI-part of the KGE acting on the SW-solution Ψ.

4.2.1 Inclusion of magnetic field

We now include the magnetic field H. In the presence of a magnetic field, the effective SW equation 4.11 reads

$$\begin{aligned} \hat{\mathcal{H}}\Psi_+(\mathbf{r}) &= \left[\nabla^2 + \bar{H}^2 + 2i\frac{\bar{H}}{c}\partial_t - \frac{i}{2}(\bar{\mathcal{D}}(\mathbf{r})\partial_x - \partial_x\bar{\mathcal{D}}(\mathbf{r}))\right]\Psi_+(\mathbf{r}) \\ &= \left[\hat{\mathcal{H}}_0^{\bar{H}} + \hat{\mathcal{H}}_1\right]\Psi_+(\mathbf{r}) \\ &= {\omega_+^*}^2\Psi_+(\mathbf{r}) \end{aligned}$$

with the operators

$$\hat{\mathcal{H}}_0^{\bar{H}} = \left[\nabla^2 + \bar{H}^2 + 2i\frac{\bar{H}}{c}\partial_t - \frac{i}{2}\bar{d}\partial_x\right]$$

where we labeled the frequency ω_+^* to denote the inclusion of the magnetic field, and the operator $\hat{\mathcal{H}}_1$ is the same as before. Assuming the time dependence of the SWs to be $\Psi_+(t) \propto e^{i\omega t}$, we can restate the problem as a *quadratic polynomial eigenvalue problem* for the eigenvalues ω_+^*. [42]

$$\left\{{\omega^*}^2 - 2\frac{\bar{H}}{c}\omega^* - \left[\nabla^2 + \bar{H}^2 - \frac{i}{2}(\bar{\mathcal{D}}(\mathbf{r})\partial_x - \partial_x\bar{\mathcal{D}}(\mathbf{r}))\right]\right\}\Psi_+(\mathbf{r}) = 0$$

The problem now has the form of a quadratic eigenvalue problem

$$\begin{aligned} (M_2\lambda^2 + M_1\lambda^1 + M_0) &= 0 \\ \lambda &= \omega_+^* \end{aligned}$$

with $\{M_0, M_1, M_2\}$ being matrices and the λ the eigenvalue. Taking the complete eigenstates to be a linear combination of Bloch states as before, and expressing the above equation in matrix form in the same way as in the last subsection, we get that the matrix $M_{1,ll'}$ multiplying the linear frequency term $\propto \omega^*$ is diagonal in this representation. The matrix $M_{0,ll'}$ is the same as before, the matrix $\mathbf{M}_{ll'}$ in eq. 4.17, but with the constant term $+\bar{H}^2$ added to σ_l. Lastly, $M_{2,ll'}$ is just the identity matrix of dimension N: $M_{2,ll'} = \mathbb{I}_N$. Thus, the central equation 4.15 for the coefficients c_l takes the form

$$\left\{\omega^{*2}\mathbb{I}_N - 2\frac{\bar{H}}{c}\omega^*\mathbb{I}_N - (\mathbf{M}_{ll'} + \bar{H}\delta_{ll'})\right\}\begin{pmatrix} c_{l_1}(\mathbf{k}_{l_1}) \\ c_{l_2}(\mathbf{k}_{l_2}) \\ \vdots \\ c_{l_N}(\mathbf{k}_{l_N}) \end{pmatrix} = 0$$

The quadratic eigenvalue problem can be solved numerically in several different ways. We apply MATLABs *polyeig*-function for obtaining the eigenvalues, which utilizes *QZ-factorization* [42] to solve the problem. We note that this approach is not suitable for large numerical accuracy, but it is sufficient for a qualitative result.

4.3 2D cosine-modulated periodic potential

We now specialize the general modulation $D(\mathbf{r})$ to a relatively simple spatial modulation in the form of 2D cosine functions in the xz-plane. This yields quantitatively the same effects as a step-modulation of the type [124]. However, the single component cosine potential is simpler to work with due to the limited number of Fourier coefficients needed to populate the matrix $\mathbf{M}_{ll'}$, for which the condition of zero determinant yields the coefficients of the eigenvalue-equation of the type seen in eq. 4.15. The 2D modulation will be taken to be in the thin film xz-plane, with the equilibrium Néel order directed along the z-axis, $\mathbf{n}_0 \perp \hat{z}$ as before. The modulation $D(\mathbf{r})$ is defined as

$$\begin{aligned} D(\mathbf{r}) &= D\left[\cos\left(\frac{2\pi}{l}x + \frac{2\pi}{l}z\right) + \cos\left(\frac{2\pi}{l}x - \frac{2\pi}{l}z\right)\right] \\ &= 2D\left[\cos(k_b x)\cos(k_b z)\right] \end{aligned} \tag{4.20}$$

where we used the identity

$$\cos(x+z) + \cos(x-z) = 2\cos x \cos z$$

in the 2nd line. l is the lattice constant of the potential in both the x- and z-directions, and $k_b \equiv 2\pi/l$. A plot of the potential and the 1BZ [45] is shown in figure 4.1. We define the primitive lattice vectors $\{\mathbf{b}_1, \mathbf{b}_2\}$ of the reciprocal lattice of the potential as

$$\mathbf{b}_1 = k_b(\hat{\mathbf{x}} + \hat{\mathbf{z}}) = k_b \begin{bmatrix} 1 \\ 0 \\ 1 \end{bmatrix}$$
$$\mathbf{b}_2 = k_b(\hat{\mathbf{x}} - \hat{\mathbf{z}}) = k_b \begin{bmatrix} 1 \\ 0 \\ -1 \end{bmatrix} \tag{4.21}$$

In app. D, the matrix elements of the modulation in eq. 4.16 are found by applying the Fourier transform to the DMI-part of the KGE $\propto [D(\mathbf{r})\partial_x - \partial_x D(\mathbf{r})]$ acting on the SW-function $\psi_\pm$. We will assume that $D(\mathbf{r})$ can be expanded in a Fourier series, which results in a simple expression for our matrix elements due to the low number of Fourier-coefficients needed to describe the potential. This approach gives the same result as evaluating eq. 4.7 directly, but it is arguably easier to follow the method in app. D. The matrix elements of the IDMI-operator in eq. 4.19, assuming a modulation of the form 4.20, takes the form

$$\begin{aligned}\frac{1}{2}\left\{\bar{\mathcal{D}}_{ll'}(\mathbf{k}_l)_x + i(\partial_x\bar{\mathcal{D}})_{ll'}\right\} &= \frac{\bar{\mathcal{D}}}{4}\sum_{i=1,2}\{\,(\mathbf{k}-\mathbf{b}_i)_x\delta_{(\mathbf{G}_l-\mathbf{G}_{l'}),\mathbf{b}_i} + (\mathbf{k}+\mathbf{b}_i)_x\delta_{(\mathbf{G}_l-\mathbf{G}_{l'}),-\mathbf{b}_i} \\ &\qquad +(\mathbf{b}_i)_x\delta_{(\mathbf{G}_l-\mathbf{G}_{l'}),-\mathbf{b}_i} - (\mathbf{b}_i)_x\delta_{(\mathbf{G}_l-\mathbf{G}_{l'}),+\mathbf{b}_i}\Big\} \\ &= \frac{\bar{\mathcal{D}}}{4}\sum_{i=1,2}\Big\{|\mathbf{k}|\cos\theta_k - 2k_b\Theta(\mathbf{G}_l-\mathbf{G}_{l'})\cos\theta_G\Big\} \\ &\qquad \times\left[\delta_{(\mathbf{G}_l-\mathbf{G}_{l'}),\mathbf{b}_i} + \delta_{(\mathbf{G}_l-\mathbf{G}_{l'}),-\mathbf{b}_i}\right]\end{aligned} \tag{4.22}$$

In the above equation, we have defined the function

$$\Theta(\mathbf{G}_l-\mathbf{G}_{l'}) = \begin{cases}(-1), & \mathbf{G}_l-\mathbf{G}_{l'} = \{\mathbf{b}_1,\mathbf{b}_2\} \\ 1, & \mathbf{G}_l-\mathbf{G}_{l'} = \{-\mathbf{b}_1,-\mathbf{b}_2\} \\ 0, & \text{else}\end{cases}$$

and used that $|\mathbf{b}_1| = |\mathbf{b}_2| = k_b$. We have defined the phase angle $\theta_k = \arctan(k_z/k_x)$ as the angle between k and the $\hat{x}$-direction, and similarly for θ_G. Again, note that the index l and the lattice constant of the modulation are unrelated.

The off-diagonal matrix elements in eq. 4.22 gives band gaps in the dispersion relation. However, we can now see a crucial difference between the case of constant DMI d_h and the inclusion of modulated DMI $\bar{\mathcal{D}}(\mathbf{r})$. The k_x-term $\propto \cos(\theta_k)$ gives rise to the nonreciprocity of the SWs. As the angle θ_k goes from $0 \to \pi/2$, the nonreciprocity of the SWs vanishes. However, a consequence of the modulation is that even for vanishing k_x, the SWs are still gapped, as can be seen from the 2nd term in eq. 4.22. These terms do not disappear, as θ_G will always be nonzero for our simple potential if the Θ-function is nonzero.

If the DMI-modulation $\bar{\mathcal{D}}(\mathbf{r})$ had been a constant term, the modulated DMI had been equivalent to the homogeneous DMI d_h. In the absence of the cosine-potential, the matrix elements in eq. 4.22 would only give a contribution when

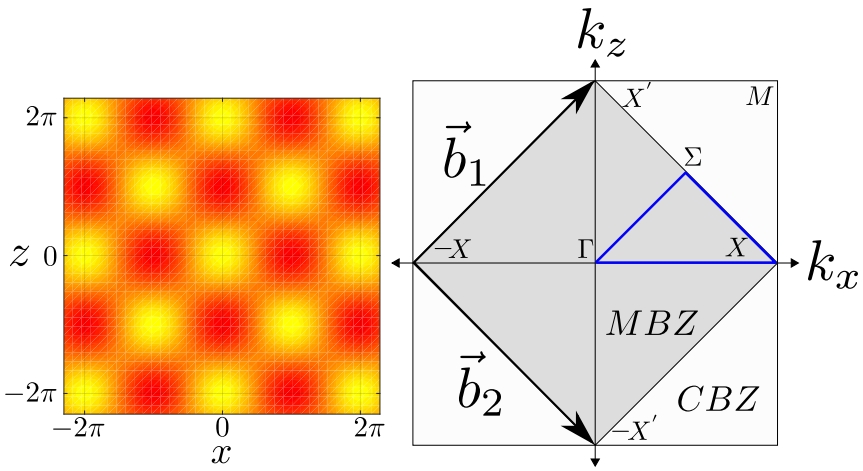

Figure 4.1: A dimensionless density/contour plot of the 2D cosine potential in eq. 4.20 in the xz-plane, with the corresponding 1BZ to the right. The AFM BZ has half the area and is rotated 45° w.r.t. the ordinary crystal Brillouin zone (CBZ) of the square lattice. This is due to the bipartite-lattice-composition of the AFM. The AFM Brillouin zone is often called the *magnetic Brillouin zone* (MBZ) [134].

$\mathbf{G}_l - \mathbf{G}_{l'} = 0$, i.e. along the diagonal. Thus, the periodic modulation is responsible for making the DMI contribute only when the quasimomenta of the PWs scatter to the shortest possible reciprocal lattice vectors $\pm\mathbf{b}_1$ or $\pm\mathbf{b}_2$. In general, one can include arbitrarily many such contributions. We will see that our single-frequency modulation will affect the lowest energy band, $\mathbf{G}_l, \mathbf{G}_{l'} = 0$, and the four next energy bands where $\{\mathbf{G}_l = 0, \mathbf{G}_{l'} = \pm\mathbf{b}_{1/2}\}$. We will mainly focus on the lowest energy gap, meaning we only care about the two or three lowest bands. If we go to much higher energy bands, the validity of our low-frequency assumption will no longer hold.

4.4 2D results

The band structure diagrams for the low frequency SW-spectrum of the AFM is presented in this section. Remember that the motivation for studying AFM magnonic crystals with IDMI of the type considered in this thesis was to create polarization-dependent band gaps for the two SW modes only present in AFM-systems. The 2D results confirms that such a mechanism is possible, in addition to other phenomena discussed in the thesis: spin wave-nonerciprocity in different k-space-directions, leading to adjustable band-gaps that become increasingly flat for large DMI lattice-parameters, and indirect bandgaps at MBZ-zone edges. In addition, we see apparent a apparent lifting of degenerate bands along certain symmetry paths due to the modulation.

In all the plots that follow, $\omega_J = 100$ THz, $\omega_{K_z} = 3$ THz and $d = 5$ Å. The

calculations were performed with 49 plane waves, corresponding to the 49 nearest neighbouring reciprocal lattice points, which for our purposes is sufficient. In many of the figures, we plot the three lowest energy bands according to our sorting scheme $l^2 = n^2 + m^2$. We list the five lowest bands , whch corresponds to $\mathbf{G}_l - \mathbf{G}_{l'} = (0,0)$ and the four nearest neighbour lattice points in reciprocal space $\pm\mathbf{b}_1, \pm\mathbf{b}_2$. However, note that the bands can be degenerate along certain symmetry paths and symmetry points for $D = 0$.

The lowest band was given above. The next band corresponds to $\mathbf{G}_l - \mathbf{G}_{l'} = \mathbf{b}_1$, which in general will be the 2^{nd}-lowest frequency-band. The bands corresponding to $\mathbf{G}_l - \mathbf{G}_{l'} = \pm\mathbf{b}_2$ are degenerate for $k_x = k_y$. The last band corresponds to $\mathbf{G}_l - \mathbf{G}_{l'} = -\mathbf{b}_1$, and is the highest in frequency for $\{k_x, k_y\} \neq 0$ on the symmetry path shown in the inset of e.g. fig 4.2.

Figures 4.2 and 4.3 show the ten lowest magnonic bands for the in-plane RH-SWs in the absence of magnetic field and DMI. The degeneracy is quite large, and there are no magnonic gaps present in the system. In fig. 4.3, we see that the degeneracy is significantly reduced at the symmetry points as the gaps open up, with the largest (and the only complete) bandgap between the 1^{st} and 2^{nd} lowest bands. The gaps at higher frequencies are significantly smaller. We also see that for $k_x \neq 0$, e.g. along $\Gamma \to \Sigma$, several branches split of into two bands. We can now see that what looked like a single band, the 3^{d} band in 4.2 on the path $\Gamma \to \Sigma$, is actually two bands.

Figures 4.4 and 4.5 gives a closer look at the three lowest energy bands, corresponding to the contributions $(0,0)$, $\mathbf{b}_1$ and $\mathbf{b}_2$. We now see that the 2^{nd} and 3^{d} bands, which are degenerate for $D = 0$ along $X \to \Gamma$, is apparently split by the modulation. We will return to this shortly.

The plots 4.6, 4.7, 4.8 and 4.9 are the main results relevant for the application of DMI-MCs as a spin-wave polarizer. The modulated DMI in combination with a magnetic field yields tunable band gaps for the two SW-modes, allowing for frequencies where both polarizations, one polarization or no modes at all can propagate. The bandwidths and their locations in the spectrum are directionally dependent due to the DMI. The separation of the ω_+- and ω_-- modes increases linearly with the magnetic field H. The gaps where none of the bands are allowed to propagate is determined by the balance between l and D, as shown in fig. 4.10 and 4.11. The gap width falls of as l increases. This is the case since $|\mathbf{G}| \propto 1/l$, so a smaller l implies that the SWs need to Bragg-scatter to larger momenta. Such events thus become less and less likely for smaller and smaller values of l, since they require higher and higher energies. This implies a larger range of forbidden frequencies for the SWs, meaning a larger bandgap. The bandwidth increases approximately linearly (fig. 4.11) with DMI-strength D up to the DMI threshold value $\sim \sqrt{JK}$, with smaller gaps for larger l as expected. As l increases, the bands become flatter. At the point where the bands are close to flat, the bandwidth becomes approximately constant with increasing D.

The nonreciprocity-effect $\omega(\mathbf{k}) \neq \omega(-\mathbf{k})$ of the SWs in the chiral MC are shown in the plots 4.12, 4.13 and 4.14. The nonreciprocity is also seen in fig. 4.11, where the bandgaps are smaller in the $\Gamma \to -X$-direction than in the

$\Gamma \rightarrow X$-direction. Frequencies that are gapped in one direction are not necessarily gapped in the opposite direction, a mechanism that can be used for the realization of one-way magnonic waveguides. The direction is equal but mirrored along the k_z-axis for the LH-mode. Applying a magnetic field H, one can tune the overlap of the gaps of the modes in both directions. This gives additional freedom in tuning the mode-selecting, one-way SW-filter.

Fig. 4.14 shows the gaps along the k_x and k_z-axes. The nonreciprocity-effect in each band only occurs for $k_x \neq 0$, as dictated by the crystal symmetry, see the discussion in app. A. The modes are still gapped for paths along the k_z-axis due to the periodic modulation, however, the gap width is the same in both directions.

The indirect bandgaps of the type shown in fig. 4.15 is a new phenomena which arises due to the modulated DMI. The top of the bottom band and the bottom of the highest band, which both are located at the BZ-edge in the absence of DMI, are shifted relative to each other by a small amount $\Delta\mathbf{k}$. Different energy bands can get k-shifted by different amounts depending on which reciprocal lattice point the band corresponds to. In this case, the matrix elements in eq. 4.22 yields different contribution for $\mathbf{G}_l - \mathbf{G}_{l'} = (0,0)$ than for the 2^{nd} band, which in this case corresponds to $\mathbf{G}_l - \mathbf{G}_{l'} = \mathbf{b}_1$. This happens even if $k_x = 0$. Thus, the bands are shifted in k by different amounts, which theoretically can allow for a fine-tuning of the bandgaps.

As a extension on these indirect bandgaps, we comment on the apparent lifting of degeneracy between the 2^{nd} and 3^{d} bands along the k_z-axis, see fig. 4.17. We note that the results on this are not assumed to be accurate due to the numerical method used, and are not important for the main results related to the mode-selective bandgaps. We have not applied special treatment to the degenerate bands in the model either (such a treatment could be e.g. *degenerate perturbation theory* [21, 115]), but we still offer it as a possible explanation for the apparent lifting of degeneracy between bands even when $k_x = 0$. Along the k_z-axis, the dispersion in each band should be nonreciprocal since $k_x = 0$. The lifting of the degeneracy between the 2^{nd} and 3^{band} is still present. When $k_x = 0$, the lowest contributing bands arise from the $\mathbf{b}_1$- and $-\mathbf{b}_2$-reciprocal lattice points. Per our discussion on the indirect bandgaps in the paragraphs above, the two gives different contributions to the matrix elements in eq. 4.22. The bands are thus able to shift relative to each other in the same manner as in fig. 4.15. However, due to the approximate nature of the calculation of the bands in this thesis, we will not draw any conclusions on this or its relation to the main-results.

In the absence of spatially modulated IDMI $D = 0$, we know that there are no gaps in the spectrum for any of the modes. The homogeneous DMI d_h does not give rise to any bandgaps either, as is evident from fig. 4.16. The homogeneous DMI-contribution is non-zero only for $k_x \neq 0$, and goes to zero as the angle between $\mathbf{k}$ and x-axis $\rightarrow \pi/2$, resulting in no contribution from the DMI whatsoever as we had in the 1D-case in chapter 3. This is in contrast to the modulated DMI $D(\mathbf{r})$, which gives bandgaps for all $\mathbf{k} \in 1BZ$. In other words, the homogeneous DMI d_h only contributes to the nonreciprocity of the SWs, but do not gap the system on its own.

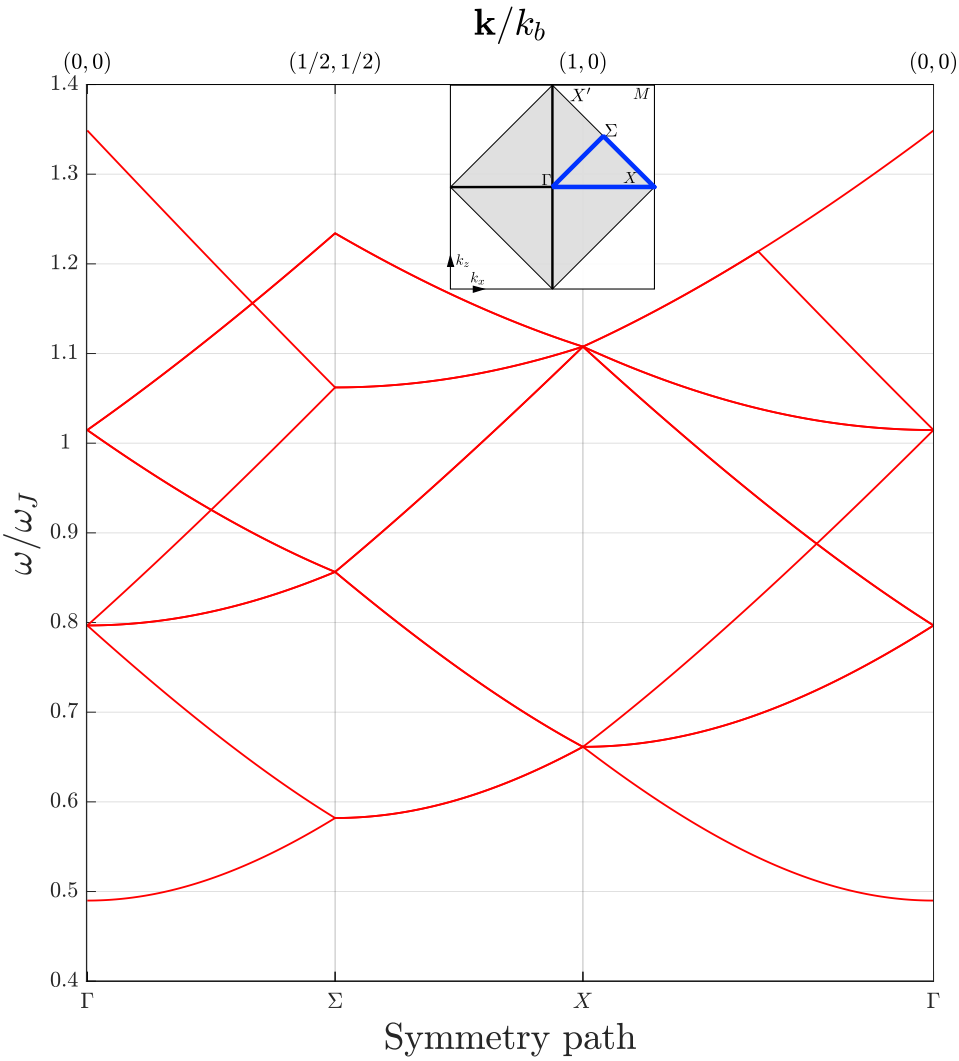

Figure 4.2: The ten lowest AFM-SW frequency bands with easy-axis anisotropy calculated from the PWE. The degree of degeneracy is large, which is expected from the square-lattice symmetry. The symmetry path is shown in the inset.

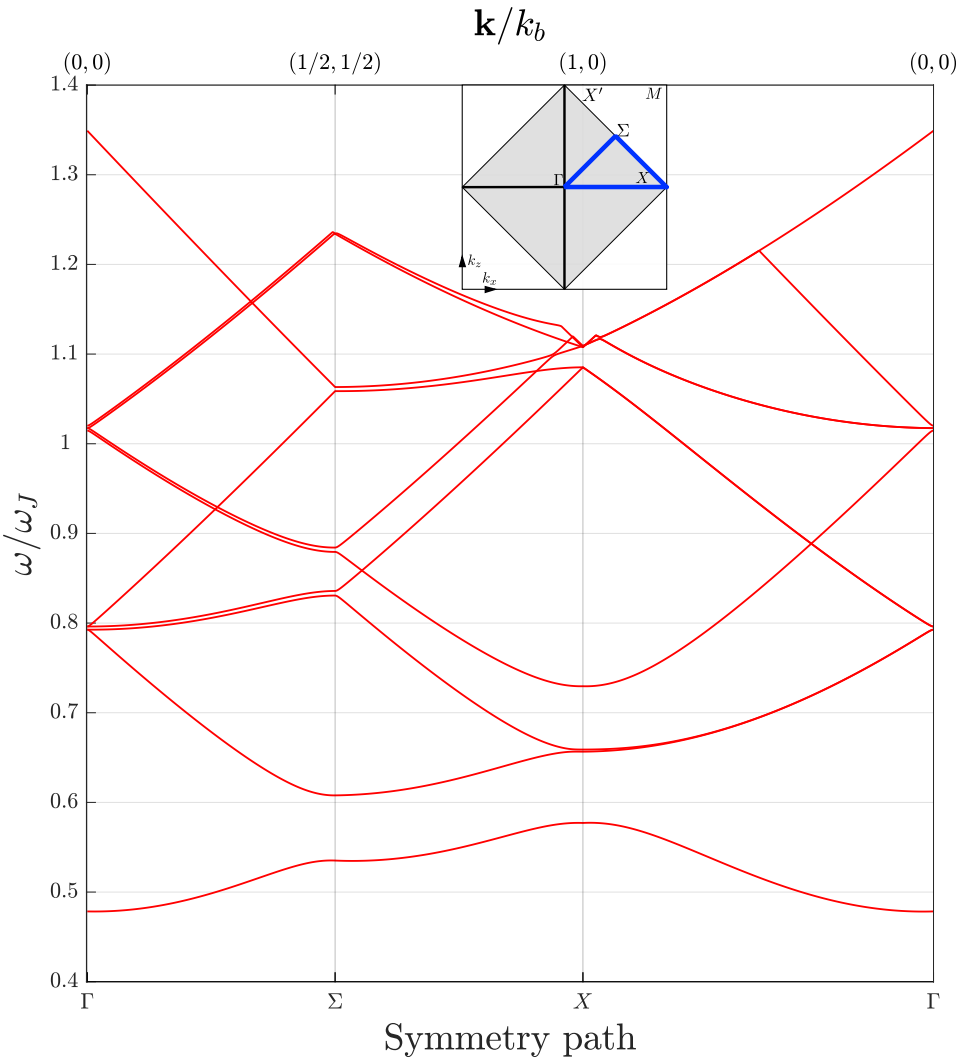

Figure 4.3: The same plot as in fig. 4.2, but with $D/J = 0.15$ and $l = 20$ nm. We see that the inclusion of periodic DMI reduces the degeneracy of the band structure. In particular, the degeneracy of the 1^{st} and 2^{nd} bands on the symmetry path $\Gamma \to \Sigma$ is lifted.

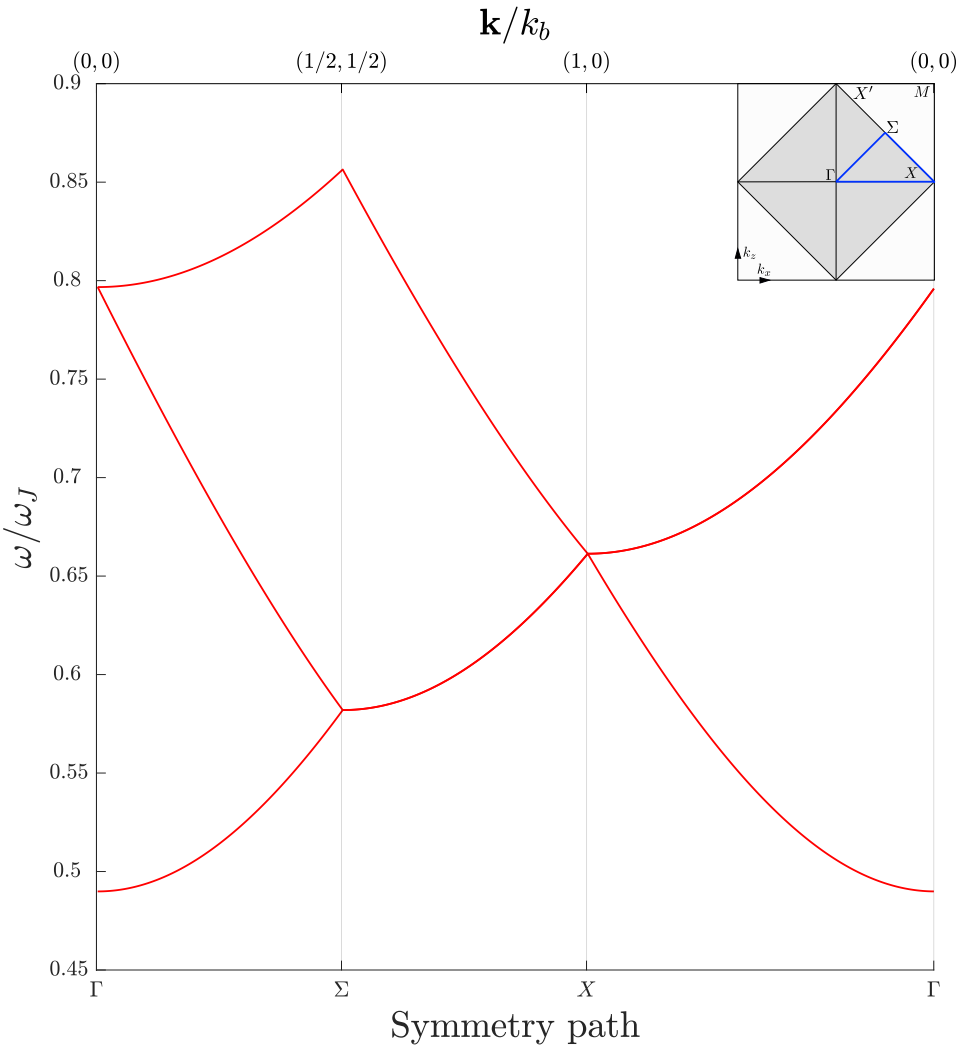

Figure 4.4: Band structure for the three lowest bands of the 2D magnonic crystal, in the absence of modulated DMI and magnetic field. The RH/LH-modes are degenerate in this case.

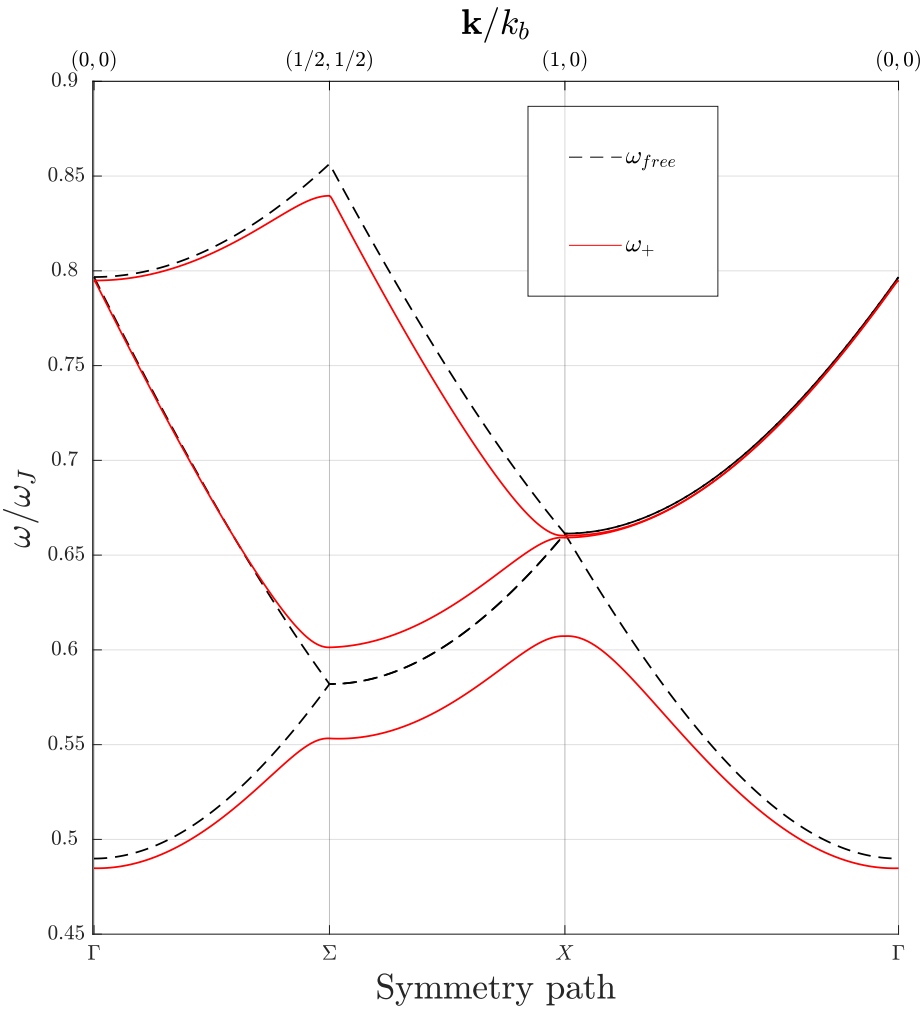

Figure 4.5: The effect of modulated DMI $D/J = 1/10$ and $l = 20$ nm on the three lowest bands of the RH-SW with no magnetic field. The dashed line shows the free dispersion in the absence of DMI.

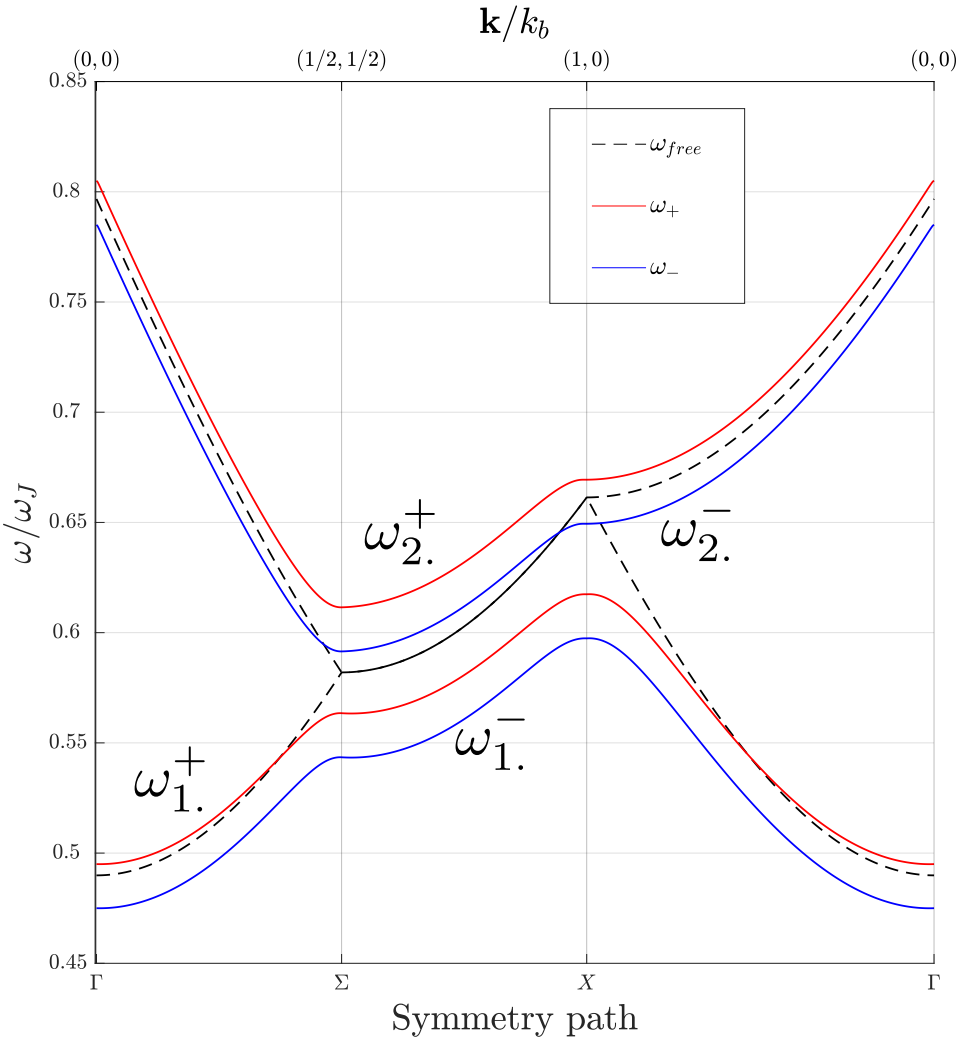

Figure 4.6: Band structure for RH/LH-modes in the presence of magnetic field and modulated DMI. The parameters are $D/J = 1/10$, $H/J = 1/100$ ($\omega_H = 1$ THz) and $l = 20$ nm.

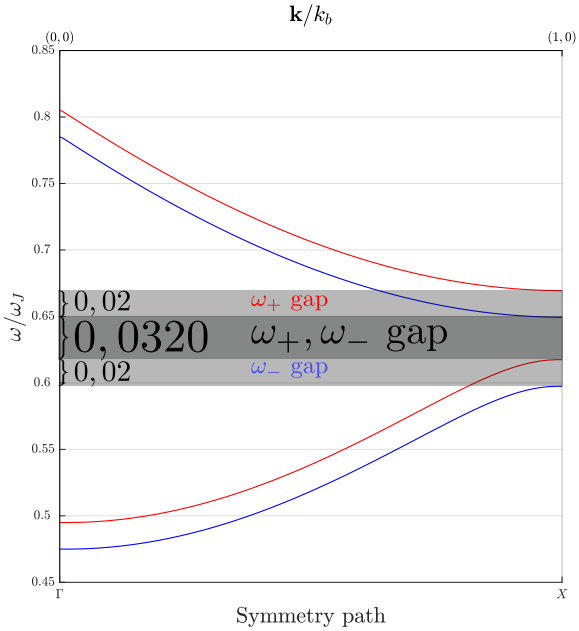

Figure 4.7: SW band gap in the $\Gamma - X$-direction. The parameters are the same as in fig. 4.6.

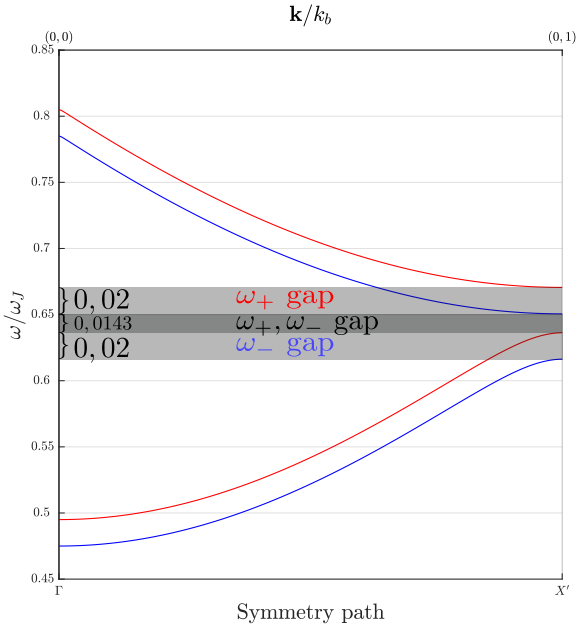

Figure 4.8: SW dispersion in the X'-direction. The parameters are the same as in fig. 4.6.

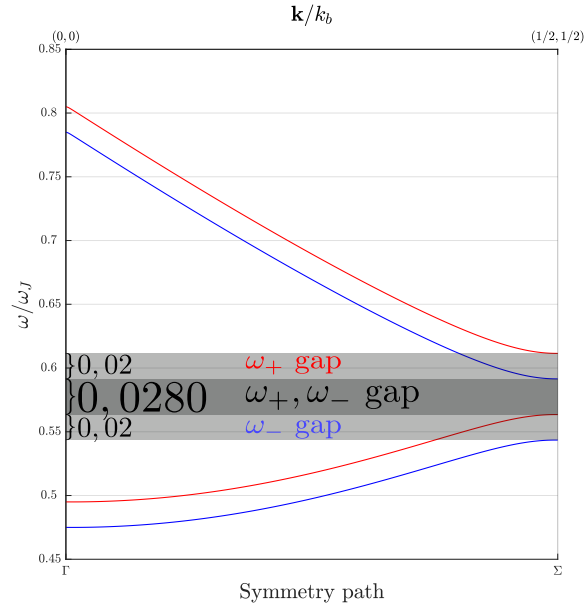

Figure 4.9: SW dispersion in the Σ-direction. The gap is the lowest in energy of the three directions plotted. The parameters are the same as in fig. 4.6.

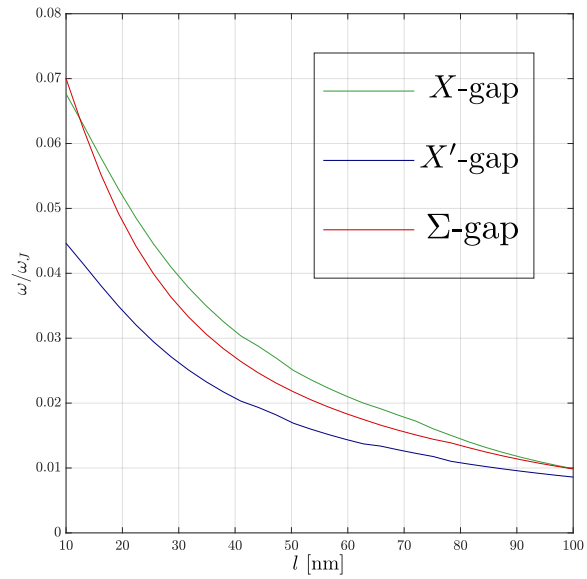

Figure 4.10: The gap width at the BZ-edge at the points X, X' and Σ as a function of the DMI lattice parameter l, with $D/J = 1/10$. The falloff in bandwidth seems to be proportional to $\sim 1/x^2$, similar to the electronic case [45].

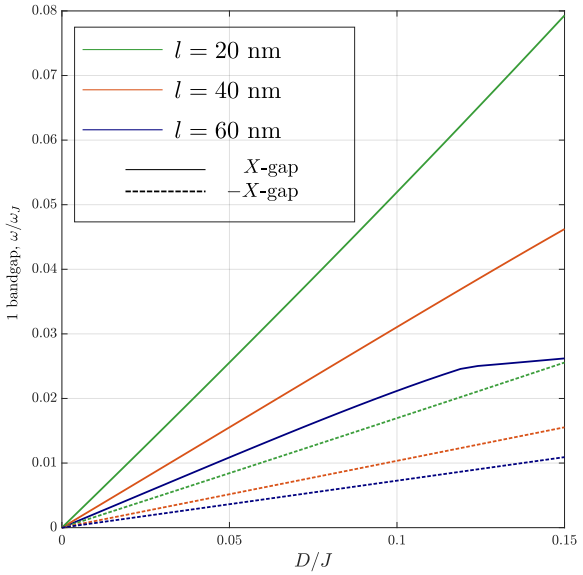

Figure 4.11: Gap width in the X- and $-X$-directions for different values of the DMI lattice-parameter l as a function of the inhomogeneous DMI-strength D.

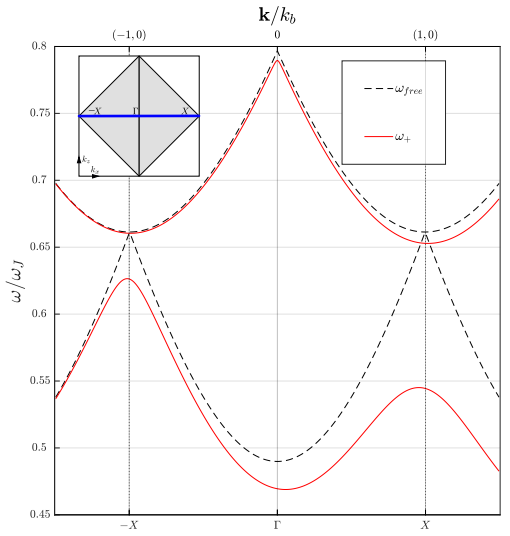

Figure 4.12: RH-SW dispersion for the two lowest bands along $-X \rightarrow X$, with $l = 20$ nm, $D/J = 1/5$. The DMI-strength is exaggerated to show the effect more clearly. Note that the gap is not centered on the BZ-edges.

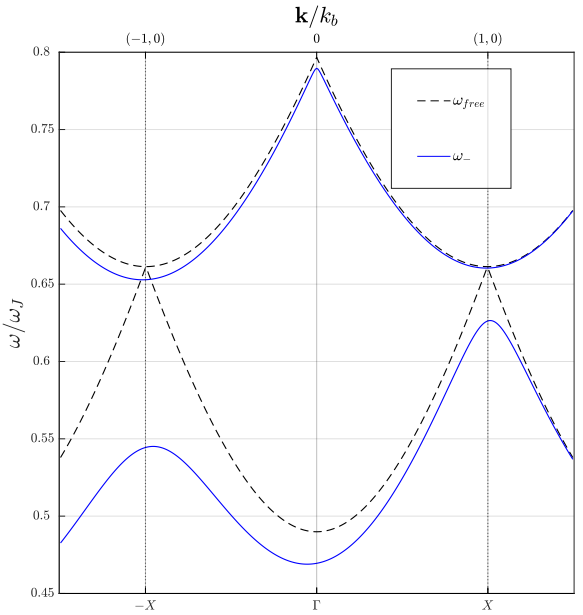

Figure 4.13: LH-SW mode along $-X \rightarrow X$, with the same parameters as in fig. 4.12. Note that the peak of the lowest LH-band at the $-X$-point is shifted slightly towards positive k, the opposite as for the RH-mode.

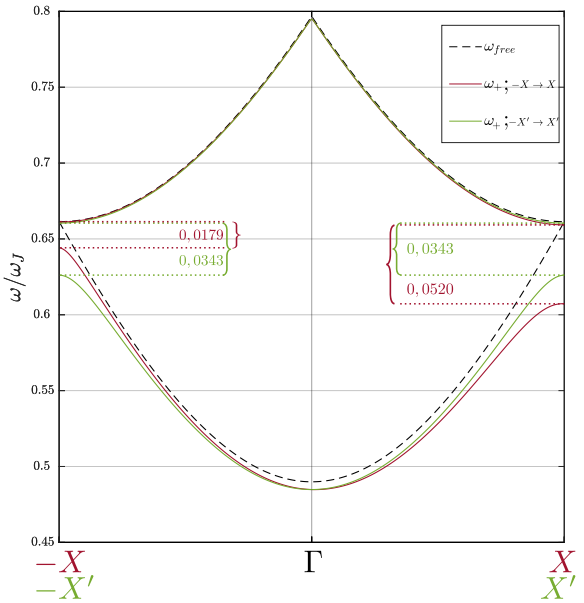

Figure 4.14: Dispersion relation along the k_x- and k_z-axes in the 1BZ, with $l = 20$ nm and $D/J = 1/10$. The modes are still gapped for $k_x = 0$ due to the periodic modulation $D(\mathbf{r})$.

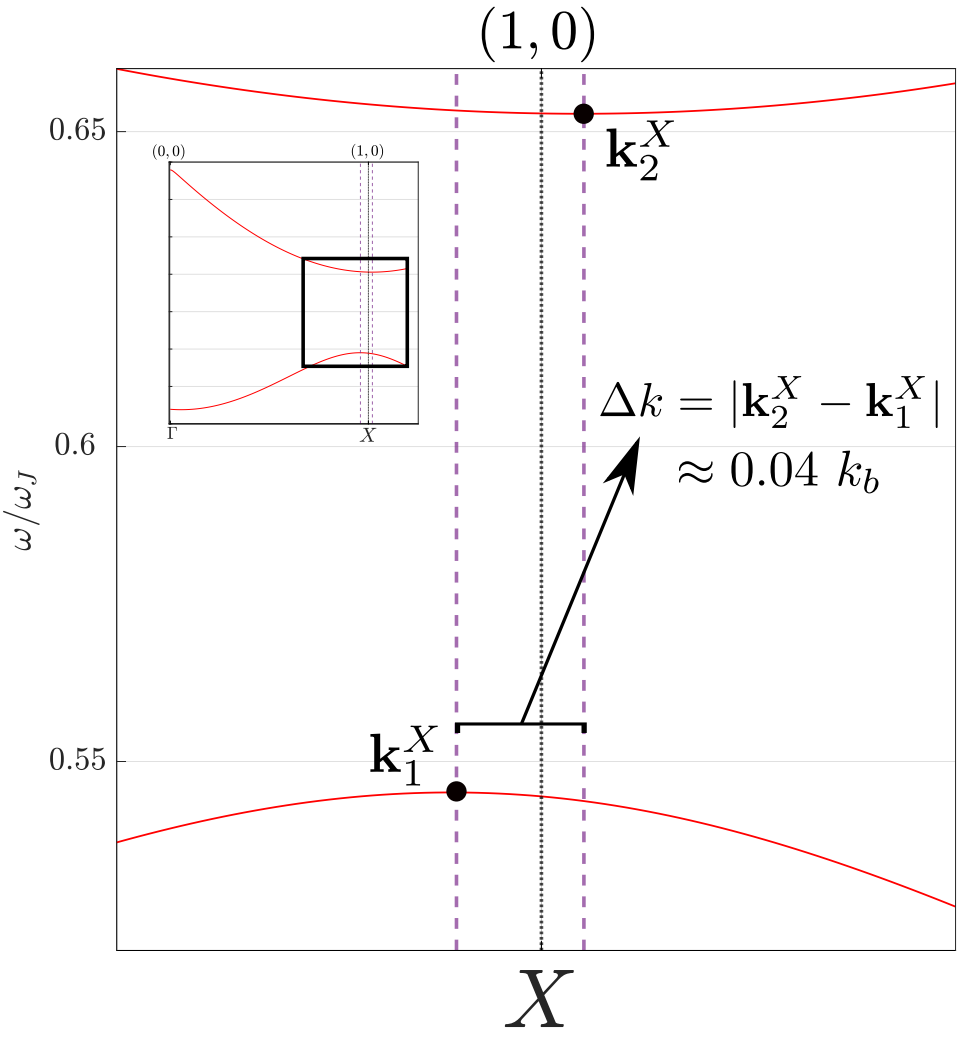

Figure 4.15: Zoom-in on the bandgap at X, with $l = 20$ nm and $D/J = 1/5$. The splitting is small, $\Delta k \approx 0.04(2\pi/l) = 0.04k_b$. This mechanism allows for fine tuning of the gaps. We note that the nonreciprocity is due to the modulated DMI alone, and not the homogeneous background DMI d_h.

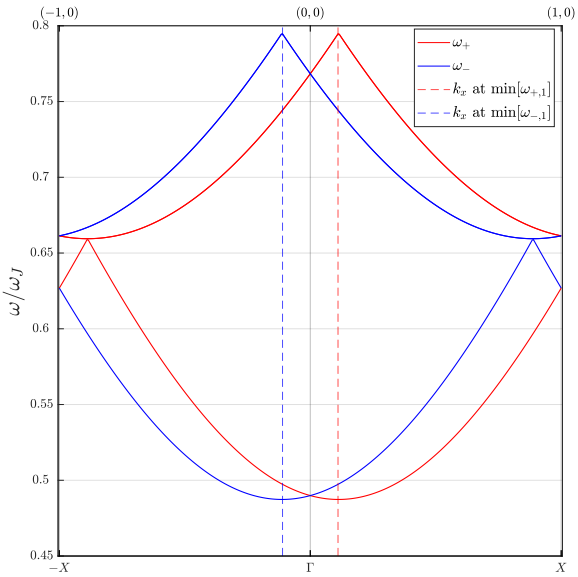

Figure 4.16: k-shift in the dispersion relation for $d/J = 1/10$ and $D = 0$. As expected, there are no complete bandgaps in the 1BZ due to the lack of periodic potential $D(\mathbf{r})$.

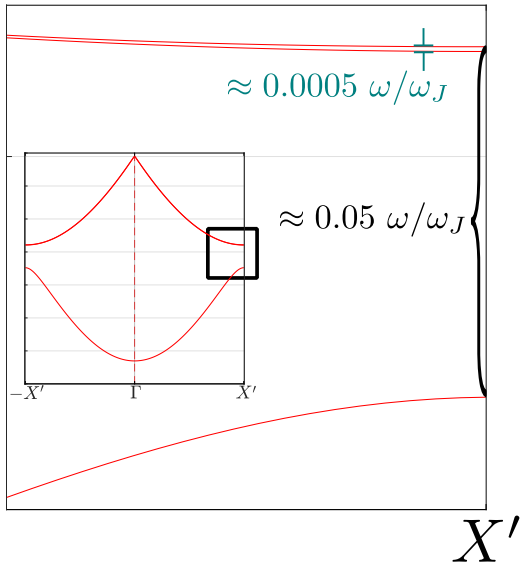

Figure 4.17: Splitting of the 2$^{\text{nd}}$ and 3$^{\text{d}}$ band for the RH-mode in the X'-direction. In the absence of DMI, these bands are degenerate. The parameters are $D/J = 1/10$ and $l = 20$ nm. The splitting is quite small, between $10 - 100$ times smaller than the 1$^{\text{st}}$ bandgap.

CHAPTER 5
SUMMARY, DISCUSSION AND OUTLOOK

In this thesis, we have calculated dispersion relations and band structure diagrams for the low-frequency spectrum of a 1D and 2D MC subject to modulated IDMI. After a general introduction in chapter 1, we explained how to describe a insulating AFM coupled spin system on a bipartite lattice with easy-axis anisotropy, modulated IDMI and in-plane external magnetic field in chapter 2. This was done in a semi-classical, phenomenological formalism in terms of the order parameters **m** and **n**, the magnetization and Néel-field respectively. The coupled EOMs describing their dynamics was reduced to a single equation in **n** in the exchange approximation. From this, we obtained a low-energy effective Klein-Gordon-equation describing the SWs. Using a plane wave-ansatz for the form of the SWs in a plane perpendicular to the Néel equilibrium-direction and the assumption of a thin film-geometry, dispersion relations and band diagrams were calculated for a 1D Krönig-Penney-DMI-MC by means of a analytical solution for the standing SW band gaps in chapter 3, and for a 2D cosine-modulation of the DMI strength with the PWE-method in chapter 4. These systems have not been previously studied with the same framework used in this thesis.

The results showcased features of the spectrum which makes DMI-modulated MCs potentially interesting for applications in wave-based computing. The degeneracy of the two RH/LH AFM-SW modes was completely lifted by means of an in-plane external magnetic field and the inversion symmetry-breaking DMI-interaction, resulting in a large degree of control of the SW-bandgaps. In particular, this allows for the creation of selective, directionally dependent band gaps in the MC, which only allow SW excitations of the correct polarization to propagate.

The spatial modulation of DMI introduced interesting effects. In addition to the usual gaps between energy bands from the periodic modulation of a physical parameter in the MC, we observe nonreciprocal SW bands and indirect bandgaps due to relative shifts in frequency branches from different Bragg-reflections. Other features that were commented on but not explored are the apparent lifting of degenerate frequency bands along certain symmetry-paths in the 1BZ, possibly due to the indirect-bandgap effect, and a tendency for the lowest energy bands to become flat for large values of the DMI lattice spacing.

We conclude that the combination of modulated IDMI and external magnetic field present a possible means of effectively selecting desired SW-polarizations in a magnonic waveguide. This can be used for several different types of applications. The nonreciprocity can e.g. be used to manufacture one-way SW waveguides. A SW-mode-filter can be realized by the inclusion of magnetic fields in such a way that only modes of the correct polarization are allowed to propagate,

which can be used in the creation of e.g. spin-polarized currents.

Regarding experimental realizations, the creation of a MC with modulated DMI can be performed by the alternate layering of heavy-metal-wires on top of a AFM thin film [132] by litography/etching [136]. The DMI lattice spacing can be varied in the thickness of the wires. The creation of a MC with potential-"bumps" as in the 2D cosine-case can be envisioned as a lattice of quantum dots [40]. Such a system might be realizable by laser-induced heating [110] or a material sputtering approach [81, 96], however, making this work with strong-SOC materials on top of thin films can present a challenge. Excitation of the SWs in the waveguide can be performed with e.g. a oscillating magnetic field perpendicular to the film [113], optical excitation [38], or thermal excitations through the spin Seebeck effect [107]. The most practical detection methods of the SWs might be magnetic probing/optical spectroscopy [73, 94], or the inverse spin Hall effect for the detection of magnonic currents [91].

It is important to emphasize that the results obtained here are very approximate, and serves to showcase only the general features of SWs in AFM-magnonic crystals, with a somewhat accurate result only expected for the lowest energy branches of the magnonic crystal [81]. We have already discussed the validity and PW-cutoff in sec. 4.2. However, a comparison with other numerical methods could be performed, such as PWM [57], solution of the EOM differential equation directly by e.g. a finite-difference method [95] or a micromagnetic simulation of the lattice spins through e.g. the Dormand-Prince-method such as in [113]. A interesting proposition is to investigate the iso-frequency contours of SWs, the magnonic analogue to Fermi-surfaces for electrons [100]. The effect of Gilbert-damping on the SWs would also be interesting to explore further.

Even if a plane wave ansatz can be justified for the non-interacting, low-frequency regime, a more thorough treatment could treat a more interesting/realistic potential than the single-frequency cosine potential used in this thesis. The PWE-calculation can be used for arbitrarily shaped scattering centers relatively easily, since the method relies on the Fourier transform of the spatial distribution of the potential, which can be readily calculated by numerical FT-routines. The method is in general most effective when the envelope function is "well behaved", and varies in a continuous fashion with the periodicity of the real-space lattice, which one must keep in mind.

The method of QZ diagonalization also has an impact on accuracy, and should not be used if one desires a high degree of accuracy for the quadratic eigenvalue problem [42]. Strictly speaking, it is not numerically stable for the quadratic eigenvalue problem in particular. The error has been attempted to be made as small as possible by rescaling the matrix such that its norm is close to one. In addition, conditioning numbers for the matrices have been checked and found to be small, in the range $\sim 1 - 10$ [60]. This number is determined by the problem itself and not the method of solution, however, a problem with high conditioning numbers can be impossible to solve due to the inaccuracy and inconsistency of the outputs.

APPENDIX A

DERIVATION OF AFM FREE ENERGY, LATTICE APPROACH

We will here derive the free energy density $\mathcal{F}_{AFM}$ of the antiferromagnet by taking the continuum limit of the Heisenberg Hamiltonian on a 2D square lattice. In deriving the free energy contributions, a number of parameters used in the thesis will be defined. These are colleced in table 2.7. This section outlines the same calculations as in the master thesis of Sørheim [131] and [118].

As noted in chapter 4, in the thesis, the magnetization $\mathbf{m}$ and staggered magnetization $\mathbf{n}$ at the cell defined by the indices $\{i, j\}$, which denotes perpendicular directions on the lattice, are defined in terms of the spins as

$$\mathbf{m}_{ij} = \frac{(\mathbf{S}^{\alpha}_{ij} + \mathbf{S}^{\beta}_{ij})}{2S}$$
$$\mathbf{l}_{ij} = \frac{(\mathbf{S}^{\alpha}_{ij} - \mathbf{S}^{\beta}_{ij})}{2S}$$

We introduce the Néel field as $\mathbf{n}_{ij} \equiv \mathbf{l}_{ij}/|\mathbf{l}_{ij}|$. Rewriting the spins in terms of the fields, we get

$$\mathbf{S}^{\alpha}_{ij} = S(\mathbf{m}_{ij} + \mathbf{n}_{ij}) \tag{A.1a}$$
$$\mathbf{S}^{\beta}_{ij} = S(\mathbf{m}_{ij} - \mathbf{n}_{ij}) \tag{A.1b}$$

Inserting the definitions of the spins into the exchange term of the Heisenberg Hamiltonian

$$\hat{\mathcal{H}}_{exch.} = J \sum_{<\mathbf{r}_1, \mathbf{r}_2>} \mathbf{S}_{\mathbf{r}_1} \cdot \mathbf{S}_{\mathbf{r}_2}$$

the sum over the vectors $\mathbf{r}_1$, $\mathbf{r}_2$ which denotes the position of all lattice points are replaced by the sums over the lattice indices $i, j \in 0, \pm 1, \pm 2, \cdots \pm N$. We now denote $\hat{\mathcal{H}}_{exch.} \rightarrow \hat{H}_{exch.}$ to mark the difference between the spin- and discrete Hamiltonians. For interaction between nearest neighbours

$$H_{exch.} = JS^2 \sum_{ij}^{N-1,N-1} (\mathbf{m}_{ij} - \mathbf{n}_{ij})\Big[(\mathbf{m}_{ij} + \mathbf{n}_{i,j}) + (\mathbf{m}_{i+1,j} + \mathbf{n}_{i+1,j}) + (\mathbf{m}_{i,j+1} + \mathbf{n}_{i,j+1}) + (\mathbf{m}_{i+1,j+1} + \mathbf{n}_{i+1,j+1})\Big]$$

Using the identities

$$\begin{aligned} 2\mathbf{n}_{ij}\mathbf{n}_{i+1,j} &= \mathbf{n}_{ij}^2 + \mathbf{n}_{i+1,j}^2 - (\mathbf{n}_{i+1,j} - \mathbf{n}_{ij})^2 \\ \mathbf{n}_{ij}\mathbf{m}_{i+1,j} - \mathbf{n}_{i+1,j}\mathbf{m}_{ij} &= \mathbf{n}_{ij}(\mathbf{m}_{i+1,j} - \mathbf{m}_{ij}) - \mathbf{m}_{ij}(\mathbf{n}_{i+1,j} - \mathbf{n}_{ij}) \end{aligned}$$

we can rewrite the discrete Heisenberg Hamiltonian into terms reminiscent of lattice differences or derivatives such as $\sim (\mathbf{n}_{i+1,j} - \mathbf{n}_{ij})$. This is done in anticipation of the transition to a continuum description.

$$\begin{aligned} H_{exch.} \simeq\ & N_n JS^2 \sum_{ij}^{N,N} (\mathbf{m}_{ij}^2 - \mathbf{n}_{ij}^2) \\ & + \frac{JS^2}{2} \sum_{ij}^{N-1,N-1} \Big[(\mathbf{n}_{i+1,j} - \mathbf{n}_{ij})^2 + (\mathbf{n}_{i,j+1} - \mathbf{n}_{ij})^2 + (\mathbf{n}_{i+1,j+1} - \mathbf{n}_{ij})^2 \\ & - (\mathbf{m}_{i+1,j} - \mathbf{m}_{ij})^2 - (\mathbf{m}_{i,j+1} - \mathbf{m}_{ij})^2 - (\mathbf{m}_{i+1,j+1} - \mathbf{m}_{ij})^2\Big] \\ & + JS^2 \sum_{ij}^{N-1,N-1} \Big[\mathbf{m}_{ij}(\mathbf{n}_{i+1,j} + \mathbf{n}_{i,j+1} + \mathbf{n}_{i+1,j+1} - 3\mathbf{n}_{ij})\Big] \\ & - \mathbf{n}_{ij}(\mathbf{m}_{i+1,j} + \mathbf{m}_{i,j+1}\mathbf{m}_{i+1,j+1} - 3\mathbf{m}_{ij})\Big] \end{aligned}$$

The $\simeq$-sign is due to the neglection of a set of small boundary terms in the sum in the 2$^{\text{nd}}$ line of the above equation, where the fields are evaluated in the unit cells at the edges of the system. These contributions arise from terms like $\sim \sum_j^N (\mathbf{n}_{N,j} - \mathbf{n}_{N,j})^2$ for both fields. Similar terms, where the sums over the terms where the index equals $i, j+1$ when $i = 1 \vee j = 1$, $i = N \vee j = 1$ and the other index is summed over, yields a vanishingly small contribution to free energy for large systems. Thus, these terms are neglected when N and S is taken to be large, which is the case for macroscopic systems.

In the continuum limit, we can rewrite the lattice differences as derivatives in the linear approximation

$$\lim_{|\Delta_i|\to 0} \sum_{ij} (\mathbf{m}_{i+1,j} - \mathbf{m}_{ij}) \to \frac{1}{V_C} \int_C d\mathbf{r} \mathcal{J}_{\mathbf{m}} \Delta_i \tag{A.2a}$$

$$\lim_{|\Delta_i|,|\Delta_j|\to 0} \sum_{ij} (\mathbf{m}_{i+1,j+1} - \mathbf{m}_{ij}) \to \frac{1}{V_C} \int_C d\mathbf{r} \Big[\mathcal{J}_{\mathbf{m}} \Delta_i + \mathcal{J}_{\mathbf{m}} \Delta_j\Big] \tag{A.2b}$$

where the expression for the linear approximation for the j-direction is identical in form to the 1st line, and the expressions for the field $\mathbf{n}$ are identical. $\Delta_{i/j}$ are vectors between the unit cells in the i, j directions. V_C is the volume of the unit cell, which for a 2D square lattice is simply $V = |\Delta_i| \cdot |\Delta_j| = \Delta^2$, with Δ being the width of the unit cell. $\mathcal{J}_{\mathbf{m}}$ is the *Jacobian matrix* of the field $\mathbf{m}$, defined componentwise in terms of partial derivatives as

$$\mathcal{J}^{\mathbf{m}}_{ij} = \frac{\partial m_i}{\partial r_j} = \begin{bmatrix} \frac{\partial m_1}{\partial r_1} & \cdots & \frac{\partial m_n}{\partial r_j} \\ \vdots & \ddots & \vdots \\ \frac{\partial m_i}{\partial r_m} & \cdots & \frac{\partial m_n}{\partial r_m} \end{bmatrix}$$

with r_i being some set of spatial components, here taken to simply be $\{x, y, z\}$. The definitions are equivalent for the $\mathbf{n}$-field. With the introduction of the above integrals ,we rewrite $H_{exch.}$ as the integral of some energy density: $H_{exch.} = 1/V_C \int d\mathbf{r}\, \mathcal{F}_{exch.}$. We thus get have in the continuum limit

$$\begin{aligned} \mathcal{F}_{exch.} = N_n J S^2 \Bigg[& 2\mathbf{m}^2 + \frac{1}{2} \sum_{i=\{x,y\}} \Delta_i^2 \left\{ (\partial_x \mathbf{n})^2 - (\partial_x \mathbf{m})^2 \right\} \\ & + \frac{1}{4} \sum_{i=\{x,y\}, i \neq j} \Delta_i \Delta_j \left\{ \partial_x \mathbf{n} \partial_j \mathbf{n} - \partial_x \mathbf{m} \partial_j \mathbf{m} \right\} + \frac{1}{2} \sum_{i=\{x,y\}} \Delta_i \left\{ \mathbf{m} \partial_x \mathbf{n} - \mathbf{n} \partial_x \mathbf{m} \right\} \Bigg] \end{aligned}$$

where the $\mathbf{n}$-term corresponding to the 1st term $2\mathbf{m}$ disappears when summing over lattice sites due to the equivalence of $\mathbf{n}$ and $-\mathbf{n}$ discussed in chapter 2 of the thesis. N_n is the number of nearest neighbours, $N_n = 4$ for a 2D square lattice. The extra factor of 1/2 in the 3d term compensates for the double counting in the sum.

Specializing to the case of 2D centered square lattices and neglecting terms of higher order in the derivative of the magnetization, $\sim \{\partial_i \mathbf{m} \partial_j \mathbf{m}, (\partial_i \mathbf{m})^2, \mathbf{n} \partial_i \mathbf{m}\}$, we obtain

$$\mathcal{F}_{exch.} = \frac{a}{2}\mathbf{m}^2 + \frac{A}{2} \left[\sum_i (\partial_i \mathbf{n})^2 + \frac{1}{2} \sum_{i \neq j} \partial_i \mathbf{n} \partial_j \mathbf{n} \right] + B \sum_i \mathbf{m} \partial_i \mathbf{n} \tag{A.3}$$

Here, $a = 4N_n J S^2$, $A = N_n \Delta^2 J S^2/2$ and $B = N_n \Delta J S^2$.

The derivation of the magnetocrystalline anisotropy free energy contribution in the continuum limit follows the same procedure, but is much simpler in comparison. The easy-axis anisotropy taken to be in the z-direction added to the Heisenberg Hamiltonian has the form

$$\hat{H}_{anis.} = -K\left[\sum_{\alpha}(\mathbf{S}_{\alpha}\cdot\hat{z})^2 + \sum_{\beta}(\mathbf{S}_{\beta}\cdot\hat{z})^2\right] \tag{A.4}$$

Inserting the definitions of the spins in eq. A.1a and A.1b into the above expression and taking the 2D continuum limit as in equations A.2a and A.2b, we get

$$\begin{aligned}
\hat{\mathcal{H}}_{anis.} &\rightarrow H_{anis.} \\
&= -KS^2\sum_{ij}^{N,N}\left[(\mathbf{m}_{ij}+\mathbf{n}_{ij})_z^2 + (\mathbf{m}_{ij}-\mathbf{n}_{ij})_z^2\right] \\
&= -2KS^2\sum_{ij}^{N,N}\left[(\mathbf{m}_{ij}\cdot\hat{\mathbf{z}})^2 + (\mathbf{n}_{ij}\cdot\hat{\mathbf{z}})^2\right] \\
\text{(Continuum limit)} \rightarrow \mathcal{F}_{anis.} &= -KS^2\left[(\mathbf{m}\cdot\hat{\mathbf{z}})^2 + (\mathbf{n}\cdot\hat{\mathbf{z}})^2\right]
\end{aligned}$$

If we take the equilibrium Néel direction to be $\hat{\mathbf{z}}$, and noting that $\mathbf{n}\cdot\mathbf{m} = 0$, we take the magnetization to be negligible in the z-direction, and subsequently drop this term. We will make use of the definition $K_z = 2KS^2$.

The DMI-contribution to the free energy is obtained in the same way by insertion of eqs. A.1a and A.1b into the micromagnetic DMI-Hamiltonian

$$\hat{\mathcal{H}}_{DMI} = \sum_{<\mathbf{r}_1,\mathbf{r}_2>}\mathbf{D}_{\mathbf{r}_1,\mathbf{r}_2}\cdot(\mathbf{S}_{\mathbf{r}_1}\times\mathbf{S}_{\mathbf{r}_2}) \tag{A.5}$$

In this thesis, we consider interfacial DMI of the form

$$\begin{aligned}
\mathbf{D}_{\mathbf{r},\mathbf{r}+\delta\mathbf{r}_x} &= -D(\mathbf{r})\hat{\mathbf{z}} \\
\mathbf{D}_{\mathbf{r},\mathbf{r}+\delta\mathbf{r}_z} &= D(\mathbf{r})\hat{\mathbf{x}}
\end{aligned}$$

where $\delta\mathbf{r}_x$, $\delta\mathbf{r}_z$ are vectors joining the the current and the closest neighbouring site in the x- and z-directions respectively. We write $D = D(\mathbf{r})$ to emphasize the spatially inhomogeneous DMI.

Inserting the definitions A.1a and A.1b into $\hat{\mathcal{H}}_{DMI}$ and summing over $\{i,j\}$ for the four neighbouring sites, neglecting the boundary terms as done earlier, we get

$$
\begin{aligned}
\hat{\mathcal{H}}_{DMI} \;&\rightarrow H_{DMI} \\
&= S^2 \sum_{ij}^{N-1,N-1} \mathbf{D}_{\mathbf{r},\mathbf{r}'} \cdot \Big\{ \Big(\mathbf{m}_{ij} + \mathbf{n}_{ij} \Big) \times \Big[(\mathbf{m}_{ij} - \mathbf{n}_{ij}) + (\mathbf{m}_{i+1,j} - \mathbf{n}_{i+1,j}) \\
&\qquad + (\mathbf{m}_{i,j+1} - \mathbf{n}_{i,j+1}) + (\mathbf{m}_{i+1,j+1} - \mathbf{n}_{i+1,j+1}) \Big] \Big\} \\
&= S^2 D(\mathbf{r}) \sum_{ij}^{N-1,N-1} \Big\{ -\hat{\mathbf{z}} \Big((\mathbf{m}_{ij} + \mathbf{n}_{ij}) \times \Big[(\mathbf{m}_{ij} - \mathbf{n}_{ij}) + (\mathbf{m}_{i+1,j+1} - \mathbf{n}_{i+1,j+1}) \Big] \Big) \Big\} \\
&\qquad + \Big\{ \hat{\mathbf{x}} \Big((\mathbf{m}_{ij} + \mathbf{n}_{ij}) \times \Big[(\mathbf{m}_{i+1,j} - \mathbf{n}_{i+1,j}) + (\mathbf{m}_{i,j+1} - \mathbf{n}_{i,j+1}) \Big] \Big) \Big\}
\end{aligned}
$$

The grouping of the terms in vector products of the two last lines in the $\hat{\mathbf{x}}$ and $\hat{\mathbf{z}}$-directions is arbitrary as long as both terms obtain contributions from the same number of unit cells an equal number of lattice vectors away from the current site $\{i, j\}$. We drop all terms containing the magnetization $\mathbf{m}$, since it is small relative to $\mathbf{n}$, and the DMI- strength is weak compared to the exchange parameters. Writing out the remaining non-zero vector products, we have

$$
H_{DMI} \;\simeq\; S^2 D(\mathbf{r}) \sum_{ij}^{N-1,N-1} \hat{\mathbf{z}} (\mathbf{n}_{ij} \times \mathbf{n}_{i+1,j+1}) - \hat{\mathbf{x}} \Big[\mathbf{n}_{ij} \times (\mathbf{n}_{i+1,j} + \mathbf{n}_{i,j+1}) \Big]
$$

We proceed to write out the terms in the cross products in the directions specified and replace the lattice differences in the fields with directional derivatives as before.

$$
\begin{aligned}
H_{DMI} \;&= S^2 D(\mathbf{r}) \sum_{ij}^{N-1,N-1} (n^x_{ij} n^y_{i+1,j+1} - n^y_{ij} n^x_{i+1,j+1}) \\
&\qquad - \Big[(n^y_{ij} n^z_{i+1,j} - n^z_{ij} n^y_{i+1,j}) + (n^y_{ij} n^z_{i,j+1} - n^z_{ij} n^y_{i,j+1}) \Big] \\
n_{i+1,j} - n_{ij} \simeq \Delta \partial_x \text{ etc...} \;&\rightarrow S^2 D(\mathbf{r}) \sum_{ij}^{N-1,N-1} n^x_{ij} (\Delta \partial_x + \Delta \partial_z + 1) n^y_{ij} - n^y_{ij} (\Delta \partial_x + \Delta \partial_z + 1) n^x_{ij} \\
&\qquad - \Big[n^y_{ij} (\Delta \partial_x + 1) n^z_{ij} - n^z_{ij} (\Delta \partial_x + 1) n^y_{ij} \Big] \\
&\qquad - \Big[n^y_{ij} (\Delta \partial_z + 1) n^z_{ij} - n^z_{ij} (\Delta \partial_z + 1) n^y_{ij} \Big] \\
&= \Delta S^2 D(\mathbf{r}) \sum_{ij}^{N-1,N-1} - n^y_{ij} (\partial_x n^x_{ij} + \partial_z n^x_{ij} + \partial_x n^z_{ij} + \partial_z n^x_{ij}) \\
&\qquad + (n^x_{ij} + n^z_{ij}) (\partial_x n^y_{ij} + \partial_z n^y_{ij})
\end{aligned} \tag{A.6}
$$

The energy contributions to the DMI is determined by the crystal symmetry of the material. In the micromagnetic limit we consider, we can write the DMI-

contribution as the integral over some energy density (as we have already done) [86]

$$\hat{\mathcal{H}}_{DMI} = \int_V dV \mathcal{F}_{DMI} = \lambda_{DMI} \int_V dV \mathcal{L}_{inv}$$

where λ_{DMI} is a material dependent constant. $\mathcal{L}_{inv}$ are so called *Lifshitz invariants* [30, 43, 86], linear combinations of spatial derivatives of the order parameter determined by the symmetry group of the magnetic material. The linear derivatives is a manifestation of the chiral nature of the DMI.

$$\mathcal{L}_{inv} = \mathcal{L}_{ij}^{k} = m_i \frac{\partial m_j}{\partial x_k} - m_j \frac{\partial m_i}{\partial x_k}$$

The most common type of symmetry is T-symmetry, which has the invariants

$$\mathcal{L} = \mathcal{L}_{yx}^{z} + \mathcal{L}_{xz}^{y} + \mathcal{L}_{zy}^{x} = \mathbf{m} \cdot (\nabla \times \mathbf{m})$$

However, we will consider IDMI in a thin film with broken inversion/mirror symmetry along the y-axis. Thus, for a centered square lattice AFM model, we are prompted to consider a system with one mirror plane and with the axis of symmetry contained in the (xz) plane, see fig. 2.2. This corresponds to the *cyclic symmetry group* C_{nv} with $n = 1$, with the subscript v denoting that we consider the *vertical* symmetry planes. The Lifshitz-invariants of the C_{nv}-group take the form [86]

$$\begin{aligned} \mathcal{L}_{ij}^{(k)C_{nv}} &= \mathcal{L}_{zy}^{z} + \mathcal{L}_{xy}^{x} \\ &= m_z \frac{\partial m_y}{\partial z} - m_y \frac{\partial m_x}{\partial z} + m_x \frac{\partial m_y}{\partial x} - m_y \frac{\partial m_x}{\partial x} \end{aligned}$$

Keeping only the terms corresponding to the Lifschitz-invariants consistent with the C_{nv}crystal symmetry for our system in eq. A.6, and replacing the sums with intergrals in the continuum limit, we obtain the free energy contribution of the interfacial DMI in the form

$$F_{DMI} = \frac{1}{V_C} \int d\mathbf{r}\, \mathcal{F}_{DMI}^{2D} = \frac{1}{V_C} \int d\mathbf{r} \mathcal{D}(\mathbf{r}) [(\mathbf{n} \cdot \hat{\mathbf{y}})(\nabla \cdot \mathbf{n}) - (\mathbf{n} \cdot \nabla)(\mathbf{n} \cdot \hat{\mathbf{y}})]$$

with $\mathcal{D}(\mathbf{r}) = \Delta S^2 D(\mathbf{r})$

The complete form of the free energy density for the collinear easy-axis AFM subject to interfacial DMI of the above type, including the magnetic field in a general direction, thus has the form

$$\mathcal{F}^{2D} \equiv \mathcal{F}_{AFM} = \mathcal{F}_{exch.} + \mathcal{F}_{anis.} + \mathcal{F}_{DMI} \tag{A.7}$$

$$= \frac{a}{2}|\mathbf{m}|^2 + \frac{A}{2}\left[\sum_i (\partial_i \mathbf{n})^2 + \frac{1}{2}\sum_{i\neq j} \partial_i \mathbf{n}\partial_j \mathbf{n}\right] + B\sum_i \mathbf{m}\partial_i \mathbf{n} - \frac{K_z}{2}(\mathbf{n}\cdot\hat{\mathbf{z}})^2 \tag{A.8}$$

$$+ \mathcal{D}(\mathbf{r})\left[(\mathbf{n}\cdot\hat{\mathbf{y}})(\nabla\cdot\mathbf{n}) - (\mathbf{n}\cdot\nabla)(\mathbf{n}\cdot\hat{\mathbf{y}})\right] - \rho\gamma(\mathbf{m}\cdot\mathbf{H}) \tag{A.9}$$

APPENDIX B

OBTAINING THE SEMI-CLASSICAL EQUATIONS OF MOTION IN THE EXCHANGE APPROXIMATION

The Lagrangian density $\mathcal{L}$ is a functional of the fields $\mathbf{n}$ and $\mathbf{m}$ and their derivatives up to 1st order, as noted in chap. 2 of the thesis.

$$\begin{aligned}\mathcal{L}[\mathbf{n}(\mathbf{r},t),\mathbf{m}(\mathbf{r},t)] &= \mathcal{K}-\mathcal{F}\\ &= \rho(\dot{\mathbf{n}}\times\mathbf{n})\cdot\mathbf{m}-\left[a\frac{|\mathbf{m}|^2}{2}+\frac{A}{2}|\partial_i\mathbf{n}|^2-\frac{K_z}{2}(\mathbf{n}\cdot\hat{z})^2-\mathbf{H}\cdot\mathbf{m}\right.\\ &\qquad\left.+\mathcal{D}(\mathbf{r})[(\mathbf{n}\cdot\hat{\mathbf{y}})(\nabla\cdot\mathbf{n})-\mathbf{n}\cdot\nabla(\mathbf{n}\cdot\hat{\mathbf{y}})]+\lambda(\mathbf{n}\cdot\mathbf{m})+\frac{\beta}{2}(\mathbf{n}^2-1)\right]\end{aligned} \tag{B.1}$$

where we have omitted the term $\sim\mathbf{m}\cdot(\nabla\times\mathbf{m})$ because it is of higher order in the magnetization. Note that the magnetic field is defined as $\mathbf{H}=g\mu_B\mathbf{H}_{ext}=\gamma\rho\mathbf{H}_{ext}$.

Before proceeding, we state some important identities which will prove useful in the derivation

$$\mathbf{a}\times(\mathbf{b}\times\mathbf{c})=(\mathbf{a}\cdot\mathbf{c})\mathbf{b}-(\mathbf{a}\cdot\mathbf{b})\mathbf{c} \tag{B.2}$$

$$\mathbf{a}\cdot(\mathbf{b}\times\mathbf{c})=\mathbf{c}\cdot(\mathbf{a}\times\mathbf{b})=\mathbf{b}\cdot(\mathbf{c}\times\mathbf{a}) \tag{B.3}$$

Invoking the *principle of least action* [16, 41], setting the variation of the action to 0, we obtain the equations of motion for the system.

$$\frac{\delta S}{\delta\psi_i} = 0 = \int d\mathbf{r}dt\left[\frac{\partial\mathcal{L}}{\partial\psi_i}-\sum_{j=1}^{n}\frac{\partial}{\partial_j}\left(\frac{\partial\mathcal{L}}{\partial(\partial_j\psi_i)}\right)\right] \tag{B.4}$$

where the *Euler-Lagrange-equations* for the i fields is given by

$$\frac{\partial\mathcal{L}}{\partial\psi_i}-\sum_{j=1}^{n}\frac{\partial}{\partial_j}\left(\frac{\partial\mathcal{L}}{\partial(\partial_j\psi_i)}\right)=0 \tag{B.5}$$

where the $\psi=\psi(\mathbf{r},t)$ is a funtion of space and time, and the sum goes over all coordinates.

We proceed to vary $\mathcal{L}$ w.r.t. $\mathbf{n}$ and $\mathbf{m}$. The equations of motion are obtained by setting this variation to zero.

$$\delta_{\mathbf{n}}\mathcal{L} \equiv \frac{\delta\mathcal{L}}{\delta\mathbf{n}} = \frac{\delta\mathcal{K}}{\delta\mathbf{n}} - \frac{\delta\mathcal{F}}{\delta\mathbf{n}} = 0 \tag{B.6}$$

$$\delta_{\mathbf{m}}\mathcal{L} \equiv \frac{\delta\mathcal{L}}{\delta\mathbf{m}} = \frac{\delta\mathcal{K}}{\delta\mathbf{m}} - \frac{\delta\mathcal{F}}{\delta\mathbf{m}} = 0 \tag{B.7}$$

The variation of the kinetic part is obtained as

$$\begin{aligned}
\frac{\delta\mathcal{K}}{\delta\mathbf{n}} &= \frac{\delta}{\delta\mathbf{n}}\left[\rho(\dot{\mathbf{n}}\times\mathbf{n})\cdot\mathbf{m}\right] \\
&= \frac{\delta}{\delta\mathbf{n}}\left[\rho(\mathbf{m}\times\dot{\mathbf{n}})\cdot\mathbf{n}\right] \\
&= \rho(\mathbf{m}\times\dot{\mathbf{n}}) - \frac{\delta}{\delta t}\frac{\partial\mathcal{K}}{\partial(\dot{\mathbf{n}})} \\
&= 2\rho(\mathbf{m}\times\dot{\mathbf{n}}) + \rho(\dot{\mathbf{n}}\times\mathbf{n}) \qquad \text{(B.8)} \\
\frac{\delta\mathcal{K}}{\delta\mathbf{m}} &= \rho(\dot{\mathbf{n}}\times\mathbf{n}) \qquad \text{(B.9)}
\end{aligned}$$

where we have left out writing the integral for clarity.

The functional derivatives of $\mathcal{F}$ w.r.t. the fields gives us the effective fields $\mathbf{f}_n$ and $\mathbf{f}_m$.

$$-\mathbf{f}_n \equiv \frac{\delta\mathcal{F}}{\delta\mathbf{n}} = -A\nabla^2\mathbf{n} - K_z(\mathbf{n}\cdot\hat{\mathbf{z}})\hat{\mathbf{z}} + \lambda\mathbf{m} + \beta\mathbf{n} + \mathcal{D}\left[\hat{\mathbf{y}}(\nabla\cdot\mathbf{n}) - \nabla(\mathbf{n}\cdot\hat{\mathbf{y}})\right] \tag{B.10}$$

$$-\mathbf{f}_m \equiv \frac{\delta\mathcal{F}}{\delta\mathbf{m}} = a\mathbf{m} - \mathbf{H} + \lambda\mathbf{n} \tag{B.11}$$

Combining all terms, we have an expression for the variation

$$\begin{aligned}
\delta_{\mathbf{n}}\mathcal{L} = 0 \implies & 2\rho(\mathbf{m}\times\dot{\mathbf{n}}) + \rho(\dot{\mathbf{m}}\times\mathbf{n}) + A\nabla^2\mathbf{n} + K_z n_{\hat{\mathbf{z}}}\hat{\mathbf{z}} \qquad \text{(B.12)} \\
& - \mathcal{D}\left[\hat{\mathbf{y}}(\nabla\cdot\mathbf{n}) - \nabla n_{\hat{y}}\right] - \lambda\mathbf{m} - \beta\mathbf{n} = 0 \\
\delta_{\mathbf{m}}\mathcal{L} = 0 \implies & \rho(\dot{\mathbf{n}}\times\mathbf{n}) - a\mathbf{m} + \mathbf{H} - \lambda\mathbf{n} = 0 \qquad \text{(B.13)}
\end{aligned}$$

The forms of the EOMs in LLG form, eq. 2.34, can be obtained by by considering the cross products of $\delta_{\mathbf{m}}\mathcal{L}$ and $\delta_{\mathbf{n}}\mathcal{L}$ with $\mathbf{n}$.

$$
\begin{aligned}
\mathbf{n}\times\delta_{\mathbf{n}}\mathcal{L} &= 2\rho\mathbf{n}\times(\mathbf{m}\times\dot{\mathbf{n}})+\rho\mathbf{n}\times(\dot{\mathbf{m}}\times\mathbf{n})+A\mathbf{n}\times(\nabla^2\mathbf{n}) \\
&\qquad + K_z n_{\hat{\mathbf{z}}}\mathbf{n}\times\hat{\mathbf{z}} - \mathcal{D}\mathbf{n}\times\left[\hat{\mathbf{y}}(\nabla\cdot\mathbf{n})-\nabla n_y\right]-\lambda\mathbf{n}\times\mathbf{m} \\
&= \rho\mathbf{n}\times\{\mathbf{m}\times\dot{\mathbf{n}}\ +\dot{\mathbf{m}}\times\mathbf{n}\}+\mathbf{n}\times\{K_z n_{\hat{\mathbf{z}}}\hat{\mathbf{z}} \\
&\qquad + A\nabla^2\mathbf{n}-\mathcal{D}\left[\hat{\mathbf{y}}(\nabla\cdot\mathbf{n})-\nabla n_y\right]-\lambda\mathbf{m}-\beta\mathbf{n}\Big\} \\
&= \rho(\dot{\mathbf{m}}-(\mathbf{n}\cdot\dot{\mathbf{m}})\mathbf{n})+\mathbf{n}\times\mathbf{f}_{\mathbf{n}}=0
\end{aligned}
$$

$$
\begin{aligned}
\mathbf{n}\times\delta_{\mathbf{m}}\mathcal{L} &= \rho\mathbf{n}\times(\dot{\mathbf{n}}\times\mathbf{n})+\mathbf{n}\times\mathbf{f}_{\mathbf{m}} \\
&= \rho\dot{\mathbf{n}}+\mathbf{n}\times\mathbf{f}_{\mathbf{m}}=0
\end{aligned}
$$

We rewrite the term $\sim(\mathbf{n}\cdot\dot{\mathbf{m}})\mathbf{n}$ in the equation for $\mathbf{n}\times\delta_{\mathbf{n}}\mathcal{L}$ as

$$
\begin{aligned}
\mathbf{n}(\mathbf{n}\cdot\dot{\mathbf{m}}) &= \mathbf{n}\left[\frac{d}{dt}\underbrace{(\mathbf{n}\cdot\mathbf{m})}_{=0}-\dot{\mathbf{n}}\cdot\mathbf{m}\right] \\
&= -\mathbf{n}\left[(\mathbf{f}_{\mathbf{m}}\times\mathbf{n})\cdot\mathbf{m}\right] \\
&= \mathbf{n}\left[\mathbf{n}\cdot(\mathbf{f}_{\mathbf{m}}\times\mathbf{m})\right] \\
&= \mathbf{f}_{\mathbf{m}}\times\mathbf{m}
\end{aligned}
$$

Thus, we have obtained the time evolution of the fields in the form of eq. 2.34.

$$
\begin{aligned}
\dot{\mathbf{n}} &= \rho\mathbf{f}_{\mathbf{m}}\times\mathbf{n} \\
\dot{\mathbf{m}} &= \rho\left[\mathbf{f}_{\mathbf{n}}\times\mathbf{n}+\mathbf{f}_{\mathbf{m}}\times\mathbf{m}\right]
\end{aligned}
\tag{B.14}
$$

To obtain the Lagrange multipliers $\{\lambda,\beta\}$, we consider the dot product of $\delta_{\mathbf{m}}\mathcal{L}$ and $\delta_{\mathbf{n}}\mathcal{L}$ with $\mathbf{n}$.

$$
\begin{aligned}
\mathbf{n}\cdot\delta_{\mathbf{m}}\mathcal{L}=0 \implies \mathbf{n}\cdot(\dot{n}\times\mathbf{n}) &= \mathbf{n}\cdot(a\mathbf{m}-\mathbf{H}+\lambda\mathbf{n}) \\
&= -\mathbf{n}\cdot\mathbf{H}+\lambda \\
\implies \lambda &= \mathbf{n}\cdot\mathbf{H}
\end{aligned}
$$

$$
\begin{aligned}
\mathbf{n}\cdot\delta_{\mathbf{n}}\mathcal{L}=0 &\implies 2\mathbf{n}\cdot(\mathbf{m}\times(\mathbf{f}_{\mathbf{m}}\times\mathbf{n}))=-A\mathbf{n}\cdot\nabla^2\mathbf{n}-K_z n_z^2+\beta+\mathcal{D}\mathbf{n}\cdot[\hat{\mathbf{y}}(\nabla\cdot\mathbf{n})-\nabla(\mathbf{n}\cdot\hat{\mathbf{y}})] \\
&\implies \beta = A\mathbf{n}\cdot\nabla^2\mathbf{n}+K_z n_z^2-\mathcal{D}\mathbf{n}\cdot[\hat{\mathbf{y}}(\nabla\cdot\mathbf{n})-\nabla(\mathbf{n}\cdot\hat{\mathbf{y}})]-2\mathbf{f}_{\mathbf{m}}\cdot\mathbf{m}
\end{aligned}
$$

The expressions for λ and β are then substituted back into the equations for the effective fields $\mathbf{f}_{\mathbf{n}}$ and $\mathbf{f}_{\mathbf{m}}$, eqs. B.10 and B.11, to obtain

$$
\begin{aligned}
\mathbf{f}_\mathbf{n} &= A\nabla^2\mathbf{n} + K_z(\mathbf{n}\cdot\hat{\mathbf{z}})\hat{\mathbf{z}} - \mathcal{D}\left[\hat{\mathbf{y}}(\nabla\cdot\mathbf{n}) - \nabla(\mathbf{n}\cdot\hat{\mathbf{y}})\right] - \lambda\mathbf{m} - \beta\mathbf{n} \\
&= A\nabla^2\mathbf{n} + K_z(\mathbf{n}\cdot\hat{\mathbf{z}})\hat{\mathbf{z}} - \mathcal{D}\left[\hat{\mathbf{y}}(\nabla\cdot\mathbf{n}) - \nabla(\mathbf{n}\cdot\hat{\mathbf{y}})\right] - (\mathbf{n}\cdot\mathbf{H})\mathbf{m} \\
&\qquad - \Big(A\mathbf{n}\cdot\nabla^2\mathbf{n} + K_z n_z^2 - \mathcal{D}\left[\hat{\mathbf{y}}(\nabla\cdot\mathbf{n}) - \nabla(\mathbf{n}\cdot\hat{\mathbf{y}})\right] - 2\mathbf{f}_\mathbf{m}\cdot\mathbf{m}\Big)\mathbf{n} \\
&= A\mathbf{n}\times(\nabla^2\mathbf{n}\times\mathbf{n}) + K_z n_z\mathbf{n}\times(\hat{z}\times\mathbf{n}) - (\mathbf{n}\cdot\mathbf{H})\mathbf{m} \\
&\qquad - \mathcal{D}\mathbf{n}\times\Big(\left[\hat{\mathbf{y}}(\nabla\cdot\mathbf{n}) - \nabla(\mathbf{n}\cdot\hat{\mathbf{y}})\right]\times\mathbf{n}\Big) + 2(\mathbf{f}_\mathbf{m}\cdot\mathbf{m})\mathbf{n} \\
\mathbf{f}_\mathbf{m} &= -a\mathbf{m} + \mathbf{n}\times(\mathbf{H}\times\mathbf{n})
\end{aligned}
$$

where we have used the identity B.2 in the 3$^{\text{d}}$ line. Upon insertion of the effective fields into the EOMs, we obtain the coupled LLG equations

$$
\begin{aligned}
\rho\dot{\mathbf{n}} &= \left[-a\mathbf{m} + \mathbf{n}\times(\mathbf{H}\times\mathbf{n})\right]\times\mathbf{n} \\
\rho\dot{\mathbf{m}} &= \Big[A\mathbf{n}\times(\nabla^2\mathbf{n}\times\mathbf{n}) + K_z n_z\mathbf{n}\times(\hat{z}\times\mathbf{n}) - (\mathbf{n}\cdot\mathbf{H})\mathbf{m} \\
&\qquad - \mathcal{D}\mathbf{n}\times\left(\left[\hat{\mathbf{y}}(\nabla\cdot\mathbf{n}) - \nabla(\mathbf{n}\cdot\hat{\mathbf{y}})\right]\times\mathbf{n}\right)\Big]\times\mathbf{n} \\
&\qquad - \left[a\mathbf{m} - \mathbf{n}\times(\mathbf{H}\times\mathbf{n})\right]\times\mathbf{m}
\end{aligned}
$$

In the exchange approximation, the dynamics of the magnetization $\mathbf{m}$ is determined completely by the staggered magnetization $\mathbf{n}$, and thus, we can write the coupled EOMs as a single differential equation in $\mathbf{n}$.

From the equation for $\dot{\mathbf{n}}$, we are able to isolate an expression for the magnetization $\mathbf{m}$

$$
\mathbf{m} = \frac{\rho}{a}\dot{\mathbf{n}}\times\mathbf{n} + \frac{1}{a}\mathbf{n}\times(\mathbf{H}\times\mathbf{n})
$$

We now substitute the expression for $\mathbf{m}$ into the Lagrangian in B.1 to obtain our effective Lagrangian density. The terms including $\mathbf{m}$ becomes

$$
\begin{aligned}
\rho(\dot{\mathbf{n}}\times\mathbf{n}) &= \frac{\rho^2}{a}|\dot{\mathbf{n}}|^2 + \frac{\rho}{a}(\dot{\mathbf{n}}\times\mathbf{n})\cdot\mathbf{H} \\
\frac{a|\mathbf{m}|^2}{2} &= \frac{\rho^2}{a}|\dot{\mathbf{n}}|^2 + \frac{2\rho}{a}(\dot{\mathbf{n}}\times\mathbf{n})\cdot\mathbf{H} + \frac{H^2}{2a} - \frac{1}{2a}(\mathbf{n}\cdot\mathbf{H})^2 \\
\mathbf{H}\cdot\mathbf{m} &= \frac{\rho}{a}(\dot{\mathbf{n}}\times\mathbf{n})\cdot\mathbf{H} + \frac{H^2}{a} - \frac{1}{a}(\mathbf{n}\cdot\mathbf{H})^2
\end{aligned}
$$

$\mathcal{L}$ then becomes

$$\mathcal{L}[\mathbf{n},\dot{\mathbf{n}},\partial_i\mathbf{n}] = \frac{\rho^2}{2a}|\dot{\mathbf{n}}|^2 - \frac{A}{2}|\partial_i\mathbf{n}|^2 + \frac{K_z}{2}(\mathbf{n}\cdot\hat{z})^2 \tag{B.15}$$

$$+ \frac{\rho}{a}(\dot{\mathbf{n}}\times\mathbf{n})\cdot\mathbf{H} + \frac{H^2}{2} - \frac{1}{2}(\mathbf{n}\cdot\mathbf{H})^2 - \mathcal{D}(\mathbf{r})\left[(\mathbf{n}\cdot\hat{\mathbf{y}})(\nabla\cdot\mathbf{n}) - \mathbf{n}\cdot\nabla(\mathbf{n}\cdot\hat{\mathbf{y}})\right] \tag{B.16}$$

$$= \frac{\rho^2}{2a}(\dot{\mathbf{n}} - \gamma\mathbf{H}_{ext}\times\mathbf{n})^2 - \frac{A}{2}|\partial_i\mathbf{n}|^2 + \frac{K_z}{2}(\mathbf{n}\cdot\hat{z})^2 - \mathcal{D}(\mathbf{r})\left[(\mathbf{n}\cdot\hat{\mathbf{y}})(\nabla\cdot\mathbf{n}) - \mathbf{n}\cdot\nabla(\mathbf{n}\cdot\hat{\mathbf{y}})\right] \tag{B.17}$$

where we in the last line inserted the definition of $\mathbf{H}$ given at the start of the appendix. We have now arrived at the classical non-linear σ-model discussed in the thesis, with the action S given by

$$S = \int dtd\mathbf{r}\,\mathcal{L} \tag{B.18}$$

$$= \int dtd\mathbf{r}\left\{\frac{A}{2}\left[\frac{1}{c^2}(\dot{\mathbf{n}} - \gamma\mathbf{H}_{ext}\times\mathbf{n})^2 - |\partial_i\mathbf{n}|^2\right]\right. \tag{B.19}$$

$$\left. + \frac{K_z}{2}(\mathbf{n}\cdot\hat{z})^2 - \mathcal{D}(\mathbf{r})\left[(\mathbf{n}\cdot\hat{\mathbf{y}})(\nabla\cdot\mathbf{n}) - \mathbf{n}\cdot\nabla(\mathbf{n}\cdot\hat{\mathbf{y}})\right]\right\}$$

To describe the spin waves in terms of the Néel field fluctuations $\delta\mathbf{n}$ around the equilibrium configuration $\mathbf{n}_0 = \hat{z}$, we introduce the complex field $\psi = \delta\mathbf{n}\cdot(\hat{e}_x + i\hat{e}_y) = \delta n_x + i\delta n_y$. The spin wave helicity is reflected in taking the complex conjugate of ψ: $\bar{\psi} = \psi_- = \delta_x - i\delta n_y$. We also define $\psi_+ = \delta n_x + i\delta n_y$, and have that $\bar{\psi}\psi = \delta n_x^2 + \delta n_y^2$.

We now linearize the action S in the absence of DMI (added later in the appendix) in the fluctuation $\delta\mathbf{n}$ and for constant magnetic field $\mathbf{H} = H\hat{z}$. We make use of the definition of the spin wave function ψ to express the components of $\delta\mathbf{n}$ as

$$\delta n_x = \frac{(\psi + \bar{\psi})}{2}$$

$$i\delta n_y = \frac{(\psi - \bar{\psi})}{2}$$

Inserting the above expressions into eq. B.18, keeping terms up to 2^{nd} order in the fields ψ and $\bar{\psi}$, and applying Euler-Lagrange's equations B.5 to the resulting expression, we obtain the equations of motion for the SW-fields. Writing the result as a matrix equation, we obtain after some calculation

$$\frac{A}{2}\frac{1}{c^2}\frac{\partial^2\mathbf{\Psi}}{\partial t^2} = \left[\frac{A}{2}\nabla^2 - \frac{K_z}{2} + \frac{A}{2}(\gamma\rho H)^2 + Ai\sigma_3\gamma\rho^2 H\partial_t\right]\mathbf{\Psi}$$

$$\rightarrow \frac{1}{c^2}\frac{\partial^2\mathbf{\Psi}}{\partial t^2} = \left[\nabla^2 - \frac{K_z}{A} + (\gamma\rho H)^2 + 2i\sigma_3\gamma\rho^2 H\partial_t\right]\mathbf{\Psi}$$

where $\mathbf{\Psi} = [\psi_+, \psi_-]^T$ and σ_3 is the 3$^{\text{d}}$ Pauli matrix for ease of notation. We take the other terms to be multiplied by the two-dimensional identity matrix $\mathbb{I}_2$.

We can rewrite the free energy contribution of the DMI F_{DMI}^{AFM} in terms of the spin wave fields $\psi, \bar{\psi}$ to acquire a Hermitian operator in a similar fashion as in [124]. The DMI-term in eq. 2.25, including homogeneous d_h and inhomogeneous DMI $D(\mathbf{r})$, is treated separately. In a effective bosonic field theory to lowest non-interacting order (quadratic), the terms in the Lagrangian must be bilinears in the fields [70, 106]. The DMI-operator must then have some bilinear form, $\psi^\dagger \hat{\mathcal{H}} \psi$ in the action S. Since $S \sim \mathcal{L} = \mathcal{K} - \mathcal{F}$, this bilinear form must be present in the free energy.

In the thin film-regime, we only allow the fluctuations $\delta\mathbf{n}$ to vary in the basal xz-plane. Thus, we establish that $\partial_y \psi \sim 0$, as discussed in the thesis. The DMI-free energy for a plane lattice with mirror symmetry breaking along the $\hat{y}$-direction [124] can be written as

$$\begin{aligned} F_{DMI} &= -\int d\mathbf{r} \mathcal{D}(\mathbf{r})\, \mathbf{n} \times [(\hat{y} \times \nabla) \times \mathbf{n}] \\ &= \int d\mathbf{r}\, \mathcal{D}(\mathbf{r}) [(\mathbf{n} \cdot \hat{\mathbf{y}})(\nabla \cdot \mathbf{n}) - \mathbf{n} \cdot \nabla(\mathbf{n} \cdot \hat{\mathbf{y}})] \\ &= \int d\mathbf{r}\, D(\mathbf{r}) \Big[n_y \partial_i n_i - n_i \partial_i n_y \Big] \\ &= \int d\mathbf{r}\, D(\mathbf{r}) \Big[n_y \partial_x n_x + n_y \partial_z n_z - n_x \partial_x n_y - n_y \partial_z n_z \Big] \end{aligned}$$

where the subscripts on the fields denote the dot product $(\mathbf{n} \cdot \hat{x})$ etc. Invoking the decomposition of the Néel order into fluctuations $\delta\mathbf{n}(x,z;t) = \delta n_x(x,z;t)\hat{x} + \delta n_y(x,z;t)\hat{y}$ orthogonal to the stationary equilibrium order direction $\mathbf{n}_0 = \hat{z}$ and inserting this into the above expression, we obtain

$$F_{DMI} = \int d\mathbf{r}\, D(\mathbf{r}) \Big[\delta n_y \partial_x \delta n_x - \delta n_x \partial_x \delta n_y \Big] \tag{B.20}$$

We now want to obtain the bilinear form $\propto \bar{\psi} \partial_x \psi$, with the spin wave function $\psi = \delta n_x + i \delta n_y$. Expressed in terms of the fluctuation components $\delta n_x, \delta n_y$, we have

$$\begin{aligned} \bar{\psi} \partial_x \psi &= (\delta n_x - i\delta n_y) \partial_x (\delta n_x + i \delta n_y) \\ &= \underbrace{\delta n_x \partial_x \delta n_x + \delta n_y \partial_x \delta n_y}_{= 0, \text{ since } \frac{1}{2}\partial_x \left[\delta n_x^2 + \delta n_y^2 + n_0 \cdot n_0 \right] = \frac{1}{2}\partial_x [1] = 0} + i \delta n_x \partial_x \delta n_y - i \delta n_y \partial_x \delta n_x \\ &= -i \Big[\delta n_y \partial_x \delta n_x - \delta n_x \partial_x \delta n_y \Big] \\ \implies & \delta n_y \partial_x \delta n_x - \delta n_x \partial_x \delta n_y \\ &= i \bar{\psi} \partial_x \psi \end{aligned} \tag{B.21}$$

We can then rewrite eq. B.20 as

$$\begin{aligned} F_{DMI} &= i\int d\mathbf{r} D(\mathbf{r})\left[\bar{\psi}\partial_x\psi\right] \\ &= \frac{i}{2}\int d\mathbf{r} D(\mathbf{r})\left[\bar{\psi}\partial_x\psi + \bar{\psi}\partial_x\psi\right] \\ &= \frac{i}{2}\int d\mathbf{r} D(\mathbf{r})\left[\bar{\psi}\partial_x\psi\right] + \frac{i}{2}\left\{D(\mathbf{r})\bar{\psi}\psi\Big|_\Omega - \int d\mathbf{r}\partial_x(D(\mathbf{r})\bar{\psi})\psi\right\} \\ &= \frac{i}{2}\int d\mathbf{r}\left[D(\mathbf{r})\bar{\psi}\partial_x\psi - \partial_x(D(\mathbf{r})\bar{\psi})\psi\right] \end{aligned} \tag{B.22}$$

where in the 3$^{\text{d}}$ line a integration by parts was performed. Summation over all indices in the derivative is implied. In the fourth line, we have neglected the boundary term since it is only expected to give rise to surface effects which we do not consider. Writing out the derivative in the 2$^{\text{nd}}$ term, we get

$$\begin{aligned} F_{DMI} =& \frac{i}{2}\int d\mathbf{r}\left[D(\mathbf{r})\bar{\psi}\partial_x\psi - \partial_x(D(\mathbf{r})\bar{\psi})\psi\right] \\ =& \frac{i}{2}\int d\mathbf{r}\ \left[D(\mathbf{r})\bar{\psi}\partial_x\psi - \bar{\psi}\psi\partial_x D(\mathbf{r}) - D(\mathbf{r})\psi\partial_x\bar{\psi}\right] \end{aligned}$$

Taking the functional derivative w.r.t. $\bar{\psi}$ with the definition of the Euler-Lagrange-equations B.5, we get

$$\begin{aligned} \frac{\delta F_{DMI}}{\delta\bar{\psi}} &= \frac{i}{2}\int d\mathbf{r}\frac{\delta}{\delta\bar{\psi}}\left(D(\mathbf{r})\bar{\psi}\partial_x\psi - \bar{\psi}\psi\partial_x D(\mathbf{r}) - D(\mathbf{r})\psi\partial_x\bar{\psi}\right) \\ &= \frac{i}{2}\int d\mathbf{r}\left(D(\mathbf{r})\partial_x\psi - \partial_x D(\mathbf{r})\psi - \partial_x\left(\psi D(\mathbf{r})\right)\right) \\ &= \frac{i}{2}\int d\mathbf{r}\ \left[D(\mathbf{r})\partial_x\psi - \partial_x D(\mathbf{r})\psi\right] \end{aligned} \tag{B.23}$$

We neglect the last term in line two because it is the integral over a total derivative. We have now obtained a Hermitian form of the effective DMI-operator analogous to the ferromagnetic effective Schrödinger equation in [124]. Our corresponding effective Klein-Gordon-equation for AFM spin waves, with definitions of the parameters given in table 2.7 and the surrounding discussion, reads

$$\frac{1}{c^2}\frac{\partial^2\boldsymbol{\Psi}}{\partial t^2} = \left[\nabla^2 - \frac{K_z}{A} + (\gamma\rho H)^2 + 2i\sigma_3\gamma\rho^2 H\partial_t - \frac{i}{A}\sigma_3\left[D^*(\mathbf{r})\partial_x - \partial_x D^*(\mathbf{r})\right]\right]\boldsymbol{\Psi}$$

APPENDIX C

EQUATIONS OF MOTION FOR NÉEL ORDER FLUCTUATIONS

As a sidenote, we here briefly obtain a equation for the fluctuations $\delta\mathbf{n}$ suitable as a continuum model for magnetic excitations in the form of textures, e.g. skyrmions, as done in [131].

We insert the form of the Néel field in the form of eq. 2.36, with the spin wave fluctuations in eq. 2.37. Expanding the EOMs in $\mathbf{n}_0$ and $\delta\mathbf{n}$, we only retain terms to linear order in the fluctuations $\delta\mathbf{n}$. We also disregard terms which are of zeroth order in $\delta\mathbf{n}$. The reason is that we are investigating the excitation spectrum of the spin waves, and the zeroth order terms only amount to an energy shift of the ground state, which for our purposes can be arbitrary. We also make use of the fact that $\mathbf{n}_0 \perp \delta\mathbf{n}$, and $\mathbf{n}_0 \times \hat{\mathbf{z}} = 0$. The equation for the magnetization in eq. 2.12 becomes

$$\begin{aligned}
\rho\dot{\mathbf{n}} &= -a\mathbf{m}\times\mathbf{n} + \Big(\mathbf{n}\times(\mathbf{H}\times\mathbf{n})\Big)\times\mathbf{n} \\
&\simeq -a\mathbf{m}\times\mathbf{n}_0 + \Big(\mathbf{H}\times\mathbf{n}_0 + \mathbf{H}\times\delta\mathbf{n}\Big) \\
\implies \mathbf{m} &= \frac{1}{a}\left[\rho(\delta\dot{\mathbf{n}}\times\mathbf{n}_0) - (\mathbf{n}_0\cdot\mathbf{H})\delta\mathbf{n}\right] \\
\implies \rho(\delta\ddot{\mathbf{n}}\times\mathbf{n}_0) &= a\dot{\mathbf{m}} - (\mathbf{n}_0\cdot\dot{\mathbf{H}})\delta\mathbf{n} - (\mathbf{n}_0\cdot\mathbf{H})\delta\dot{\mathbf{n}}
\end{aligned}$$

The 3$^{\text{d}}$ line of the above equation establishes a connection between the magnetization and the spin wave excitations, as discussed in the thesis. Inserting the expression for $\dot{\mathbf{m}}$ into the fourth equation and only keeping the terms of linear order in the fluctuations as before, we get

$$\begin{aligned}
\rho(\delta\ddot{\mathbf{n}}\times\mathbf{n}_0) &= \frac{a}{\rho}\Big\{A(\nabla^2\delta\mathbf{n}\times\mathbf{n}_0 + \nabla^2\mathbf{n}_0\times\delta\mathbf{n}) + K_z((\delta\mathbf{n}\cdot\hat{\mathbf{z}})(\hat{\mathbf{z}}\times\mathbf{n}_0) + (\mathbf{n}_0\cdot\hat{\mathbf{z}})(\hat{\mathbf{z}}\times\delta\mathbf{n})) \\
&\quad - (\mathbf{n}_0\cdot\mathbf{H})\mathbf{m}\times\mathbf{n}_0 + [\mathbf{H} - (\mathbf{n}_0\cdot\mathbf{H})\mathbf{n}_0]\times\mathbf{m} \\
&\quad - \mathcal{D}[(\hat{\mathbf{y}}\times\mathbf{n}_0)\nabla\cdot\delta\mathbf{n} + (\hat{\mathbf{y}}\times\delta\mathbf{n})\nabla\cdot\mathbf{n}_0 - (\nabla\times\mathbf{n}_0)(\delta\mathbf{n}\cdot\hat{\mathbf{y}}) - (\nabla\times\delta\mathbf{n})(\mathbf{n}_0\cdot\hat{\mathbf{y}})]\Big\} \\
&\quad - (\mathbf{n}_0\cdot\dot{\mathbf{H}})\delta\mathbf{n} - (\mathbf{n}_0\cdot\mathbf{H})\delta\dot{\mathbf{n}} \\
&= \frac{a}{\rho}\Big\{A(\nabla^2\delta\mathbf{n}\times\mathbf{n}_0 + \nabla^2\mathbf{n}_0\times\delta\mathbf{n}) + K_z((\delta\mathbf{n}\cdot\hat{\mathbf{z}})(\hat{\mathbf{z}}\times\mathbf{n}_0) + (\mathbf{n}_0\cdot\hat{\mathbf{z}})(\hat{\mathbf{z}}\times\delta\mathbf{n})) \\
&\quad - \mathcal{D}[(\hat{\mathbf{y}}\times\mathbf{n}_0)\nabla\cdot\delta\mathbf{n} + (\hat{\mathbf{y}}\times\delta\mathbf{n})\nabla\cdot\mathbf{n}_0 - (\nabla\times\mathbf{n}_0)(\delta\mathbf{n}\cdot\hat{\mathbf{y}}) - (\nabla\times\delta\mathbf{n})(\mathbf{n}_0\cdot\hat{\mathbf{y}})]\Big\} \\
&\quad \mathbf{H}\times\left[(\delta\dot{\mathbf{n}}\times\mathbf{n}_0) - \frac{1}{\rho}(\mathbf{n}_0\cdot\mathbf{H})\delta\mathbf{n}\right] - (\mathbf{n}_0\cdot\dot{\mathbf{H}})\delta\mathbf{n} - (\mathbf{n}_0\cdot\mathbf{H})\delta\dot{\mathbf{n}}
\end{aligned}$$

where the term $[\mathbf{n} \times (\mathbf{H} \times \mathbf{n})] \times \mathbf{m}$ was rewritten with the identity B.2. In the last equality, the terms $\sim (\mathbf{n}_0 \cdot \mathbf{H})\mathbf{m} \times \mathbf{n}_0$ cancel, and the expression for $\mathbf{m}$ in the exchange approximation was inserted. Taking the vector product with $\mathbf{n}_0$ yields an expression for $\delta\ddot{\mathbf{n}}$

$$\begin{aligned}\frac{\rho^2}{a}\delta\ddot{\mathbf{n}} \;=\; & A(\nabla^2\delta\mathbf{n} - (\mathbf{n}_0 \cdot \nabla^2\mathbf{n}_0)\delta\mathbf{n}) + K_z((\delta\mathbf{n}\cdot\hat{\mathbf{z}})\hat{\mathbf{z}} - (\mathbf{n}_0\cdot\hat{\mathbf{z}})^2\delta\mathbf{n}) \\ & - \mathcal{D}[\hat{\mathbf{y}}(\nabla\cdot\delta\mathbf{n}) - (\mathbf{n}_0\cdot\hat{\mathbf{y}})(\nabla\cdot\mathbf{n}_0)\delta\mathbf{n} - (\nabla\delta\mathbf{n}\cdot\hat{\mathbf{y}}) + (\mathbf{n}_0\cdot(\nabla\mathbf{n}_0\cdot\hat{\mathbf{y}}))\delta\mathbf{n}] \\ & \frac{1}{a}(\mathbf{H}\cdot\mathbf{n}_0)^2\delta\mathbf{n} + \frac{2\rho}{a}(\mathbf{H}\cdot\mathbf{n}_0)\mathbf{n}_0\times\delta\dot{\mathbf{n}} + \frac{\rho}{a}(\dot{\mathbf{H}}\cdot\mathbf{n}_0)\mathbf{n}_0\times\delta\mathbf{n}\end{aligned}$$

APPENDIX D

FOURIER TRANSFORM OF THE EFFECTIVE DZYALOSHINSKII-MORIYA TERM AND MATRIX ELEMENTS

We here perform the Fourier transform of the Dzyaloshinskii-Moriya-operator in the effective spin wave Hamiltonian acting on the spin wave function $\psi(\mathbf{r})$. This will yield the matrix-elements used to calculate the SW-band diagrams in chap. 4. We will write D for the inhomogeneous DMI instead of the redefined parameter $\bar{D}$ to keep the notation simple.

The DMI-part of the effective KGE is given by

$$\hat{\mathcal{H}}_{DMI} = -\frac{i}{2}\left[D(\mathbf{r})\partial_x - \partial_x D(\mathbf{r})\right] \tag{D.1}$$

where $D(\mathbf{r})$, as introduced in chap. 4, takes the form

$$\begin{aligned} D(\mathbf{r}) &= D\left[\cos\left(\frac{2\pi}{l}x + \frac{2\pi}{l}z\right) + \cos\left(\frac{2\pi}{l}x - \frac{2\pi}{l}z\right)\right] \\ &= 2D\left[\cos(k_b x)\cos(k_b z)\right] \end{aligned} \tag{D.2}$$

with $k_b = 2\pi/l$, where l is the DMI lattice spacing. The reciprocal lattice vectors $\mathbf{b}_1, \mathbf{b}_2$ are defined as

$$\begin{aligned} \mathbf{b}_1 &= k_b(\hat{\mathbf{x}} + \hat{\mathbf{z}}) = k_b \begin{bmatrix} 1 \\ 0 \\ 1 \end{bmatrix} \\ \mathbf{b}_2 &= k_b(\hat{\mathbf{x}} - \hat{\mathbf{z}}) = k_b \begin{bmatrix} 1 \\ 0 \\ -1 \end{bmatrix} \end{aligned} \tag{D.3}$$

The real space lattice periodicity of the modulation, $D(\mathbf{r} + \mathbf{R}) = D(\mathbf{r})$, allows us to expand the function in a set of reciprocal lattice vectors and weighting coefficients $D_{\mathbf{G}}$.

$$D(\mathbf{r}) = \sum_{\mathbf{G}} D_{\mathbf{G}} e^{i\mathbf{G}\cdot\mathbf{r}} \tag{D.4}$$

The coefficients $D_{\mathbf{G}}$ are calculated as [24]

$$\begin{aligned} D_{\mathbf{G}} &= \frac{1}{V_C}\int_C d\mathbf{r}\; D(\mathbf{r})e^{-i\mathbf{G}\mathbf{r}} \\ &= \frac{D}{V_C}\int_C d\mathbf{r}\;\left[\cos\left(\frac{2\pi}{l}x+\frac{2\pi}{l}z\right)+\cos\left(\frac{2\pi}{l}x-\frac{2\pi}{l}z\right)\right]e^{-i\mathbf{G}\mathbf{r}} \\ &= \frac{D}{2V_C}\int_C d\mathbf{r}\;\left[e^{i\mathbf{b}_1\cdot\mathbf{r}}+e^{i\mathbf{b}_2\cdot\mathbf{r}}+e^{-i\mathbf{b}_1\cdot\mathbf{r}}+e^{-i\mathbf{b}_2\cdot\mathbf{r}}\right]e^{-i\mathbf{G}\cdot\mathbf{r}} \\ &= \frac{D}{2}\;\left[\delta(\mathbf{G}-\mathbf{b}_1)+\delta(\mathbf{G}-\mathbf{b}_2)+\delta(\mathbf{G}+\mathbf{b}_1)+\delta(\mathbf{G}+\mathbf{b}_2)\right] \end{aligned}$$

where D is the modulated DMI-strength. The spatial part of the spin wave function $\psi(\mathbf{r})$ can be represented as

$$\psi(\mathbf{r}) \;=\; \int d\mathbf{k}\;\psi(\mathbf{k})\;e^{-i\mathbf{k}\cdot\mathbf{r}} \tag{D.5}$$

We apply the transform to each term of the operator separately. We omit the minus-sign in front of the operator for now. The 1st term of $\hat{\mathcal{H}}_{DMI}$ yields

$$\begin{aligned} \mathcal{F}\left[\frac{i}{2}D(\mathbf{r})\partial_x\psi(\mathbf{r})\right] &= \frac{i}{2}\int_C d\mathbf{r}\,[D(\mathbf{r})\partial_x\psi(\mathbf{r})]\,e^{i\mathbf{q}\cdot\mathbf{r}} \\ &= \frac{i}{2}\int_C d\mathbf{r}\left[\sum_{\mathbf{G}} D_{\mathbf{G}}\;e^{i\mathbf{G}\cdot\mathbf{r}}\;\partial_x\left(\int d\mathbf{k}\psi(\mathbf{k})e^{-i\mathbf{k}\cdot\mathbf{r}}\right)\right]e^{i\mathbf{q}\cdot\mathbf{r}} \\ &= \frac{1}{2}\sum_{\mathbf{G}}\int_C d\mathbf{r}\int d\mathbf{k}\;D_{\mathbf{G}}k_x\;\psi(\mathbf{k})e^{i(\mathbf{q}-\mathbf{k}+\mathbf{G})\cdot\mathbf{r}} \\ &= \frac{D}{4}\sum_{\mathbf{G}}\int d\mathbf{r}\int d\mathbf{k}\,[\delta(\mathbf{G}-\mathbf{b}_1)+\delta(\mathbf{G}-\mathbf{b}_2)+\delta(\mathbf{G}+\mathbf{b}_1)+\delta(\mathbf{G}+\mathbf{b}_2)] \\ &\qquad \times k_x\;e^{i(\mathbf{q}-\mathbf{k}+\mathbf{G})\cdot\mathbf{r}}\;\psi(\mathbf{k}) \\ &= \frac{DV_C}{4}\int d\mathbf{k}\,[\delta(\mathbf{q}-\mathbf{k}+\mathbf{b}_1)+\delta(\mathbf{q}-\mathbf{k}+\mathbf{b}_2)+\delta(\mathbf{q}-\mathbf{k}-\mathbf{b}_1)+\delta(\mathbf{q}-\mathbf{k}-\mathbf{b}_2)] \\ &\qquad \times k_x\;\psi(\mathbf{k}) \\ &= \frac{D}{4}\sum_{i=1,2}[(\mathbf{q}+\mathbf{b}_i)_x\psi(\mathbf{q}+\mathbf{b}_i)+(\mathbf{q}-\mathbf{b}_i)_x\psi(\mathbf{q}-\mathbf{b}_i)] \end{aligned}$$

The 2nd term gives

$$
\begin{aligned}
\mathcal{F}\left[-\frac{i}{2}\partial_x D(\mathbf{r})\psi(\mathbf{r})\right] &= -\frac{i}{2}\int_C d\mathbf{r}\,[\partial_x D(\mathbf{r})\psi(\mathbf{r})]\,e^{i\mathbf{q}\cdot\mathbf{r}} \\
&= -\frac{i}{2}\int_C d\mathbf{r}\left[\partial_x\left(\sum_{\mathbf{G}} D_{\mathbf{G}} e^{i\mathbf{G}\cdot\mathbf{r}}\right)\left(\int d\mathbf{k}\psi(\mathbf{k})e^{-i\mathbf{k}\cdot\mathbf{r}}\right)\right]e^{i\mathbf{q}\cdot\mathbf{r}} \\
&= \frac{D}{4}\sum_G \int d\mathbf{r}\,[\delta(\mathbf{G}-\mathbf{b}_1)+\cdots]\;G_x e^{i\mathbf{G}\cdot\mathbf{r}}\left(\int d\mathbf{k}\psi(\mathbf{k})e^{-i\mathbf{k}\cdot\mathbf{r}}\right)e^{i\mathbf{q}\mathbf{r}} \\
&= \frac{D}{4}\sum_G \int d\mathbf{r}\int d\mathbf{k}\,[\delta(\mathbf{G}-\mathbf{b}_1)+\cdots]\;G_x\psi(\mathbf{k})\;e^{i(\mathbf{q}-\mathbf{k}+\mathbf{G})\cdot\mathbf{r}} \\
&= \frac{DV_C}{4}\int d\mathbf{k}\,[b_{1,x}\delta(\mathbf{q}-\mathbf{k}+\mathbf{b}_1)+b_{2,x}\delta(\mathbf{q}-\mathbf{k}+\mathbf{b}_2)-b_{1,x}\delta(\mathbf{q}-\mathbf{k}-\mathbf{b}_1) \\
&\qquad -b_{1,x}\delta(\mathbf{q}-\mathbf{k}-\mathbf{b}_2)]\,\psi(\mathbf{k}) \\
&= \frac{D}{4}\left[b_{1,x}\psi(\mathbf{q}+\mathbf{b}_1)+b_{2,x}\psi(\mathbf{q}+\mathbf{b}_2)-b_{1,x}\psi(\mathbf{q}-\mathbf{b}_1)-b_{2,x}\psi(\mathbf{q}-\mathbf{b}_2)\right] \\
&= \frac{D}{4}\sum_{i=1,2}\left[b_{i,x}\psi(\mathbf{q}+\mathbf{b}_i)-b_{i,x}\psi(\mathbf{q}-\mathbf{b}_i)\right]
\end{aligned}
$$

Combining the two terms, we get

$$
\begin{aligned}
&\mathcal{F}[\hat{\mathcal{H}}_{DMI}\psi(\mathbf{r})] = \\
&\quad \frac{D}{4}\sum_{i=1,2}([(\mathbf{q}+\mathbf{b}_i)_x\;\psi(\mathbf{q}+\mathbf{b}_i)+(\mathbf{q}-\mathbf{b}_i)_x\;\psi(\mathbf{q}-\mathbf{b}_i)] \\
&\qquad\quad +[b_{i,x}\psi(\mathbf{q}+\mathbf{b}_i)-b_{i,x}\psi(\mathbf{q}-\mathbf{b}_i)]) \\
&\quad = \frac{D}{4}\sum_{i=1,2}[(\mathbf{q}+\mathbf{b}_i+\mathbf{b}_i)_x\psi(\mathbf{q}+\mathbf{b}_i)+(\mathbf{q}-\mathbf{b}_i-\mathbf{b}_i)_x\psi(\mathbf{q}-\mathbf{b}_i)] \\
&\quad = \frac{Dk_b}{4}\sum_{i=1,2}[(q_x+2)\psi(\mathbf{q}+\mathbf{b}_i)+(q_x-2)\psi(\mathbf{q}-\mathbf{b}_i)]
\end{aligned}
$$

where $q'_x = q_x/k_b \equiv q_x$, and used that $b_{1,x} = b_{2,x} = k_b$ to simplify the expression. We have also put back the minus-sign in front of the operator $\hat{\mathcal{H}}_{DMI}$. We have thus obtained the matrix elements $D_{l,l'}$ discussed in the end of chap. 4, with the matrix elements written out explicitly in eq. 4.22. In eq. 4.22, the evaluation of ψ at the reciprocal lattice vectors $\mathbf{b}_i$ is written out as the corresponding δ-functions, and the vector components have been written out explicitly.

BIBLIOGRAPHY

[1] F. Bloch, "Zur Theorie des Ferromagnetismus", *Zeitschrift fur Physik*, vol. 61, 1930. DOI: 10.1007/BF01339661.

[2] H. Kramers, "L'interaction entre les atomes magnétogènes dans un cristal paramagnétique", *Physica*, vol. 1, 1934. DOI: 10.1016/S0031-8914(34)90023-9.

[3] T. Holstein and H. Primakoff, "Field dependence of the intrinsic domain magnetization of a ferromagnet", *Phys. Rev.*, vol. 58, 12 1940. DOI: 10.1103/PhysRev.58.1098.

[4] J. H. E. GRIFFITHS, "Anomalous high-frequency resistance of ferromagnetic metals", *Nature*, vol. 158, 1946. DOI: 10.1038/158670a0.

[5] P. W. Anderson, "Antiferromagnetism. theory of superexchange interaction", *Phys. Rev.*, vol. 79, 2 1950. DOI: 10.1103/PhysRev.79.350.

[6] C. G. Shull, W. A. Strauser, and E. O. Wollan, "Neutron diffraction by paramagnetic and antiferromagnetic substances", *Phys. Rev.*, vol. 83, 2 1951. DOI: 10.1103/PhysRev.83.333.

[7] P. W. Anderson, "An approximate quantum theory of the antiferromagnetic ground state", *Phys. Rev.*, vol. 86, 5 1952. DOI: 10.1103/PhysRev.86.694.

[8] F. J. Dyson, "Thermodynamic behavior of an ideal ferromagnet", *Phys. Rev.*, vol. 102, 5 1956. DOI: 10.1103/PhysRev.102.1230.

[9] F. J. Dyson, "General theory of spin-wave interactions", *Physical Review - PHYS REV X*, vol. 102, 1956. DOI: 10.1103/PhysRev.102.1217.

[10] I. Dzyaloshinsky, "A thermodynamic theory of weak ferromagnetism of antiferromagnetics", *Journal of Physics and Chemistry of Solids*, vol. 4, 1958. DOI: 10.1016/0022-3697(58)90076-3.

[11] T. Moriya, "Anisotropic superexchange interaction and weak ferromagnetism", *Phys. Rev.*, vol. 120, 1 1960. DOI: 10.1103/PhysRev.120.91.

[12] "Magnetostatic modes of a ferromagnet slab", *Journal of Physics and Chemistry of Solids*, vol. 19, 1961. DOI: 10.1016/0022-3697(61)90041-5.

[13] E. Lieb and D. Mattis, "Ordering energy levels of interacting spin systems", *Journal of Mathematical Physics*, vol. 3, 1962. DOI: 10.1063/1.1724276.

[14] L. M. Roth, "Theory of the faraday effect in solids", *Phys. Rev.*, vol. 133, 2A 1964. DOI: 10.1103/PhysRev.133.A542.

[15] C. Elachi, "Magnetic wave propagation in a periodic medium", *IEEE Transactions on Magnetics*, vol. 11, 1975. DOI: 10.1109/TMAG.1975.1058546.

[16] L. D. Landau and E. M. Lifshitz, *The classical theory of fields (course of theoretical physics, volume 2)*. Pergamon Press, 1975.

[17] A. P. Cracknell, J Lorenc, and J. A. Przystawa, "Landau's theory of second-order phase transitions and its application to ferromagnetism", *Journal of Physics C: Solid State Physics*, vol. 9, 1976. DOI: 10.1088/0022-3719/9/9/015.

[18] W. F. Brown, *Micromagnetics*. Krieger Pub Co, 1978.

[19] A. F. Andreev and V. I. Marchenko, "Symmetry and the macroscopic dynamics of magnetic materials", *Soviet Physics Uspekhi*, vol. 23, 1980. DOI: 10.1070/pu1980v023n01abeh004859.

[20] A. Fert and P. M. Levy, "Role of anisotropic exchange interactions in determining the properties of spin-glasses", *Phys. Rev. Lett.*, vol. 44, 23 1980. DOI: 10.1103/PhysRevLett.44.1538.

[21] L. Landau and E. Lifshitz, *Statistical physics: Part 2*. Pergamon Press, 1980, vol. 9.

[22] F. D. M. Haldane, "Nonlinear field theory of large-spin heisenberg antiferromagnets: Semiclassically quantized solitons of the one-dimensional easy-axis néel state", *Phys. Rev. Lett.*, vol. 50, 15 1983. DOI: 10.1103/PhysRevLett.50.1153.

[23] K Binder, "Theory of first-order phase transitions", *Reports on Progress in Physics*, vol. 50, 1987. DOI: 10.1088/0034-4885/50/7/001.

[24] N. W. Ashcroft and N. D. Mermin, *Solid state physics*. Saunders College, 1988.

[25] M. N. Baibich, J. M. Broto, A. Fert, F. N. Van Dau, F. Petroff, P. Etienne, G. Creuzet, A. Friederich, and J. Chazelas, "Giant magnetoresistance of (001)fe/(001)cr magnetic superlattices", *Phys. Rev. Lett.*, vol. 61, 21 1988. DOI: 10.1103/PhysRevLett.61.2472.

[26] *Continuum mechanics of electromagnetic solids (north-holland series in applied mathematics and mechanics)*. Elsevier Science Ltd, 1988.

[27] N. Kurti, *Selected works of louis neel*. CRC Press, 1988.

[28] I Affleck, "Quantum spin chains and the haldane gap", *Journal of Physics: Condensed Matter*, vol. 1, 1989. DOI: 10.1088/0953-8984/1/19/001.

[29] G. Binasch, P. Grünberg, F. Saurenbach, and W. Zinn, "Enhanced magnetoresistance in layered magnetic structures with antiferromagnetic interlayer exchange", *Phys. Rev. B*, vol. 39, 7 1989. DOI: 10.1103/PhysRevB.39.4828.

[30] A. N. Bogdanov and D. A. Yablonskii, "Thermodynamically stable "vortices" in magnetically ordered crystals. the mixed state of magnets", *Zh. Eksp. Teor. Fiz.*, vol. 95, 1989.

[31] A. Fert, "Magnetic and transport properties of metallic multilayers", in *Metallic Multilayers*, ser. Materials Science Forum, vol. 59, Trans Tech Publications Ltd, Jan. 1991, pp. 439–480. DOI: 10.4028/www.scientific.net/MSF.59-60.439.

[32] R. Shankar, "Renormalization-group approach to interacting fermions", *Rev. Mod. Phys.*, vol. 66, 1 1994. DOI: 10.1103/RevModPhys.66.129.

[33] N. Papanicolaou, "Antiferromagnetic domain walls", *Phys. Rev. B*, vol. 51, 21 1995. DOI: 10.1103/PhysRevB.51.15062.

[34] "Current-driven excitation of magnetic multilayers", *Journal of Magnetism and Magnetic Materials*, vol. 159, 1996. DOI: 10.1016/0304-8853(96)00062-5.

[35] A. Auerbach, *Interacting electrons and quantum magnetism (graduate texts in contemporary physics)*. Springer, 1998.

[36] R. P. Feynman, *Quantum electrodynamics (frontiers in physics)*. Westview Press, 1998.

[37] J. D. Jackson, *Classical electrodynamics third edition*. Wiley, 1998.

[38] J. S. Dodge, A. B. Schumacher, J.-Y. Bigot, D. S. Chemla, N. Ingle, and M. R. Beasley, "Time-resolved optical observation of spin-wave dynamics", *Phys. Rev. Lett.*, vol. 83, 22 1999. DOI: 10.1103/PhysRevLett.83.4650.

[39] D. J. Griffiths, *Introduction to electrodynamics (3rd edition)*. Prentice Hall, 1999.

[40] A. D. Andreev and E. P. O'Reilly, "Theory of the electronic structure of gan/aln hexagonal quantum dots", *Phys. Rev. B*, vol. 62, 23 2000. DOI: 10.1103/PhysRevB.62.15851.

[41] H. Goldstein, C. P. P. Jr., and J. L. Safko, *Classical mechanics (3rd edition)*. Pearson, 2001.

[42] F. Tisseur and K. Meerbergen, "The quadratic eigenvalue problem", *SIAM Review*, vol. 43, 2001. DOI: 10.1137/S0036144500381988.

[43] A. N. Bogdanov, U. K. Roessler, M. Wolf, and K. H. Muller, "Magnetic structures and reorientation transitions in noncentrosymmetric uniaxial antiferromagnets", 2002. DOI: 10.1103/PhysRevB.66.214410.

[44] N. B. Weber, H. Ohldag, H. Gomonaj, and F. U. Hillebrecht, "Magnetostrictive domain walls in antiferromagnetic nio", *Phys. Rev. Lett.*, vol. 91, 23 2003. DOI: 10.1103/PhysRevLett.91.237205.

[45] C. Kittel, *Introduction to solid state physics*, Eight edition. Wiley, 2005.

[46] L. S. Schulman, *Techniques and applications of path integration (dover books on physics)*. Dover Publications, 2005.

[47] B. Thaller, *Advanced visual quantum mechanics*. Springer, 2005.

[48] S. O. Demokritov, V. E. Demidov, O. Dzyapko, G. A. Melkov, A. A. Serga, B. Hillebrands, and A. N. Slavin, "Bose-einstein condensation of quasi-equilibrium magnons at room temperature under pumping", *Nature*, vol. 443, 2006. DOI: 10.1038/nature05117.

[49] R. Wehrspohn, A von Rhein, and T. Geppert, *Photonic crystals: Principles and applications*. Dec. 2006. DOI: 10.1016/B0-08-043152-6/02021-0.

[50] M. Bode, M. Heide, K. von Bergmann, P. Ferriani, S. Heinze, G. Bihlmayer, A. Kubetzka, O. Pietzsch, S. Blügel, and R. Wiesendanger, "Chiral magnetic order at surfaces driven by inversion asymmetry", *Nature*, vol. 447, 2007. DOI: 10.1038/nature05802.

[51] S. T. Ochsenbein, O. Waldmann, A. Sieber, G. Carver, R. Bircher, H. U. Güdel, R. S. G. Davies, G. A. Timco, R. E. P. Winpenny, H. Mutka, and F. Fernandez-Alonso, "Standing spin waves in an antiferromagnetic molecular cr6 horseshoe", 2007. DOI: 10.1209/0295-5075/79/17003.

[52] a. V. K. V. Ya. Demikhovski and A. A. Perov, "Periodic structures with spin-orbit coupling", *Low Temperature Physics 33*, vol. 115, 2007. DOI: 10.1063/1.2409644.

[53] Z. Wei, A. Sharma, A. S. Nunez, P. M. Haney, R. A. Duine, J. Bass, A. H. MacDonald, and M. Tsoi, "Changing exchange bias in spin valves with an electric current", *Phys. Rev. Lett.*, vol. 98, 11 2007. DOI: 10.1103/PhysRevLett.98.116603.

[54] Y. D. Chong, X.-G. Wen, and M. Soljacic, "Effective theory of quadratic degeneracies", 2008. DOI: 10.1103/PhysRevB.77.235125.

[55] N. Grigoryeva, A Ustinov, and B A. Kalinikos, "Observation of spin-wave envelope solitons in periodic magnetic film structures", *JETP Letters*, vol. 88, 2008. DOI: 10.1134/S0021364008130079.

[56] M. C. Hickey and J. S. Moodera, "Origin of intrinsic gilbert damping", 2008. DOI: 10.1103/PhysRevLett.102.137601.

[57] M. Krawczyk and H. Puszkarski, "Plane-wave theory of three-dimensional magnonic crystals", *Physical Review B*, vol. 77, 2008. DOI: 10.1103/PhysRevB.77.054437.

[58] P. Landeros, R Arias, and D L. Mills, "Two magnon scattering in ultrathin ferromagnets: The case where the magnetization is out of plane", *Physical Review B*, vol. 77, 2008. DOI: 10.1103/PhysRevB.77.214405.

[59] V. Vlaminck and M. Bailleul, "Current-induced spin-wave doppler shift", *Science*, vol. 322, 2008. DOI: 10.1126/science.1162843.

[60] D. Bindel and J. Goodman, *Principles of scientific computing*. 2009.

[61] A. V. Chumak, T Neumann, A. A. Serga, B Hillebrands, and M. P. Kostylev, vol. 42, 2009. DOI: 10.1088/0022-3727/42/20/205005.

[62] R. A. Duine, *Spintronics*. 2009, Lecture notes for the course Spintronics at Utrecht University, spring 2009.

[63] G. I. Japaridze, H. Johannesson, and A. Ferraz, "Metal-insulator transition in a quantum wire driven by a modulated rashba spin-orbit coupling", 2009. DOI: 10.1103/PhysRevB.80.041308.

[64] ——, "Metal-insulator transition in a quantum wire driven by a modulated rashba spin-orbit coupling", 2009. DOI: 10.1103/PhysRevB.80.041308.

[65] A. V. Kimel, B. A. Ivanov, R. V. Pisarev, P. A. Usachev, A. Kirilyuk, and T. Rasing, "Inertia-driven spin switching in antiferromagnets", *Nature Physics*, vol. 5, 2009. DOI: 10.1038/nphys1369.

[66] S. Mühlbauer, B. Binz, F. Jonietz, C. Pfleiderer, A. Rosch, A. Neubauer, R. Georgii, and P. Böni, "Skyrmion lattice in a chiral magnet", *Science*, vol. 323, 2009. DOI: 10.1126/science.1166767.

[67] "Phononic crystals and acoustic metamaterials", *Materials Today*, vol. 12, 2009. DOI: 10.1016/S1369-7021(09)70315-3.

[68] D. D. Stancil and A. Prabhakar, *Spin waves: Theory and applications*. Springer, 2009.

[69] Z. K. Wang, V. L. Zhang, H. S. Lim, S. C. Ng, M. H. Kuok, S. Jain, and A. O. Adeyeye, "Observation of frequency band gaps in a one-dimensional nanostructured magnonic crystal", *Applied Physics Letters*, vol. 94, 2009. DOI: 10.1063/1.3089839.

[70] A. Altland and B. D. Simons, *Condensed matter field theory*. Cambridge University Press, 2010.

[71] T. Brauner, "Spontaneous symmetry breaking and nambu-goldstone bosons in quantum many-body systems", 2010. DOI: 10.3390/sym2020609.

[72] T. Kampfrath, A. Sell, G. Klatt, A. Pashkin, S. Mährlein, T. Dekorsy, M. Wolf, M. Fiebig, A. Leitenstorfer, and R. Huber, "Coherent terahertz control of antiferromagnetic spin waves", *Nature Photonics*, vol. 5, 2010. DOI: 10.1038/nphoton.2010.259.

[73] V. V. Kruglyak, S. O. Demokritov, and D Grundler, "Magnonics", *Journal of Physics D: Applied Physics*, vol. 43, 2010. DOI: 10.1088/0022-3727/43/26/264001.

[74] R. Magaraggia, M. Kostylev, K. Kennewell, R. L. Stamps, M. Ali, D. Greig, B. J. Hickey, and C. H. Marrows, "Exchange anisotropy pinning of a standing spin wave mode", 2010. DOI: 10.1103/PhysRevB.83.054405.

[75] Y. Onose, T. Ideue, H. Katsura, Y. Shiomi, N. Nagaosa, and Y. Tokura, "Observation of the magnon hall effect", *Science*, vol. 329, 2010. DOI: 10.1126/science.1188260.

[76] T. Satoh, S.-J. Cho, R. Iida, T. Shimura, K. Kuroda, H. Ueda, Y. Ueda, B. A. Ivanov, F. Nori, and M. Fiebig, "Spin oscillations in antiferromagnetic nio triggered by circularly polarized light", 2010. DOI: 10.1103/PhysRevLett.105.077402.

[77] P. Strange, *Relativistic quantum mechanics: With applications in condensed matter and atomic physics*. Cambridge University Press, 2010.

[78] J. Thomson, "Cathode rays", *Philosophical Magazine*, vol. 90, 2010. DOI: 10.1080/14786431003659214.

[79] X. yu, Y Onose, N Kanazawa, J.-H. Park, J H Han, Y. Matsui, N Nagaosa, and Y Tokura, "Real-space observation of a two-dimensional skyrmion crystal", *Nature*, vol. 465, 2010. DOI: 10.1038/nature09124.

[80] S. Heinze, K. von Bergmann, M. Menzel, J. Brede, A. Kubetzka, R. Wiesendanger, G. Bihlmayer, and S. Bl/"ugel, "Spontaneous atomic-scale magnetic skyrmion lattice in two dimensions", *Nat Phys*, vol. 7, 2011. DOI: 10.1038/nphys2045.

[81] B. Lenk, H. Ulrichs, F. Garbs, and M. Münzenberg, "The building blocks of magnonics", 2011. DOI: 10.1016/j.physrep.2011.06.003.

[82] B. G. Park, J. Wunderlich, X. Martí, V. Holý, Y. Kurosaki, M. Yamada, H. Yamamoto, A. Nishide, J. Hayakawa, H. Takahashi, A. B. Shick, and T. Jungwirth, "A spin-valve-like magnetoresistance of an antiferromagnet-based tunnel junction", *Nature Materials*, vol. 10, 2011. DOI: 10.1038/nmat2983.

[83] A. C. Swaving and R. A. Duine, "Current-induced torques in continuous antiferromagnetic textures", *Phys. Rev. B*, vol. 83, 5 2011. DOI: 10.1103/PhysRevB.83.054428.

[84] R. Cheng and Q. Niu, "Electron dynamics in slowly varying antiferromagnetic texture", *Physical Review B*, vol. 86, 2012. DOI: 10.1103/PhysRevB.86.245118.

[85] F. Han, *A modern course in the quantum theory of solids*. World Scientific Pub Co Inc, 2012.

[86] D Cortés-Ortuño and P Landeros, "Influence of the dzyaloshinskii–moriya interaction on the spin-wave spectra of thin films", *Journal of Physics: Condensed Matter*, vol. 25, 2013. DOI: 10.1088/0953-8984/25/15/156001.

[87] S. Emori, U. Bauer, S.-M. Ahn, E. Martinez, and G. Beach, "Current-driven dynamics of chiral ferromagnetic domain walls", *Nature materials*, vol. 12, 2013. DOI: 10.1038/nmat3675.

[88] R. Gieniusz, H. Ulrichs, V. D. Bessonov, U. Guzowska, A. I. Stognii, and A. Maziewski, "Single antidot as a passive way to create caustic spin-wave beams in yttrium iron garnet films", *Applied Physics Letters*, vol. 102, 2013. DOI: 10.1063/1.4795293.

[89] M. Jamali, J. H. Kwon, S.-M. Seo, K.-J. Lee, and H. Yang, "Spin wave nonreciprocity for logic device applications", *Scientific Reports*, vol. 3, 2013. DOI: 10.1038/srep03160.

[90] M. Mruczkiewicz, M. Krawczyk, V. K. Sakharov, Y. V. Khivintsev, Y. A. Filimonov, and S. A. Nikitov, "Standing spin waves in magnonic crystals", *Journal of Applied Physics*, vol. 113, 2013. DOI: 10.1063/1.4793085.

[91] H. Nakayama, M. Althammer, Y.-T. Chen, K. Uchida, Y. Kajiwara, D. Kikuchi, T. Ohtani, S. Geprägs, M. Opel, S. Takahashi, R. Gross, G. E. W. Bauer, S. T. B. Goennenwein, and E. Saitoh, "Spin hall magnetoresistance induced by a nonequilibrium proximity effect", *Phys. Rev. Lett.*, vol. 110, 20 2013. DOI: 10.1103/PhysRevLett.110.206601.

[92] R. Shindou, J. ichiro Ohe, R. Matsumoto, S. Murakami, and E. Saitoh, "Chiral spin-wave edge modes in dipolar magnetic thin films", 2013. DOI: 10.1103/PhysRevB.87.174402.

[93] R. Cheng, J. Xiao, Q. Niu, and A. Brataas, "Spin pumping and spin-transfer torques in antiferromagnets", *Phys. Rev. Lett.*, vol. 113, 5 2014. DOI: 10.1103/PhysRevLett.113.057601.

[94] M Krawczyk and D Grundler, "Review and prospects of magnonic crystals and devices with reprogrammable band structure", *Journal of Physics: Condensed Matter*, vol. 26, 2014. DOI: 10.1088/0953-8984/26/12/123202.

[95] D. Kumar, J. W. Kłos, M. Krawczyk, and A. Barman, "Magnonic band structure, complete bandgap, and collective spin wave excitation in nanoscale two-dimensional magnonic crystals", *Journal of Applied Physics*, vol. 115, 2014. DOI: 10.1063/1.4862911.

[96] T. Liu, H. Chang, V. Vlaminck, Y. Sun, M. Kabatek, A. Hoffmann, L. Deng, and M. Wu, "Ferromagnetic resonance of sputtered yttrium iron garnet nanometer films", *Journal of Applied Physics*, vol. 115, 2014. DOI: 10.1063/1.4852135.

[97] F. Ma and Y. Zhou, "Interfacial dzialoshinskii–moriya interaction induced nonreciprocity of spin waves in magnonic waveguides", *RSC Adv.*, vol. 4, 87 2014. DOI: 10.1039/C4RA07326F.

[98] R. Tomasello, E. Martinez, R. Zivieri, L. Torres, M. Carpentieri, and G. Finocchio, "A strategy for the design of skyrmion racetrack memories", *Scientific Reports*, vol. 4, 2014. DOI: 10.1038/srep06784.

[99] G Bihlmayer, O Rader, and R Winkler, "Focus on the rashba effect", *New Journal of Physics*, vol. 17, 2015. DOI: 10.1088/1367-2630/17/5/050202.

[100] C. Davies and V. Kruglyak, "Graded-index magnonics", *Fizika Nizkikh Temperatur*, vol. 41, 2015. DOI: 10.1063/1.4932349.

[101] P. Gentile, M. Cuoco, and C. Ortix, "Edge states and topological insulating phases generated by curving a nanowire with rashba spin-orbit coupling", *Phys. Rev. Lett.*, vol. 115, 25 2015. DOI: 10.1103/PhysRevLett.115.256801.

[102] J. Hagemeister, N. Romming, K. von Bergmann, E. Y. Vedmedenko, and R. Wiesendanger, "Stability of single skyrmionic bits", *Nature Communications*, vol. 6, 2015. DOI: 10.1038/ncomms9455.

[103] J. Lan, W. Yu, R. Wu, and J. Xiao, "A spin wave diode", 2015. DOI: 10.1103/PhysRevX.5.041049.

[104] M. Mruczkiewicz, P. Gruszecki, M. Zelent, and M. Krawczyk, "Collective dynamical skyrmions excitations in magnonic crystal", 2015. DOI: 10.1103/PhysRevB.93.174429.

[105] H. T. Nembach, J. M. Shaw, M. Weiler, E. Jué, and T. J. Silva, "Linear relation between heisenberg exchange and interfacial dzyaloshinskii-moriya interaction in metal films", *Nature Physics*, vol. 11, 2015. DOI: 10.1038/nphys3418.

[106] M. Peskin, *An introduction to quantum field theory, student economy edition (frontiers in physics)*. CRC Press, 2015.

[107] S. Seki, T. Ideue, M. Kubota, Y. Kozuka, R. Takagi, M. Nakamura, Y. Kaneko, M. Kawasaki, and Y. Tokura, "Thermal generation of spin current in an antiferromagnet", *Phys. Rev. Lett.*, vol. 115, 26 2015. DOI: 10.1103/PhysRevLett.115.266601.

[108] A. A. Stashkevich, M. Belmeguenai, Y. Roussigné, S. M. Cherif, M. Kostylev, M. Gabor, D. Lacour, C. Tiusan, and M. Hehn, "Experimental study of spin-wave dispersion in py/pt film structures in the presence of an interface dzyaloshinskii-moriya interaction", *Phys. Rev. B*, vol. 91, 21 2015. DOI: 10.1103/PhysRevB.91.214409.

[109] R. E. Troncoso, C. Ulloa, F. Pesce, and A. S. Nunez, "Antiferromagnetic magnonic crystals", *Phys. Rev. B*, vol. 92, 22 2015. DOI: 10.1103/PhysRevB.92.224424.

[110] M. Vogel, A. V. Chumak, E. H. Waller, T. Langner, V. I. Vasyuchka, B. Hillebrands, and G. von Freymann, "Optically reconfigurable magnetic materials", *Nature Physics*, vol. 11, 2015. DOI: 10.1038/nphys3325.

[111] H. Yang, A. Thiaville, S. Rohart, A. Fert, and M. Chshiev, "Anatomy of dzyaloshinskii-moriya interaction at Co/Pt interfaces", *Phys. Rev. Lett.*, vol. 115, 26 2015. DOI: 10.1103/PhysRevLett.115.267210.

[112] X. Yongbing, D. Awschalom, and N Junsaki, *Handbook of spintronics*. Springer, 2015.

[113] R. Cheng, M. W. Daniels, J.-G. Zhu, and D. Xiao, "Antiferromagnetic spin wave field-effect transistor", *Scientific Reports*, vol. 6, 2016. DOI: 10.1038/srep24223.

[114] M. L. Cohen and S. G. Louie, *Fundamentals of condensed matter physics*. Cambridge University Press, 2016.

[115] D. J. Griffiths, *Introduction to quantum mechanics*. Cambridge University Press, 2016.

[116] C. Moreau-Luchaire, C. Moutafis, N. Reyren, J. Sampaio, C. A. F. Vaz, N. Van Horne, K. Bouzehouane, K. Garcia, C. Deranlot, P. Warnicke, P. Wohlhüter, J.-M. George, M. Weigand, J. Raabe, V. Cros, and A. Fert, "Additive interfacial chiral interaction in multilayers for stabilization of small individual skyrmions at room temperature", *Nature Nanotechnology*, vol. 11, 2016. DOI: 10.1038/nnano.2015.313.

[117] R. L. Pavelich and F. Marsiglio, "Calculation of 2d electronic band structure using matrix mechanics", 2016. DOI: 10.1119/1.4964353.

[118] E. G. Tveten, T. Müller, J. Linder, and A. Brataas, "Intrinsic magnetization of antiferromagnetic textures", *Phys. Rev. B*, vol. 93, 10 2016. DOI: 10.1103/PhysRevB.93.104408.

[119] X. Zhang, Y. Zhou, and M. Ezawa, "Antiferromagnetic skyrmion: Stability, creation and manipulation", *Scientific Reports*, vol. 6, 2016. DOI: 10.1038/srep24795.

[120] S. Bhatti, R. Sbiaa, A. Hirohata, H. Ohno, S. Fukami, and S. Piramanayagam, "Spintronics based random access memory: A review", *Materials Today*, vol. 20, 2017. DOI: 10.1016/j.mattod.2017.07.007.

[121] G. Gitgeatpong, Y. Zhao, P. Piyawongwatthana, Y. Qiu, L. W. Harriger, N. P. Butch, T. J. Sato, and K. Matan, "Nonreciprocal magnons and symmetry-breaking in the noncentrosymmetric antiferromagnet", *Phys. Rev. Lett.*, vol. 119, 4 2017. DOI: 10.1103/PhysRevLett.119.047201.

[122] J. H. Han, *Skyrmions in condensed matter (springer tracts in modern physics book 278)*. Springer, 2017.

[123] J. Lan, W. Yu, and J. Xiao, "Antiferromagnetic domain wall as spin wave polarizer and retarder", *Nature Communications*, vol. 8, 2017. DOI: 10.1038/s41467-017-00265-5.

[124] S. J. Lee, J. H. Moon, H.-W. Lee, and K.-J. Lee, "Spin-wave propagation in the presence of inhomogeneous dzyaloshinskii-moriya interactions", *Physical Review B*, vol. 96, 2017. DOI: 10.1103/PhysRevB.96.184433.

[125] S. Tacchi, R. E. Troncoso, M. Ahlberg, G. Gubbiotti, M. Madami, J. Åkerman, and P. Landeros, "Interfacial dzyaloshinskii-moriya interaction in Pt/CoFeB films: Effect of the heavy-metal thickness", *Phys. Rev. Lett.*, vol. 118, 14 2017. DOI: 10.1103/PhysRevLett.118.147201.

[126] P. Taivansaikhan, D. Odkhuu, S. H. Rhim, and S. C. Hong, "Gigantic perpendicular magnetic anisotropy of heavy transition metal cappings on fe/mgo(001)", *Journal of Magnetism and Magnetic Materials*, vol. 442, 2017. DOI: 10.1016/j.jmmm.2017.06.110.

[127] W. Wang, C. Gu, Y. Zhou, and H. Fangohr, "Magnonic analog of relativistic zitterbewegung in an antiferromagnetic spin chain", *Phys. Rev. B*, vol. 96, 2 2017. DOI: 10.1103/PhysRevB.96.024430.

[128] S. Woo, K. M. Song, X. Zhang, Y. Zhou, M. Ezawa, X. Liu, S. Finizio, J. Raabe, N. J. Lee, S.-I. Kim, S.-Y. Park, Y. Kim, J.-Y. Kim, D. Lee, O. Lee, J. W. Choi, B.-C. Min, H. C. Koo, and J. Chang, "Current-driven dynamics and inhibition of the skyrmion hall effect of ferrimagnetic skyrmions in gdfeco films", 2017. DOI: 10.1038/s41467-018-03378-7.

[129] S. A. Owerre, "Two-dimensional dirac nodal loop magnons in collinear antiferromagnets", *Journal of Physics: Condensed Matter*, vol. 30, 2018. DOI: 10.1088/1361-648x/aac8b5.

[130] A. Qaiumzadeh, L. A. Kristiansen, and A. Brataas, "Controlling chiral domain walls in antiferromagnets using spin-wave helicity", *Phys. Rev. B*, vol. 97, 2 2018. DOI: 10.1103/PhysRevB.97.020402.

[131] S. B. Sørheim, "Magnon excitations of a dzyaloshinskiimoriya coupled insulating 2d antiferromagnetic skyrmion", Master's thesis, 2018.

[132] R. A. Gallardo, D. Cortés-Ortuño, T. Schneider, A. Roldán-Molina, F. Ma, R. E. Troncoso, K. Lenz, H. Fangohr, J. Lindner, and P. Landeros, "Flat bands, indirect gaps, and unconventional spin-wave behavior induced by a periodic dzyaloshinskii-moriya interaction", *Phys. Rev. Lett.*, vol. 122, 6 2019. DOI: 10.1103/PhysRevLett.122.067204.

[133] A. V. Chumak, "Fundamentals of magnon-based computing",

[134] J. O. Fjærestad, *Lecture notes, quantum theory of many-particle systems*.

[135] T. Gilbert and J. Kelly, "Anomalous rotational damping in ferromagnetic sheets", *American Institute of Electrical Engineers*,

[136] S. Yeong-Ah and K. R. K., "Spintronics in antiferromagnets", *Philosophical Transactions of the Royal Society A: Mathematical, Physical and Engineering Sciences*,